

Kinetics of Block Copolymer Micelles Studied by Small-Angle Scattering Methods

Reidar Lund, Lutz Willner, and Dieter Richter

Abstract This article reviews recent progress in studying the kinetics of block copolymer micellar systems by time-resolved small angle scattering techniques. The review includes an overview of the theoretical background concerning block copolymer micellar structure and kinetics, with a clear distinction between equilibrium and non-equilibrium processes. Basic principles of both static and time-resolved small-angle X-ray and neutron scattering (TR-SAXS and TR-SANS) techniques are summarized, with a special emphasis on the characterization of block copolymer micellar systems. In particular, the principle of SANS in combination with hydrogen/deuterium (H/D) contrast variation for the determination of chain exchange under equilibrium conditions is highlighted. In the experimental part, we first review results on equilibrium kinetics obtained within the last decade by the TR-SANS/H/D labeling technique. In general, the experimental results strongly indicate that the component exchange between different micelles proceeds via the exchange of single unimers. In agreement with the theoretical prediction, chain expulsion is the rate-determining step. The corresponding activation energy is mainly governed by the interfacial tension and the length of the insoluble block, which determine the exchange rate with a double exponential dependence. Thus, due to this extremely strong dependence, even synthetic polymers with modest chain length distribution show a logarithmic time dependence instead of the theoretically expected single exponential decay. In the second part, the kinetic results obtained under non-equilibrium conditions, i.e., relaxation processes obtained after perturbations from equilibrium, are reviewed. This part covers formation kinetics as well as reorganization and morphological transition kinetics. We present, as a special highlight, TR-SAXS

R. Lund (✉)

Department of Chemistry, University of Oslo, Postboks 1033 Blindern, 0315 Oslo, Norway
e-mail: reidar.lund@kjemi.uio.no

L. Willner (✉) and D. Richter

Jülich Centre for Neutron Science JCNS and Institute for Complex Systems ICS,
Forschungszentrum Jülich GmbH, 52425 Jülich, Germany
e-mail: l.willner@fz-juelich.de; d.richter@fz-juelich.de

measurements with millisecond resolution on the formation of star-like micelles after stopped-flow mixing of molecularly dissolved block copolymers with a selective solvent. The micellization process could be modelled as a nucleation & growth process with unimer exchange as the elemental mechanism. The resulting scenario could be described as a three step process that includes a fast nucleation event, a region of micellar growth, and a final equilibration to thermodynamically stable micelles. In summary, this review demonstrates the importance of small angle scattering techniques for studying fundamental aspects of kinetics in block copolymer micelles and in soft matter materials in general.

Keywords Block copolymer micelles · Contrast variation · Equilibrium and non-equilibrium kinetics · Morphology · Small-angle neutron and X-ray scattering · Time-resolved SAXS/SANS

Contents

1	Introduction	54
2	Theoretical Background	58
2.1	Structure and Thermodynamics	58
2.2	Chain Exchange Kinetics in Equilibrium	66
2.3	Non-equilibrium Micellization Kinetics	77
3	Experimental Techniques	83
3.1	Small-Angle Scattering Methods	83
3.2	Time-Resolved Small-Angle Scattering as a Technique for Studying Micellar Kinetics	99
4	Equilibrium Kinetics in Block Copolymer Micelles	108
4.1	Quasi-equilibrium Kinetics of PEO-PPO-PEO in Temperature-Jump Experiments	110
4.2	PEP-PEO Block Copolymers in Aqueous Solution	111
4.3	Block Copolymer Micelles in Organic Solvents	122
4.4	<i>n</i> -Alkyl-PEO Polymeric Micelles	126
4.5	Chain Exchange in Soft Solids: Effect of Concentration	128
4.6	Cylinders Versus Spheres: Effect of Morphology	130
4.7	Summary	132
5	Non-equilibrium Kinetics in Block Copolymer Micelles	133
5.1	Formation and Micellization Kinetics	133
5.2	Morphological Transition Kinetics	149
6	Concluding Remarks and Future Challenges	152
	References	153

Symbols

$\frac{d\Sigma}{d\Omega}$	Macroscopic differential scattering cross-section per unit volume in cm^{-1}
k_p^+	Rate constant for unimer insertion from micelle of size P
k_p^-	Rate constant for unimer expulsion from micelle of size P

$ \mathbf{Q} = Q$	Scattering vector in \AA^{-1}
A	Area
a	Elementary lattice size
$A(Q)$	Scattering amplitude in cm
A_2, A_3	Second and third virial coefficient
b	Scattering length in cm
C_F, C_H	Numerical prefactors
d	Density in g/cm^3
D	Diffusion coefficient
d_f	Fractal dimension
E_a	Activation energy
F	Free energy
f	Ratio between degree of polymerization of soluble and insoluble block
F_{micelle}	The mixing term of free block copolymers and solvent
F_{mix}	Free energy of mixing
$G(P, \phi_1)$	Chemical potential
H/D	Hydrogen/deuterium
j_P	Flux of unimers to micelle of size P
k_B	Boltzmann constant: $1.38 \times 10^{-23} \text{ J/K}$
L	Cylinder length in \AA
l_i	Monomer segment length of block i
M_w	Weight average molecular weight in g/mole
$n(r)$	Density profile
N_A	Degree of polymerization of soluble block
N_{Avo}	Avogadro's number: $6.022 \times 10^{23} \text{ mole}^{-1}$
N_B	Degree of polymerization of insoluble block
N_m	Total particle number
P	Micellar aggregation number
$P(Q)$	Form factor
$R(t)$	Relaxation function (TR-SANS)
R_c	Micellar core radius in \AA
R_g	Radius of gyration
R_m	Total micellar radius in \AA
s	Grafting density (area available per chain)
$S(Q)$	Structure factor
S_m	Translational entropy of micelles
t_{dead}	Dead time of mixing
ν	Flory exponent
V_i	Volume of component i
V_s	Sample volume in cm^3
γ	Interfacial tension in mN/m
ζ	Fraction of block copolymer in the micellar state
η	Corona density
ξ	Blob radius/correlation length

ρ	Scattering length density in cm^{-2}
σ_{int}	Gaussian width of core–corona interface
σ_{m}	Smearing parameter for micellar radius
τ_1	Slow relaxation time (Aniansson and Wall)
τ_2	Fast relaxation time (Aniansson and Wall)
Φ_0	Solvent fraction in micellar core
ϕ_0	Total amphiphile volume fraction
ϕ_1	Unimer concentration
Φ_p	Concentration of micelle of size p
χ	Flory–Huggins interaction parameter

1 Introduction

Self-assembly is responsible for the formation of essential structures in nature, including lipid membranes and living cells. The resulting structures are formed as a consequence of a delicate balance between hydrophilic and hydrophobic contributions and/or enthalpic and entropic forces. Whereas the surface tension drives the formation of such systems, entropy and stochastic fluctuations try to rip the structures apart. This has important consequences. First of all, self-assembled structures are classified as soft materials meaning that the properties are rather susceptible to intensive parameters such as temperature and pressure and that the structures are easily perturbed and deformed by external fields. Secondly, they are intrinsically dynamic structures; both their formation and stability are potentially governed by their kinetics. Additionally, self-assembled systems are often only metastable, i.e., they are long-lived non-equilibrium structures. Whereas molecular thermodynamics can be used as a quantitative tool to predict structural parameters for systems in equilibrium, there is no general facile approach for non-equilibrium systems. A great challenge is therefore to understand the underlying physics and use this to understand the design rules for non-equilibrium structures. However, this requires advanced instrumentation tools capable of a full four-dimensional characterization of materials, i.e., providing full spatiotemporal information on the nanoscale.

Experimental observation of the kinetic processes of self-assembly is very challenging due to the wide range of time scales involved. Typically, a nucleation event takes place on a short time scale of the order of microseconds to milliseconds, which contrasts with the slower time scale for reorganization processes that can occur on time scales as slow as hours to years. Ideally, it is desirable to watch the structural evolution of the process to keep track of possible metastable intermediates, in analogy with what is commonly observed under chemical reactions. For this, time-resolved small-angle neutron and X-ray scattering (TR-SANS and TR-SAXS) techniques are ideal because the structure is encoded in the angular dependence of

the scattered intensity. In fact, with the advent of ever more powerful X-ray sources such as the third-generation synchrotrons, state-of-the-art SAXS gives access to spatiotemporal resolution of the order of only micro- to milliseconds up to hours, directly on the relevant length scales of about 1–100 nm. With more powerful neutron sources such as the high-flux reactor at Institut Laue Langevin (ILL), it is now also possible to access time scales down to about 100 ms with SANS. With even more powerful spallation sources such as the SNS, Oak Ridge in the USA and the future European Spallation Source (ESS) at Lund, Sweden, SANS is expected to catch up with the synchrotron and more easily give time resolutions approaching milliseconds and microseconds. Here in particular, neutron scattering will be useful as selective deuteration of molecules or parts of molecules, opening up many possibilities for contrast variation to label and highlight specific parts of the structure or to watch specific kinetic processes. In this review, we will focus on how these methods can be applied to investigate kinetics in micellar systems, in particular block copolymer systems.

Amphiphilic molecules such as surfactants and block copolymers containing hydrophobic (water-insoluble) and hydrophilic (water-soluble) parts, serve as simple synthetic model systems for understanding self-assembly. Micellization is a common self-assembly process whereby amphiphilic molecules spontaneously aggregate into various nanostructures that are usually of spherical, ellipsoidal, cylindrical, or vesicular shapes [1, 2]. These processes usually occur in selective solvents, i.e., solvents that are good for one part but poor for the other. Here, self-assembly is primarily driven by the incompatibility of the insoluble (hydrophobic or more generally “solvophobic”) part with water or other solvents, and is mainly counteracted by repulsions or unfavorable configurations experienced in the swollen corona of the resulting micelles.

Block copolymer micelles are macromolecular analogues to ordinary surfactant micelles. These systems generally consist of two or more distinct types of polymeric blocks covalently linked together. Because of the wealth of possible combinations of chemistry and compositions of such polymers, the possibilities for tailoring self-assembly and resulting structures are virtually endless, leading to a wide range of applications. Common for micellization is that the aggregates are formed above a certain threshold concentration, called the critical micelle concentration (cmc). As block copolymers often contain large insoluble blocks, the cmc in these systems can be almost immeasurably small and micelles are spontaneously formed at almost any concentration in solvents where the interfacial tension is high, such as in water. An idealized example of how micelles are formed from block copolymers is shown in Fig. 1. Here, a sudden micellization is induced from a homogeneous solution of dissolved block copolymer chains by suddenly altering the conditions (change in solubility by addition of co-solvents, salts, etc.). This micelle formation process is a typical non-equilibrium kinetic process. Once micelles are formed, the classical view for micellar solutions is that the system attains its equilibrium by continuously exchanging the constituting chains. An example of such scenario is also shown in Fig. 1, where a single chain (unimer) is released and reabsorbed into the micelle. In much the same way as in chemical reactions, such a unimer exchange process is a

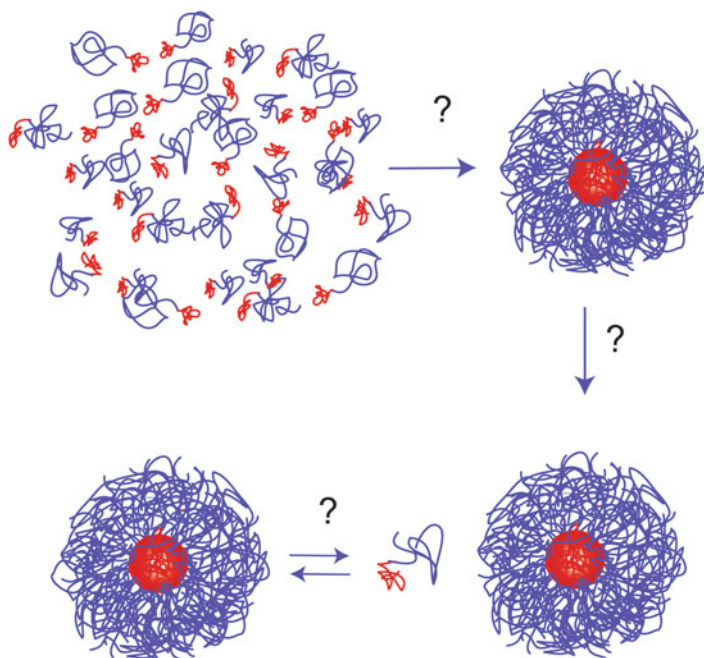


Fig. 1 Illustration of two kinetic processes in micellar systems. (a) Micelle formation, i.e., the kinetics associated with aggregation of single amphiphiles (unimers) into micelles and (b) the equilibrium kinetics characterizing a dynamic equilibrium of unimers exchanging between micelles

prerequisite for a dynamic equilibrium. However, for block copolymers characterized by a vanishingly small cmc, the question is: how can equilibrium be expected to be achieved?

As has been increasingly recognized over the last decade, block copolymer micelles are often characterized by exceedingly slow kinetics and, consequently, equilibrium is not necessarily achieved on a global scale. The system is then non-ergodic and the structure is thus generally path dependent, i.e., dependent on the sample preparation method [3–6]. This has significant implications in both nanotechnological and biomedical applications as the system is no longer just determined by thermodynamics (i.e., the global minimum in the parameter landscape), but rather by the kinetic pathways and the stability of the metastable state, in particular towards intramicellar reorganization processes. Recently, this property has been utilized to gain control over the nanostructures via kinetic control [5, 7–9] whereby the morphology and chemical composition can be manipulated via their non-equilibrium growth mechanism, etc. Kinetic control also represents a convenient methodology to use these “trapped” metastable states in order to create various non-equilibrium nanostructures that would otherwise not form under equilibrium conditions. While in equilibrium, most systems form either spherical, cylindrical, or vesicular structures; however, a notable computer simulation study [10] has shown that exotic (metastable) structures such as toroidal as well as intertwined and perforated shapes

can be formed in a simple A-B amphiphile system. Such structures are likely to be more long-lived in block copolymer systems due to their slower dynamics and kinetics. This opens up exciting possibilities for achieving well-defined intricate structures in simple two-component systems. However, in order to take full advantage of these possibilities, the kinetic pathways and the kinetics of block copolymer systems must be understood. On a more fundamental note, kinetic pathways in self-assembled systems and kinetic control are integral parts of the understanding and intelligent use of these materials in a nanotechnological setting. Their importance can be understood in much the same way as the importance of kinetics in chemical reactions and how an understanding of kinetics has helped design products and extended the use of both inorganic and organic chemistry in the twentieth century. Apart from kinetic control and manipulation of structures, kinetics is also essential in controlling the size and stability of nanoparticles formed by block copolymers for their use as, e.g., drug delivery systems [11] or in industrial applications as components of emulsions or non-foaming surfactant systems [12]. A great deal of effort must therefore be made towards studies assessing kinetic processes and in development of suitable experimental techniques.

Time resolved SAXS/SANS allow a structural observation of kinetic processes on the nanoscale (1–100 nm) on a time scale ranging from milliseconds to hours. This allows micellar kinetics to be followed in real time, giving direct structural information of the process and its evolution. Synchrotron SAXS can reach smaller time scales and exhibits better resolution compared to neutron-based methods. However, SANS offers the possibility for contrast variation via simple H/D exchange chemistry, which opens up a world of possibilities for the investigation of kinetics in soft matter systems, in particular transport and exchange processes that otherwise would be invisible in scattering experiments. As most of these techniques have become available over recent years with advancements in both instrumentation and sample environments, there is a need for an overview of the development and the possibilities that are now available in the field of soft matter in general and micellar systems in particular.

To this end, in this review we focus on the study of kinetic processes in micellar systems using time-resolved SAXS and SANS. Particular attention will be given to block copolymer systems and novel methodologies to study the kinetics using TR-SAXS or TR-SANS. Secondly, labeling experiments to study equilibrium kinetics using SANS will be thoroughly presented. While several related reviews have been presented [13–19], these contributions have been mostly devoted to low molecular weight surfactant systems and/or only focused on the general methodology of either SANS or SAXS. Here, we will give a thorough overview of results on block copolymer systems and show how both SAXS and SANS can be used as complementary methods to study kinetic processes in these systems. We will discuss both the strength and weaknesses of these methods and compare the results with investigations using other methods. Small-angle scattering methods are low-resolution methods that give ensemble averages over a large number of (most often orientational averaged) particles. The technique therefore requires a significant effort in data modeling and the development of methodology to analyze the data and thereby optimize the information content. Significant attention is therefore devoted to data modeling, in

particular with respect to time-resolved data and mechanistic models for kinetics. The fundamentals of scattering techniques and their application to micellar systems will be reviewed together with fundamentals of thermodynamics and kinetic models for block copolymer self-assembly. In the literature there is often an unclear terminology regarding the use of “kinetics of micelles”. The terms “micelle dynamics” or “micelle kinetics” are often used for equilibrium kinetics (exchange kinetics), relaxation kinetics (micelle–micelle relaxation kinetics) and micellization kinetics (unimer–micelle transition). Here, we will attempt to clarify this subject and give a broader overview of the different processes encountered in micellar solutions. A particular focus will be on equilibrium kinetics and non-equilibrium micellization kinetics, although other processes will be covered as well.

2 Theoretical Background

In this section, we give a brief review of important selected theories for surfactant and block copolymer micelles. First, the classical thermodynamic theories covering both mean-field and scaling approaches are briefly reviewed before discussing kinetics. Classical theories for equilibrium and near-equilibrium surfactant and block copolymer micelle kinetics will be briefly reviewed before covering non-equilibrium kinetics in the final part.

2.1 *Structure and Thermodynamics*

The molecular organization and morphologies of micellar structures depend intimately on a delicate balance between hydrophobic and hydrophilic interactions as well as, if charges are present, electrostatic interactions. In addition, translational entropy may play an important role. Thermodynamics permits the determination of the structural micellar parameters, cmc (the concentration above which a significant aggregation occurs), micellar size distributions, etc. via molecular parameters. The earliest, most extensive descriptions of micellization were presented by Hill [20], who developed a molecular thermodynamic theory in which the individual micelles were considered as “small” phase-separated entities in equilibrium with other micelles, unimers, and solvent. This microscopic phase-separation picture was further developed by Hall and Pethica [21] and provides the most fundamental basis for many later developments. Tanford later made seminal contributions to an understanding of the effect of hydrophobicity and its driving force for micellization in aqueous solutions [22–24]. He showed that the hydrophobicity of hydrocarbons and organic molecules is mainly related to the entropy of water associated with hydrogen bonds.

In order to calculate the free energy of micellization accurately, one needs to take into account the enthalpic terms describing the interactions between the block copolymer and solvent, the free energy of the micelle (F_{micelle}), the mixing free energy (F_{mix}), as well as the translational entropy associated with micelles and free chains (S_{m}).

2.1.1 Mean-Field Theories

Mean-field theories are common in statistical physics and have been used to describe a wide range of phenomena ranging from magnetism to micelles. The common basis is the assumption that the local potential felt by all the neighboring particles is replaced by an effective field. The field is constant in time, isotropical and its strength depends on the number, coordination, and nature of its neighbors. This means that a multibody problem is reduced into effective interactions. In polymer physics, a familiar version is the Flory–Huggins solution theory whereby polymer segments are distributed together with the solvent molecules on a lattice. The thermodynamic properties can thereby be derived by calculating the distribution and resulting enthalpic interactions on such a lattice [25]. These ideas have been used by several authors to calculate the structural properties in micellar solutions [26–28].

A very complete and detailed model was presented by Leibler, Wheeler and Orland in the early 1980s [26]. The model uses a Flory–Huggins framework to calculate the mixing free energy and the free energy of the reference disordered state. The theory was originally developed for symmetric A-B type block copolymers (where A is the soluble block and B the insoluble block) in an A-homopolymer “solvent” and is thus restricted to a situation with no excluded volume effects in the corona ($\chi = 0.5$) (true mean field). Although the theory was originally formulated for symmetric block copolymers, Balsara and coworkers extended the theory for asymmetric B-A-B type systems and also considered “loops” in the corona [29]. Lund et al. later extended the model further to allow for a partial mixing between the B-type chain and a solvent for micelles in solutions [30]. As the model also applies relatively well for some block copolymer/solvent systems and provides a very useful starting point for discussing micellization theoretically, we will describe the theory in some detail.

Within this classical theory by Leibler and coworkers, the total free energy can be written as a sum of three contributions: the free energy of a micelle (F_{micelle}), the mixing term of free block copolymers and solvent (F_{mix}), and finally the entropic term (TS_m) describing the gas of micelles and block copolymers. In units per lattice site, this can be written as:

$$F_{\text{total}} = \frac{\phi_0 \zeta}{P \cdot N} \cdot F_{\text{micelle}} + F_{\text{mix}} - TS_m \quad (1)$$

where ζ is the fraction of block copolymers in the micellar state and ϕ_0 is the total volume fraction of block copolymers. P denotes the aggregation number (number of chains per micelle).

The individual terms can be written as:

$$F_{\text{mix}} = (1 - \xi \phi_0 \zeta) \left(\frac{\phi_1 \ln(\phi_1)}{N} + (1 - \phi_1) \frac{\ln(1 - \phi_1)}{N_s} + \chi \frac{\phi_1}{1 + f} \cdot (1 - \phi_1 / (1 + f)) \right) \quad (2)$$

where N_s is the number of lattice points occupied by the solvent molecules and ϕ_1 the unimer volume fraction. Note that because ϕ_0 is typically 1% (dilute solution), this term is negligible in most practical situations. $\xi = (f + \eta)/[\eta(f + 1)]$; $N = N_A + N_B$ is the total number of polymer segments; $f = N_A/N_B$ the ratio of the repeat unit of the soluble, N_A , and insoluble block, N_B ; η is the volume fraction of the A-polymer block in the corona; $\eta = PV_A/V_{\text{corona}}$ where V_A is the molecular volume of a single A-block; $V_{\text{corona}} = 4\pi/3(R_m^3 - R_c^3)$ is the volume of the corona; and R_c and R_m are the radii of core and micelle, respectively.

The translational entropy associated with the micelles and the unaggregated block copolymer chains can be written using the Flory–Huggins theory as:

$$S_m/k_B = -\left(\frac{\phi_0 \zeta}{P \cdot N} \ln(\xi \phi_0 \zeta) + \frac{1 - \xi \phi_0 \zeta}{\xi \cdot P \cdot N} \ln(1 - \xi \phi_0 \zeta)\right) \quad (3)$$

The micellar free energy, F_{micelle} , can be approximated to consist of mainly three terms:

$$F_{\text{micelle}} = F_{\text{core}} + F_{\text{shell}} + F_{\text{int}} \quad (4)$$

Within the classical Leibler, Orland, and Wheeler mean-field theory, the free energy is mainly dominated by the balance between stretching and swelling of the polymer chains and the interfacial energy. Here, the interactions between the coronal chains are assumed to be zero while the interactions between the two blocks are implicitly assumed to be equal to those between the solvent and insoluble B-block. Being a mean-field theory, no fluctuations are considered and the density of micelles is considered to be constant. Possible distribution in terms of the aggregation number is thereby neglected.

The free energy term of a micellar core consisting entirely of B-polymer segments can be written as:

$$F_{\text{core}} = \frac{3}{2} \cdot P \cdot \left(\frac{R_c^2}{N_B \cdot a^2} + \frac{N_B \cdot a^2}{R_c^2} - 2 \right) \quad (5)$$

where a denotes the lattice size. However, in order to take into account swelling of the micellar core (i.e., when solvent molecules penetrate the core), one can modify the theory by introducing a Flory–Huggins expression describing the enthalpic and entropic interactions between the solvent molecules and the polymer segments within the core. This can be done by adding the term $F_{\text{core}}^{\text{swollen}}$ to Eq. 5 [30]:

$$F_{\text{core}}^{\text{swollen}} = F_{\text{core}} + \frac{4\pi R_c^3}{3a^3} \left(\Phi_0 \cdot \frac{\ln(\phi_0)}{N_0} + \Phi_0 \cdot (1 - \Phi_0) \cdot \chi \right) \quad (6)$$

where N_0 is the number of lattice sites occupied by a solvent molecule and Φ_0 is the fraction of solvent molecules in the core (homogeneously distributed).

The contribution from the shell consisting of A-block polymers with concentration η , homogeneously distributed in the radial direction, is written in the form:

$$F_{\text{shell}} = \frac{3}{2} \cdot P \cdot \left(\frac{R_{\text{corona}}^2}{N_B \cdot a^2} + \frac{N_B \cdot a^2}{R_{\text{corona}}^2} - 2 \right) + \frac{4\pi(R_m^3 - R_c^3)}{3a^3} \cdot \frac{(1 - \eta) \ln(1 - \eta)}{N_0} \quad (7)$$

The interfacial energy for a swollen core (assuming equal composition at surface and volume) may be written as:

$$F_{\text{int}} = \frac{4\pi R_c^2}{a^2} \gamma (1 - \Phi_0) \quad (8)$$

where $\gamma = \frac{k_B T}{a^2} \sqrt{\frac{z}{6}}$ is the interfacial tension and χ is the Flory–Huggins solubility parameter between A and B; in micellar solutions, between B and the solvent.

By minimizing the expressions above (Eq. 1) with respect to the independent parameters, the micellar parameters, including the cmc, for a given system can in principle be obtained.

In the case where interfacial energy (i.e. interfacial tension, γ) is large, then large micelles with only a very small fraction of unaggregated block copolymers are expected. Thus, the cmc (equal to ϕ_1 in equilibrium) is small and aggregation number $P \gg 1$, which in a dilute solution ($\phi_0 \approx 1\%$) leads to a negligible mixing free energy (i.e., F_{mix} and $S_m \approx 0$) and the total free energy of micellization is essentially given by the internal free energy of the micelle, F_{micelle} . This approximation is sometimes called the pseudo-phase approximation because physically this picture corresponds to a view in which the micelles constitute a thermodynamic “phase”. However, since micelles are a sort of mesophase structure rather than a distinct state of matter, micellization is not called a phase transition. An extensive molecular thermodynamic mean-field theory has also been developed by Nagarayan (see, e.g., [31]) to calculate the micellar free energy in great detail. Quantitative predictions were made that gave reasonable agreement with experimental results in the case of polystyrene–polybutadiene (PS-PB) and polystyrene–polyisoprene (PS-PI) diblock copolymer systems. Mean-field approaches can be expected to work only for relatively homogeneous systems with weak interactions. A more recent example concerns PS-PB diblock copolymers in *n*-alkane solvents, which at room temperature are close to θ conditions [30]. It was shown that the structural properties measured by SANS, could be well described by the Leibler mean-field approach, provided that the swelling and penetration of solvent molecules into the micellar cores is included. In the case of polymeric systems that exhibit strong excluded volume interactions or repulsions, a mean-field approach is not appropriate.

2.1.2 Scaling Theories

For systems exhibiting strong excluded volume interactions, a mean-field approach is no longer realistic and spatial correlations must be taken into account. Although this is a notorious deep problem in theoretical statistical physics in general and polymers in particular, a relatively simple way of calculating free energies for micellar systems is represented by so-called “scaling theories”, which have an origin in Kadanoff’s approach and renormalization group theories developed to treat interactions in magnetic systems and critical phenomena [32, 33].

Scaling theory is a quite simple approach, which in the realm of polymer science was pioneered mainly by de Gennes [34]. Scaling theories apply a “coarse-grained” approach whereby the molecular details of the system is only indirectly considered using simplified geometrical descriptions. Complicated structural and thermodynamic features of polymeric systems are estimated using simple geometrical and physical arguments. Thereby, problems associated with mathematical complexities imposed by long-range excluded volume effects are partially circumvented. The central idea utilizes the fractal properties of polymeric chains and the scale invariance of such systems.¹ Introducing a characteristic length scale, ξ (the blob size), defined as regions of non-overlapping polymer segments, the polymer chains can be pictured as a “necklace” of connected “blobs”. Inside the blobs, the potential of neighboring chains are not felt and the chains effectively behave as single isolated chains. The blob size scales as: [34]:

$$\xi \sim g^\nu \quad (9)$$

where ν is the Flory exponent, taking the value 0.5 for a Gaussian chain and 0.588² for swollen chains [35]. g is the effective number of segments inside a blob. Furthermore, realizing that the blob size is defined by the fluctuations of the chain, the standard equipartition theorem in statistical physics suggests that its energy should be of the order of $k_B T$, where k_B is the Boltzmann constant. de Gennes further hypothesized that the free energy contribution of such a system can be calculated simply by counting the numbers of blobs and multiplying by $k_B T$. This can be called the de Gennes’ $k_B T$ per blob recipe [34].

For block copolymer micelles there are many applications of such theories [36–42] generally using the pseudo-phase approximation.

We will first concentrate on the thermodynamics of spherical micelles that are generally formed for block copolymers having asymmetric compositions. Here, it is

¹ Renormalization group theory (see, e.g., [35]) lies at the heart of this theory, justifying the use of scaling laws in the asymptotic limit, i.e., for infinitely long polymer chains and for dilute solutions. For semidilute solutions, however, this criterion is not so crucial because the polymer chains are overlapping and many properties, e.g., osmotic pressure, are independent of the chain length.

² The fractal dimension d_f is given by $1/\nu \approx 1.7$ in this case, i.e., the chain is more extended than a Gaussian chain with $d_f = 2$. We also note here that the blob concept obviously only applies to systems with excluded volume effects, i.e., where $d_f < 2$.

possible to make several simplifications and consider limiting cases or classes of micelles. We will assume that the pseudo-phase approximation is fulfilled and that mixing entropy terms are negligible and can be ignored.

In all models (as for mean-field theories), the reduction of interfacial area upon micellization is considered to be the driving force for micellization. Thus, the interfacial tension is an important parameter. The interfacial free energy per chain of a spherical micelle (Eq. 8) can be written as:

$$F_{\text{int}} = \frac{4\pi R_c^2 \gamma}{P} \sim P^{-1/3} \gamma \quad (10)$$

where R_c is the micellar core radius and P is the aggregation number of the micelle that would scale with the volume, and thus $P \sim R_c^3$.

This term will favor micellar growth and, in the absence of other effects, lead to a macroscopic phase separation. However, in a real micellar system, growth will be primarily counteracted by a repulsion between the head groups or a finite extension of the surfactant tails. In polymeric systems, entropic contributions become dominant, e.g., stretching of chains. The major difference between the models is the way in which the counteracting free energy is calculated, in particular the free energy of the corona.

Within scaling theories, it is possible to distinguish three limiting cases for spherical polymeric micelles: crew-cut, intermediate and star-like micelles. For crew-cut micelles, characterized by having the number of repeat units of the B-block, N_B , much larger than of the soluble A-block, N_A (i.e. $N_A \ll N_B$), the free energy of the corona is assumed to be negligible compared with the stretching contribution in the core. As seen in Eq. 5, this contribution can be estimated from the rubber elasticity. Furthermore, ignoring prefactors and the finite extension of the chain, this can be simply written as:

$$F_{\text{core}} \sim \frac{R_c^2}{N_B l_B^2} \sim P^{2/3} \quad (11)$$

with l_B , the corresponding characteristic monomer length of the insoluble polymer B-block.

For the other two cases, it is assumed that the balancing free energy is determined by the free energy of the corona, which is calculated by assuming a flat core–corona interface for intermediate micelles (i.e., suitable when the B-block is relatively large) and a highly curved interface when $N_A \gg N_B$ for star-like micelles. Using the analogy to grafted polymer chains, the free energy of the corona can be calculated using the physics of polymer brushes [36–38, 41, 43].

This gives the following free energies of the corona:

$$F_{\text{corona}}/k_b T \sim \begin{cases} P^{1/2} \ln(N_A^{3/5} P^{-2/15} N_B^{-1/3}) & \text{Star-like} \\ P^{5/18} N_B^{-5/9} N_A & \text{Intermediate} \end{cases} \quad (12)$$

From this formalism, the dependence of the various micellar parameters on, for example, molecular weight, composition, interfacial tension, etc. can be estimated. The results seem to compare rather well with experimental data, see, e.g., [44, 45]. For example, for intermediate and star-like micelles, the aggregation number would scale as:

$$P_{\text{scaling}} \sim \begin{cases} \gamma^{6/5} N_B^{4/5} l_B^{12/5} & \text{Star-like} \\ \gamma^{18/11} N_B^2 N_A^{-18/11} l_A^{-30/11} l_B^{30/11} & \text{Intermediate} \end{cases} \quad (13)$$

2.1.3 Thermodynamics of Morphological Transitions

Under certain conditions, cylindrical micelles or even vesicles can be formed instead of spherical symmetric micelles. Cylindrical micelles are usually formed as a consequence of a delicate balance between the different terms, most notably governed by the chain stretching in the micellar core. Compared to spherical micelles, the core radius of a cylinder for an equivalent area or volume can easily be evaluated to be 2/3 smaller. Hence, in a cylindrical micelle, the amount of chain stretching is expected to be less pronounced than in a spherical one. On the other hand, chain interactions in the corona of a cylindrical micelle is expected to be more severe due to the smaller area available for each chain. All terms must thus be included and a more detailed thermodynamic evaluation should be performed. For vesicles, the bending modulus is additionally expected to be important [46].

A very detailed and accurate theoretical description of the problem concerning the cylinder–sphere transition was made by Zhulina et al. [47].

For this approach, the same total free energy as in Eq. 4 was used. As before, the interface contribution can be calculated in a straightforward way and equals the area of the micellar core times the interfacial tension, γ :

$$F_{\text{int}} = \frac{A_j \cdot \gamma}{P \cdot k_B T} \begin{cases} A_j = 4\pi R_c^2 & \text{Spheres} \\ A_j = 2\pi R_c L & \text{Cylinders} \end{cases} \quad (14)$$

The aggregation number P can be related to other micellar parameters assuming a compact (solvent-free) core: $P = \pi R_c^2 L / (V_B / N_{\text{AvO}})$ and $P = 4\pi R_c^3 / (3 \cdot V_B / N_{\text{AvO}})$ for cylinders and spheres, respectively. Here V_B is the molar volume of the insoluble B-block and N_{AvO} is Avogadro's number.

For the corona contribution, some care has to be taken. In order to calculate the free energy of this part, the number of blobs has to be calculated for each morphology, taking into account that the radial dependence of the density changes with the curvature. For a completely planar surface, de Gennes and Alexander [36, 37] showed that the blob size will be constant and scale by $\xi \approx s$, where s is the area available per chain. For a curved micellar core, the surface per corona chain will naturally increase

with the radial distance r away from the core $r > R_c$ and thus the area per chain will also be a function of r , i.e., $s = s(r)$.

Following the approach by Zhulina et al. [47], the energy density is thus $\Phi(r) = C_F \cdot k_B T / s(r)^{3/2}$ and the corona free energy per $k_B T$ can be calculated from $F_{\text{corona}} = \int_{R_c}^{R_m} \Phi(r) / k_B T s(r) dr = C_F \cdot \int_{R_c}^{R_m} s(r)^{-1/2} dr$. C_F is a numerical scaling factor of order unity.

The area per chain is found to have the following approximate form:

$$s(r) \begin{cases} s(r) = s_0 \left(\frac{r}{R_c} \right)^2 & \text{Spheres} \\ s(r) = s_0 \frac{r}{R_c} & \text{Cylinders} \end{cases} \quad (15)$$

These give the following results:

$$F_{\text{corona}} = C_F \int_{R_c}^{R_c+D} s(r)^{-1/2} dx; \begin{cases} s(r) = s_0 \left(\frac{r}{R_c} \right)^2 & \text{Spheres} \\ s(r) = s_0 \frac{r}{R_c} & \text{Cylinders} \end{cases} \quad (16)$$

where $s(r)$ is a function that describes the radial dependence of the grafting density, s (area available per chain), which on the core surface ($r = 0$) is equal to $s_0 = 4\pi R_c^2 / P$ for spherical micelles and $s_0 = 2\pi R_c \times L/P$ for cylindrical micelles (where L is the cylinder length). After some calculus, Zhulina et al. showed that the analytical expressions of F_{corona} can be written as:

$$F_{\text{corona}} = \begin{cases} \frac{v C_F R_c}{\sqrt{s}} \ln \left(1 + \frac{l_A C_H N_A (s l_A^{-2})^{(v-1)/2v}}{v R_c} \right) & \text{Spheres} \\ \frac{2 C_F R_c}{\sqrt{s}} \left[\left(1 + \frac{(1+v) \cdot l_A C_H N_A (s l_A^{-2})^{(v-1)/2v}}{2 v R_c} \right)^{v/(v+1)} - 1 \right] & \text{Cylinders} \end{cases} \quad (17)$$

Here C_F and C_H are numerical prefactors; l_B and l_A the effective segment lengths of insoluble and soluble blocks; N_B and N_A denote the respective number of repeat units; and v is the excluded volume parameter controlling the conformation of the chain. In a good solvent, v takes the well-known value 0.588.

F_{core} corresponds to the elastic energy associated with stretching the chains beyond their unperturbed end-to-end distance to the radius of the core. If this contribution is to be determined accurately, the fraction of chains needed to stretch must be evaluated. This was carefully worked out for various geometries by Semenov [39], who also calculated the fraction of chain-ends needed to effectively fill the core for each geometry. The results are:

$$F_{\text{core}} = k_j \cdot \frac{R_c^2}{R_{\text{ce}}^2}; \begin{cases} k_j = \frac{\pi^2}{16} & \text{Spheres} \\ k_j = \frac{3\pi^2}{80} & \text{Cylinders} \end{cases} \quad (18)$$

where R_c is the core radius and $R_{ee} \approx N_B^{1/2} l_B$ is the unperturbed (bulk) end-to-end distance of the core-forming polymer. The units are, as before, in $k_B T$. The total free energy can be found by summing Eqs. 14–18 according to Eq. 4 and the stability of sphere and cylinder can be estimated by the respective free energy. Minimalization with respect to the independent variables (P , R_m , etc.) will give the equilibrium values.

In a recent work on symmetric poly(ethylene-*alt*-propylene)–poly(ethylene oxide) (PEP-PEO) block copolymers in various *N,N*-dimethylformamide (DMF) and water mixtures, this model was used to analyze the structural data and the cylinder-to-sphere transition by minimizing the total free energy using Eq. 4 combined with Eqs. 14–18 above [48]. The values obtained by fitting the model after numerical minimization were in good accordance with the experimental data, and the resulting free energy profiles could describe the transition quite well. For transitions from cylinders to vesicles, a corresponding detailed thermodynamic model is yet to be presented and compared with experimental values. However, a useful compilation of theoretical considerations concerning the free energy contributions has been published [46].

2.2 Chain Exchange Kinetics in Equilibrium

Micelles can attain and maintain their global equilibrium by constantly redistributing their chains. This can predominantly occur via two main mechanisms³: unimer exchange and fusion/fission, as schematically illustrated in Fig. 2. These two mechanisms will be discussed in the context of different thermodynamic and kinetic models.

Exchange and relaxation kinetics of surfactant micelles are classical topics from the 1970s and 1980s [16, 50–54]. Because exchange kinetics are usually very fast for surfactant micelles, the process was more indirectly measured using a perturbation scheme like, e.g., temperature or pressure jumps. The relaxation to the new equilibrium is subsequently followed by light-scattering and other suitable methods. Such processes can be referred to as near-equilibrium relaxation kinetics and involve a transition from one micellar equilibrium to another mediated by a small change in the thermodynamic conditions. An illustration of such a process is depicted in Fig. 3.

As a consequence of available experimental data from relaxation experiments, most of the early theoretical work has been focused on this, in particular in the equilibrium regime where perturbations are small, which facilitates the treatment. Most notable is the work by Aniansson and Wall [54–56], valid for neutral surfactants, and that of Kahlweit [57], who also takes into account fusion of micelles

³ Other mechanism such as concerted insertion, i.e., the scenario that two micelles exchange an unimer upon direct overlap [49], have also been proposed although these are expected to be less probable, at least for low concentrations.

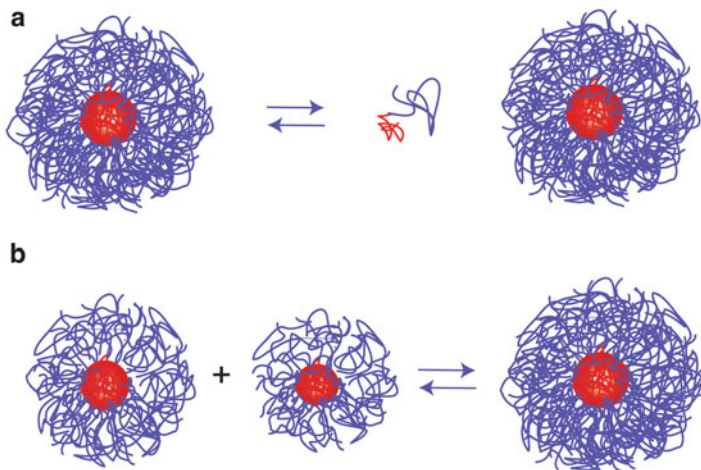


Fig. 2 Illustration of two important mechanisms involved in various kinetic processes in micellar systems. **(a)** Unimer exchange, single surfactant/block copolymer chains are interchanged one by one via the solvent medium. **(b)** Fusion/fission, where two micelles fuse or are fragmented to smaller micelles, respectively

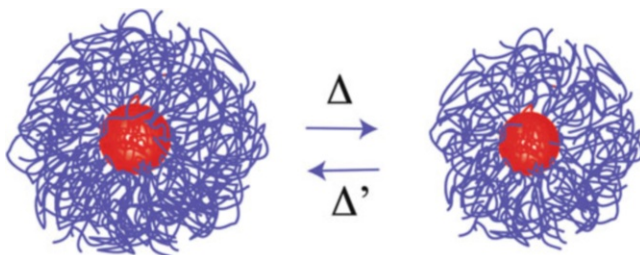


Fig. 3 Illustration of a relaxation process from one micellar equilibrium to another upon a small perturbation, Δ (the reverse perturbation, Δ') can either be due to a change in an intensive variable (temperature, pressure, electric field, etc.) or extensive variables such as pH, added salt, etc.

and the effect of charge screening. Here, we will focus on neutral systems where electrostatic effects are not relevant.

We will briefly review the available classical theories relevant to both surfactant and block copolymer micelle kinetics.

2.2.1 Aniansson and Wall Mechanism: Unimer Exchange and Linear Relaxation Experiments

The Aniansson and Wall theory (A-W theory) [55, 56] was developed for the near equilibrium relaxation kinetics of neutral low molecular weight micelles. It was

assumed that all changes in the association/dissociation involve individual unitary steps where only an exchange of one surfactant molecule is allowed at a time (Fig. 2a). This can be written as:



where U is the unimer, M_P is a micelle with aggregation number P , and k_p^+ and k_p^- are the corresponding rate constants for the insertion and expulsion. The corresponding rate equation is:

$$\frac{d[U]}{dt} = -k_p^+[M_P][U] + k_p^-[M_{P+1}] \quad (20)$$

Using a system of rate equations constructed from the above mechanism, Aniansson and Wall showed that in a relaxation experiment close to equilibrium, in the linear regime, the relaxation is determined by two relaxation time constants. The first time constant characterizes the fast relaxation associated with a readjustment of the unimer concentration, without a change in the number density of micelles. As shown by Aniansson and Wall, this contribution depends on the expulsion rate constant, the width of the distribution of the micellar population, σ , and the fraction of unimers, X .

$$\frac{1}{\tau_1} = \frac{k_-}{\sigma^2} + \frac{k_-}{\langle P \rangle} \cdot X(1 + C_{\text{dev}}) \quad (21)$$

where k_- is the expulsion rate constant for micelles at their equilibrium size (independent of P) and C_{dev} is a number that describes the relative deviation from equilibrium. For relaxation experiments performed in the linear regime (i.e. for very small perturbations), $C_{\text{dev}} \approx 0$.

The second relaxation time τ_2 , is related to a change in the number of micelles and is much slower because the surfactants have to be rearranged between the micelles in a cooperative fashion (formation/dissociation of micelles limited by unimer exchange). Again under the assumption of unimer exchange, this can be written as:

$$\frac{1}{\tau_2} = \frac{\langle P \rangle^2}{\phi_0} \frac{1}{R} \cdot \left(1 + \frac{\sigma^2}{\langle P \rangle} \right)^{-1} \quad (22)$$

where

$$\frac{1}{R} = \frac{1}{\sum_p k_p^- \cdot \phi_p} \quad (23)$$

The time scale of the first process is seen to decrease linearly with micellar density. The reason is that the larger the number of micelles, the more unimers are

consumed or expelled, which leads to a faster net growth or reduction of the micelles towards a new equilibrium. The second process is characterized by τ_2 ; however, it is expected to have a more complex concentration dependence. This comes from the fact that since the micelle equilibration only proceeds via unimer exchange, any intermediate metastable aggregates will consume unimers and hinder the formation of the final stable micellar state. The time scale thereby depends on the concentration and kinetics of all improper micelles ($P < P_{eq}$ or $P > P_{eq}$) and thus more than the width of the mean distribution. As seen in Eqs. 22–23, A-W theory predicts that the τ_2 increases with R , which characterizes the population and in some sense the lifetime of the improper (out of equilibrium) micelles as ϕ_0 is the total concentration. The quantity R thus depends on the thermodynamic stability and, hence, on the lifetime of improper, metastable micelles. This concentration dependence is thus difficult to predict because τ_2 depends on the concentration of the different types of micelles of size P , ϕ_P . This highlights the fact that micelle formation is an activated process because metastable micelles must dissolve by unimer expulsion before the equilibrium micelles can be formed. This issue will be discussed in more detail later when we return to non-equilibrium micellization kinetics in section 2.3.

Note that the A-W theory was derived under the assumption that the micellar size distribution is Gaussian, independent of concentration, and can be taken to be essentially the equilibrium distribution. Thus, in this linear relaxation process, the micellar population is imagined to be “shifted” to a new mean aggregation value.

The existence of two relaxation constants and the corresponding concentration dependence predicted by Aniansson and Wall has been well corroborated in many experiments, especially for surfactant systems with large hydrophobic tails, where the two processes can be observed more clearly [54]. It has been shown that for classical ionic surfactants $1/\tau_1$ shows a consistent increase with concentration, whereas the second process, characterized by τ_2 , seems to first increase and then decrease again upon higher micelle concentration [51, 54]. This complex concentration dependence of τ_2 was later addressed in a work by Lessner and coworkers [52, 53] and attributed to previously ignored effects of charge screening, which can promote micellar fusion or fission [57]. This conclusion was based on temperature-jump experiments where the mechanism seemingly changed on going from low to high concentrations. Screening of the charges at high ionic strengths in ionic surfactants lowers the repulsion, facilitating fusion as an increasingly important exchange mechanism. Fusion/fission is in general expected to play more of a role in micellar systems with low repulsion, such as in nonionic micelles [58]. The relaxation time for the fusion/fission mechanism is expected to decrease with concentration, and a tentative description was given by Lessner et al. [53]. However, this does not seem to be strictly necessary to understand the experimental results because the A-W theory also predicts a complicated concentration dependence of τ_2 simply because metastable micelles restrict micellar growth by consuming and depleting unimers [54]. In any case, a complication for charged micelles, not considered in the original A-W theory, is the effect of co-solutes such as counter-ions accompanying the main surfactant chain. These ions will additionally affect the thermodynamics by lowering the cmc, which in turn leads

to slower τ_2 at higher concentrations (increasing ionic strengths). Some corrections along these lines, explicitly taking into account issues of charge screening, have been done by Kahlweit and coworkers [52, 53].

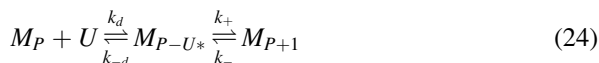
2.2.2 Rate Constants for Unimer Exchange in Equilibrium

Most of the experimental and theoretical work concerning kinetics of micellar systems in the 1970s and 1980s were concerned with the outcome of so-called linear relaxation experiments. There was also an attempt to relate the kinetics with the general diffusion in micellar systems [50]. NMR experiments as well as later experiments using fluorescence spectroscopy or neutron scattering are able to follow labeled entities and the signal is not related to changes in sizes and their distributions. For example, in temperature-jump experiments followed by light scattering, the changes in concentration and size of all micelles and unimers are monitored. A labeling experiment is thus “cleaner” and provides a more direct access to the rate constants. In addition, for neutron scattering, the structure can also be analyzed simultaneously with nanometer resolution. In the subsequent section, rate constants associated with micellar kinetics and their dependence on molecular parameters will be discussed.

2.2.3 Reaction-Limited Versus Diffusion-Limited Exchange Kinetics

The situation for low molecular weight surfactant micelles might be different to that for polymeric micelles. In the former case, the kinetics is close to being “diffusion-limited” [54], i.e., the diffusion of chains between the micellar droplets is comparable to the time scale of the expulsion/insertion process.

In general, exchange “reactions” should be analyzed with respect to both transport between micelles (diffusion) and expulsion/insertion. In complete analogy with chemical reaction kinetics known in physical chemistry (see, e.g., Atkins [59]) this can be formulated as:



Here, the diffusion rate constant to (k_d) and from (k_{-d}) the micelle is included. The intermediate micelle–unimer complex (the fictive activated complex) is denoted as M_{P-U*} .

Assuming that the intermediate configuration is rare (low concentration of fictive reaction intermediate), one can assume $d[M_{P-U*}]/dt \approx 0$. This yields:

$$\frac{d[U]}{dt} = \left(\frac{k_d k_{-d}}{k_{-d} + k_+} - k_d \right) [M_P][U] + \frac{k_{-d} k_-}{k_{-d} + k_+} [M_{P+1}] \quad (25)$$

In general, the diffusion of single polymers in a low molecular weight solvent such as water is relatively fast, $D \approx 10^{-11} \text{ m}^2/\text{s}$ and thus a typical distance of about 10 nm would be covered in a few microseconds. Hence, we can assume that $k_{-d} \gg k_+$, leading to the simple equation:

$$\frac{d[U]}{dt} \approx k_- [M_{P+1}] \quad (26)$$

Thus, this simple result suggests that the rate of unimer exchange is governed by the expulsion rate constant. We will see later that this approximation is indeed a good assumption when we compare with the proposed models for unimeric expulsion/insertion.

2.2.4 Exchange Kinetics in Surfactant Micelles

Given the central role of the expulsion rate constant for micellar stability, formation, and dissociation, it is essential to determine the physical governing factors and functional form. Aniansson and Wall based their calculations [54] on a general diffusion in an external potential. In this approach, the diffusion coefficient, $D(\mathbf{r})$ is dependent on the position, \mathbf{r} , due to the potential $V(\mathbf{r})$. In a sphero-symmetric system, we can imagine that the diffusion of a unimer only depends on the distance, r , from the origin and this problem can be summarized in a Einstein–Smoluchowski type equation:

$$J = -D(r) \left[\frac{\partial \phi(r)}{\partial r} + \frac{1}{k_B T} \frac{\partial V(r)}{\partial r} \phi(r) \right] \quad (27)$$

where $\phi(r)$ is the concentration at radius r and $V(r)$ is the corresponding potential. In order to solve Eq. 27 self-consistently, the potential, $V(r)$, must be specified. Aniansson and Wall considered a situation where the potential increases linearly with r until $V(\text{max}) = \varepsilon$ at $x = l_{\text{tail}}$ (i.e., when the surfactant tail is outside the micelle) where it drops to 0. This corresponds to the physical picture in which the surfactant is treated as a straight rod moving along its axis normal to the surface of the micelles. The motion is diffusive and affected by the interfacial (hydrophobic) energy, which increases linearly with the extent of diffusion out of the micelle. No interactions in the corona are considered. The equilibrium concentration of the segment would be $c(r) = c(0)\exp(-V(r)/k_B T)$. With these assumptions, Aniansson and Wall deduced for the expulsion rate constant:

$$k_- = P \frac{D_m}{l_r' l_0'} \exp(-\varepsilon/k_B T) \quad (28)$$

where l_r' and l_0' are two characteristic sizes related to the actual shape of the potential (both close to the unit length of the surfactant) and D_m is the free diffusion of the surfactant.

It is important to stress that the activation energy, ε , which is related to the surface energy of the exposed hydrocarbon part, is here expected to grow linearly with the length of surfactant:

$$\varepsilon \sim l_{\text{tail}} = N \cdot l_0 \quad (29)$$

where l_0 is the bond length. This is a consequence of the rather stiff nature of alkyl-chain-type surfactants and is equivalent to Tanford's classical results of the hydrophobic energy of alkyl chains, which have the form: $\varepsilon_H = \text{constant} + k_B T(N - 1)$ [22–24]. This has important consequences for the kinetics, which we will come back to later (sections 4.3–4.6).

Halperin and Alexander extended the theory of the Aniansson and Wall approach to calculate the detailed rate constants and the associated activation energies for polymeric materials, i.e., block copolymer micelles. We briefly review the central results in the following section.

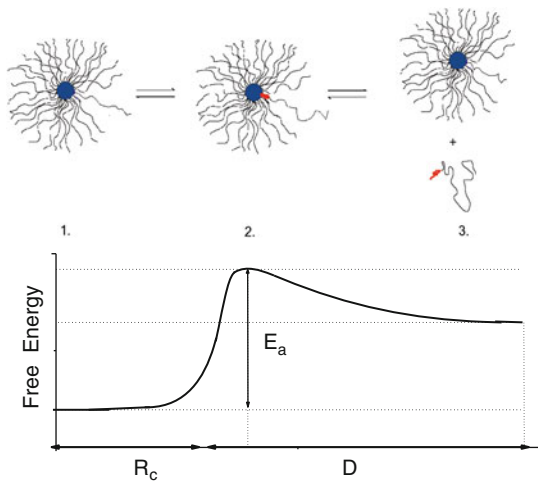
2.2.5 Exchange Kinetics in Block Copolymer Micelles: Halperin and Alexander Theory

The theory proposed by Halperin and Alexander (H-A theory) [60] is based on the structural scaling description of polymeric micelles outlined in Sect. 2.1.2. Using a combination of scaling theory and Kramers' rate theory for diffusion in an external potential [61], the expulsion rate for both “crew-cut” and “star-like” spherical micelles was derived. Moreover, Halperin and Alexander discussed different scenarios of chain exchange between micelles.

Hence, the most important process for the equilibrium kinetics is the unimer exchange mechanism which, as expected from the Aniansson–Wall scenario, is mainly governed by the expulsion rate constant. In the model of Halperin and Alexander this release of a single unimer from the micelle is pictured to go through two stages:

1. Ejection of the solvophobic part of the block copolymer to form a “bud” on the interface of the micellar core. Thereby, an extra area $\left(\approx l_B^2 N_B^{2/3}\right)$ is exposed to the solvent.
2. Diffusion of the whole block copolymer through the micellar corona.

Fig. 4 Illustration of the chain expulsion process of a single chain from a star-like micelle with core radius R_c and corona thickness D and a corresponding schematic free energy profile, $F(y)$, along the reaction coordinate. In the calculations given in the text the reference state is chosen according to $F(P+1) \equiv 0$ so that $F^* = E_a$ for the expulsion process



The corresponding free energy profile is shown in Fig. 4.

For one-dimensional stationary flow in a potential well, Kramers' rate theory gives the following expression for the outgoing flux, J :

$$J = -D \exp(-F(r)/k_B T) \frac{\partial}{\partial r} \phi(r) \exp(F(r)/k_B T) \quad (30)$$

where $F(y)$ is the free energy profile along the “reaction coordinate”, y . As a polymer is expected to follow a curvilinear rather than a straight path, y is not necessarily the spatial coordinate r as for rod-like surfactants. $\phi(y)$ is the local polymer concentration of the diffusing block copolymer characterized by a typical diffusion coefficient D . Halperin and Alexander demonstrated that the flux could be rewritten as:

$$J \sim \exp(-F^*/k_B T) v_{\text{diffusion}} \quad (31)$$

where $v_{\text{diffusion}}$ is the chain velocity over the barrier and $F^* = F(y^*)$ is the maximum free energy. This is principally determined by the interfacial energy penalty due to the expelled B-blocks, i.e., $F^* \sim r_{\text{bud}}^2 \gamma \sim N_B^{2/3} l_B^2 \gamma$, with r_{bud} being the radius of the collapsed B-block.

For micelles with a thin corona, $N_B \ll N_A$, $v_{\text{diffusion}}$ is roughly determined by the time, τ_B , necessary to diffuse the length of its insoluble block, i.e., $\tau_B \sim N_B^{2/3}/D$. Assuming classical diffusion of polymer segments in homogeneous surroundings, Stoke–Einstein's law gives $D \sim 1/N_B^{1/3} l_B$ and $\tau_B \sim N_B^{2/3} l_B^2 / (N_B^{-1} l_B^{-1}) = N_B l_B^3 = v_B$ where v_B is the molecular volume of the B-block.

The above-mentioned expression is valid whenever the core is large compared to the corona. In the opposite limit, as in star-like micelles, the diffusion through the corona has to be considered instead. Using the Langevin equation to describe the

stochastic passage of the chain through the corona, Halperin and Alexander obtained for the characteristic velocity of diffusion through the corona $v_{\text{diffusion}} \sim L^{-2} P^{1/2} \sim N_B^{2/25} N_A^{-6/5}$.

Thus, the velocity of the block copolymers over the activation barrier is in the two limiting cases given by:

$$v_{\text{diffusion}} \sim \begin{cases} \frac{N_B^{1/3} l_B}{\tau_B} \sim N_B^{-2/3}, & N_B \gg N_A \\ L^{-2} P^{1/2} \sim N_B^{2/25} N_A^{-6/5}, & N_A \gg N_B \end{cases} \quad (32)$$

The expulsion rate can be obtained using $k_- = \exp(-F^*) v_{\text{diffusion}} / R_c$ and $k_- = \exp(-F^*) v_{\text{diffusion}} / L$ for crew-cut and star-like micelles, respectively. In this way, the following expressions are obtained:

$$k_- \sim \begin{cases} \exp\left(-N_B^{2/3} \gamma l_B^2 / k_B T\right) N_B^{-4/3}, & N_B \gg N_A \\ \exp\left(-N_B^{2/3} \gamma l_B^2 / k_B T\right) N_B^{-2/25} N_A^{-9/5}, & N_A \gg N_B \end{cases} \quad (33)$$

Thus, in all cases the activation energy has the form:

$$E_a \sim N_B^{2/3} \gamma l_B^2 \quad (34)$$

2.2.6 Modified Halperin and Alexander Theory

According to the H-A theory, the chain exchange is dominated by chain expulsion and follows a first-order kinetic process characterized by a single exponential:

$$R(t) = \exp(-k_- t) \quad (35)$$

with a rate constant of the Boltzmann/Arrhenius form $k = 1/\tau_0 \exp(-E_a/k_B T)$, where τ_0 is a characteristic time. In this model, the activation energy, E_a , is given by the product of the interfacial area and the interfacial tension γ of the single (collapsed) B-block. In the original paper by Halperin and Alexander, this was written as $E_a = \gamma \cdot N_B^{2/3} \cdot l_B^2$, where N_B is the degree of polymerization of the insoluble block B and l_B the monomer length. However, as recently recognized [62, 63] this is only correct up to a prefactor (scaling law). In fact, if we assume that the hydrophobic part of the expelled chain is a compact globule, we can calculate the prefactor and Eq. 34 takes the form:

$$E_a = \gamma \cdot (\alpha 36\pi)^{1/3} \cdot (V_0)^{2/3} \cdot N_B^{2/3} \quad (36)$$

where V_0 is the monomer volume of the hydrophobic block.

Deviation from this conformation would give different prefactors and, importantly, a different N_B -dependence. In order to take this into account, we write the following for the rate constant:

$$k(N_B) = (1/\tau_0) \exp(-\alpha \cdot \gamma \cdot (36\pi)^{1/3} (V_0)^{2/3} N_B^\beta / k_B T) \quad (37)$$

where β is a scaling exponent that is $2/3$ for spherical globules and 1 in the case of linear chains where all segments are in contact with the solvent. Thus, we would expect an exponent that has the following validity range: $2/3 \leq \beta \leq 1$. α is a prefactor that, together with β , corrects for deviations from a spherical shape, and/or interpenetration of solvent. The prefactor α is more complicated to estimate as it would be associated to both a change in chain conformation and interactions between the hydrophobic part of the ejected bud and the corona. Prefactor α would also represent a general correction factor for entropic and enthalpic interactions with coronal chains.

2.2.7 Unimer Exchange Kinetics at Higher Concentrations: Effect of Osmotic Pressure

In a recent work, the original Halperin and Alexander model was, in light of new experimental data, extended for the case of high concentrations and particularly for the case of overlapping coronal A-chains [64]. As noted, Eq. 34 is only approximately correct and several corrections should be included. In particular, as is evident from Fig. 4, Eq. 34 does not give a complete description of the activation barrier. In addition to the surface free energy of the exposed insoluble B-block, the expulsion process involves interactions with the corona chains. The free energy of the “activated state” must therefore be calculated in more detail.

As noted by Halperin, the expulsion steps involve three additional free energy changes that should be included: (1) the free energy term ΔF_{ins} arising from the osmotic pressure “felt” by the expelled B-bud when inserted into the semi-dilute concentration of A-chain; (2) the lowering of the surface free energy after losing one chain ($\Delta F \sim (P_{\text{eq}} - 1)^{3/2} - P_{\text{eq}}^{2/3}$); and (3) the increase in free energy of the corona (increased crowding) due to the small reduction of the core radius and small increase in curvature. For a system of star-like micelles, this leads to a term that scales as $\Delta F \sim \gamma^{2/5} N_B^{2/5}$ and thus imposes a correction to Eq. 34 according to:

$$E_{a,\phi} \sim N_B^{2/3} \gamma \left(1 + \gamma^{-2/5} N_B^{-4/15} \right) \quad (38)$$

As discussed later, this might lead to an apparent modification of the prefactor of the activation energy seen in experiments (See sect. 4.5).

The osmotic insertion term ΔF_{ins} evidently changes with the corona density, which is a function of concentration, through screening effects or as an effect of

direct overlap of the corona belonging to two adjacent micelles. Alternatively, a similar effect can be induced by adding A-type homopolymers [64].

Halperin also considered the screening-induced growth of micelles that occurs when the repulsion within the corona decreases. In this case one can write:

$$E_{a,\phi} = E_a + \Delta F = N_B^{2/3} \gamma + R_c^{3/2}(\eta) N_B^{-1/2} \quad (39)$$

where the last term reflects the concentration-dependent corona density (η). Because the rate is sensitive to the exponential of this term, small variations are sufficient for a notable acceleration or deceleration.

2.2.8 Other Mechanisms for Chain Exchange: Fusion and Fission

So far, we have considered unimer exchange as the only (main) equilibration mechanism. However, other important mechanism may come into play. As depicted in Fig. 2, the most likely candidates are fusion and fission mechanisms:



The question is, however, with what probability does fusion or fission occur in comparison with unimer exchange, i.e., how important are they? Halperin and Alexander performed a rather straightforward calculation of the activation energy for fusion of two micelles of size P_1 and P_2 under the assumption that the corona free energy (star-like) of the micelle dominates. For star-like micelles they obtained:

$$E_a^{\text{fusion}}(P)/k_B T \sim \begin{cases} P^{3/2} & \text{for } P_1 \approx P_2 \approx P \\ P_1 \cdot P_2^{1/2} & \text{for } P_1 \ll P_2 \approx P \end{cases} \quad (41)$$

whereas for micelles with thin coronas:

$$E_a^{\text{fusion}}(P)/k_B T \sim \begin{cases} P^2 & \text{for } P_1 \approx P_2 \approx P \\ P_2^{2/9} & \text{for } P_1 = 1 \ll P_2 \approx P \end{cases} \quad (42)$$

As seen, the activation energy for fusion rapidly increases and grows to unfavorable values with increasing P . In comparison, fusion of dissimilar micelles is more probable. The most favored (lowest activation barrier), however, corresponds to the case where one of the fusing entities is a unimer. This corresponds to an insertion of a unimer into a micelle, which will have the following insertion rate constant:

$$k_+^P \sim \frac{1}{\tau_0} \exp(-\beta P^\alpha) \quad (43)$$

where τ_0 is a typical factor setting the time scale and $\alpha = 1/2$ and $2/9$ for a star-like and crew-cut micelles, respectively.

For micellar fission, the activation energy is given by the free energy difference: $F(P_1) + F(P_2) - F(P)$ for a micelle of size P splitting into two micelles of size P_1 and P_2 . This gives:

$$E_a^{\text{fission}}(P)/k_B T = (36\pi)^{1/3} P^{2/3} \cdot N_B^{2/3} \frac{\gamma \cdot l_B^2}{k_B T} \left[x^{2/3} + (1-x)^{2/3} - 1 \right] \\ + \frac{1}{2} \cdot P^{5/3} N_B^{-1/3} \left[x^{5/3} + (1-x)^{5/3} - 1 \right] - \frac{1}{6} [x \ln x + (1-x) \ln(1-x)] \quad (44)$$

where $x = \frac{P_1}{P}$. Obviously, $P_2 = P - P_1$

As seen, the activation energy assumes rather big values for fission. The value, however, is greatly reduced for smaller x . For small x we can approximately write $E_a^{\text{fission}}(P) \sim P^{2/3} N_B^{2/3} x^{2/3}$. Because x must be multiples i of P , one obtains $E_a^{\text{fission}}(P) \sim N_B^{2/3} i^{2/3}$. Hence, fission into a micelle of size $P - 1$ and a unimer ($i = 1$) has the smallest activation energy and thus the highest probability.

Hence, from these calculations it can be deduced that fusion/fission is not important for polymeric micelles because the associated activation energies are very large, especially when the corona is rather dense/extended. This is reasonable, at least in the case of star-like micelles or whenever the micelles are well-developed, i.e., at the end of the equilibration process or at equilibrium. However, this has been challenged in a more recent work by Dormidontova [65]. In this work, the theory was extended to also include nonlinear kinetics, e.g., the kinetics of micelle formation. In this respect, all relevant rate constants and the proper dependence on block copolymer characteristics, concentration, etc., were reconsidered and calculated in great detail by taking into account polymer-specific dynamics such as Reptation- and Rouse-like dynamics [66]. By using a full chemical reaction scheme (coupled reactions of all possible micellar sizes), the corresponding formation kinetics were simulated on the basis of the calculated rate constants. An important outcome of this work is that micellar fusion/fission is not negligible and plays an important role for the formation kinetics. This is particularly the case at short times where micelles tend to be less compact and more unstable.

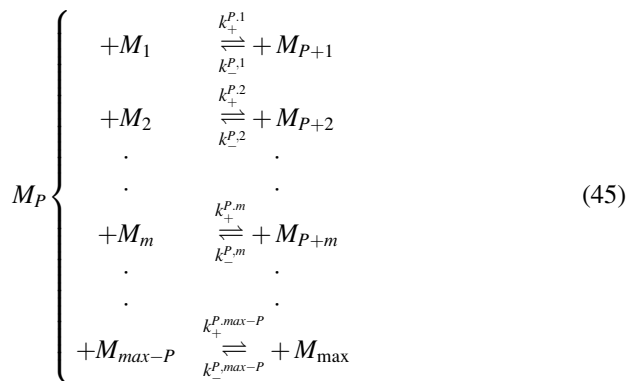
2.3 Non-equilibrium Micellization Kinetics

Contrary to the case of equilibrium kinetics, micellization of block copolymers proceeds from unimers and potentially involves any aggregate size up to or even above the equilibrium size. Hence, a theoretical treatment of the problem involves finding the concentration of the set of aggregates at all times: $\{\phi_1(t), \phi_2(t), \dots, \phi_n(t), \dots, \phi_{\max}(t)\}$. This is a quite challenging task, for which the detailed mechanisms must be established and then all activation energies, rate constants, etc.

must be calculated. There are several approaches to this problem, which we will briefly go through in the next section.

2.3.1 Chemical Reaction Approach

A brute force method for calculation of the micellization kinetics is to treat the problem as series of chemical reactions. Such an approach has been developed extensively within chemical engineering to treat complex coupled reactions. For micelles, we can write the reaction scheme on the general form:



where P is aggregation number and $1 \leq P \leq \max - P$ indicates the range in aggregation number. Here $k_{-}^{P,m}$ and $k_{+}^{P,m}$ are the rate constants for dissociation of two aggregates into sizes P and m and the inverse reaction, respectively.

The time evolution of the species are given by the resulting coupled differential equations:

$$\frac{\partial \phi_P}{\partial t} = \left[\sum_m k_{+}^{P,m} \phi_P \cdot \phi_m - k_{-}^{P,m} \phi_{P+m} \right] \quad (46)$$

This set of differential equations must then be solved numerically in a computer program.

Utilizing this kind of scheme and a detailed energetic analysis of the rate constants, Dormidontova [65] obtained a full description of a typical micellization process for a system with $1 \leq P \leq 35$ with an equilibrium size P_{eq} . The results show that fusion/fission occurs, but mainly at short times.

While this approach is quite attractive from the point of view of versatility and flexibility, the main disadvantage is that this method is heavy and computationally very demanding.

2.3.2 Free Energy Landscape Formalism

The previous “brute force” method is rather ineffective as all “reactions” and species are treated equally, regardless of the probability of formation or the stability. It may very well be that most of the pathways are so improbable or so energy-costly that they can be completely ignored.

In another approach, the micellization can be seen as a journey on a multidimensional energy landscape (phase space, i.e., a space spanned by all parameters) towards an equilibrium state that represents a global minimum on the landscape. One can imagine that the most probable path corresponds to the path of minimal energy, which naturally introduces a constraint. Such an approach was recently used by Diamant and coworkers for surfactant micelles [67]. Here, we will briefly review a generic model for block copolymers.

The Theory of Nyrkova and Semenov

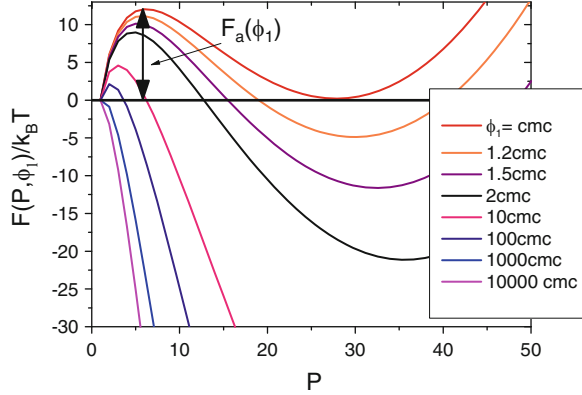
For block copolymer micelles, a conceptual model was developed by Nyrkova and Semenov [68] who considered the difference between the total free energy of a micelle compared with that of unimers:

$$F(P, \phi_1) = F_{\text{micelle}}(P) - P \cdot F_1 - (P - 1) \ln(\phi_1) \quad (47)$$

The concentration of a given aggregate is thereby determined by: $\phi_P = \phi_0 \exp[F(P, \phi_0)]$, where ϕ_1 is the concentration of unimers (at equilibrium $\phi_1 = \text{cmc}$). In Fig. 5, the potential is plotted for some representative values (for details see [68]).

Nyrkova and Semenov further assumed that only unimer exchange is active (i.e., dominant). By considering the aggregation number as representative of the mean micellar size and the unimer concentration, the free energy landscape is reduced and solely spanned by these two variables. In this way, the path from single chains (unimers) to equilibrium micelles is naturally the path with minimal energy. The local minima along the path thus represent metastable micelles. These metastable micelles considerably slow down the growth to the equilibrium micellar state and can, in some cases, completely deplete unimers and arrest further growth. This makes micellization an activated process in the sense that there is a (collective) entropic and enthalpic barrier to overcome in order to form micelles from unimers. In the words of Nyrkova and Semenov: “The main point is that micelle formation and their relaxation are activation processes involving collective energy barriers which can be high enough to considerably slow down or even to virtually suppress certain channels of relaxation.” These ideas are very similar to those presented earlier by Aniansson and Wall [54–56]. A very important contribution is thus the entropic barrier for micellization.

Fig. 5 The micellar free energy, $F(P, \phi_1)$ (in $k_B T$ units) versus the aggregation number plotted for different unimer concentrations. The curves were calculated using the typical potential: $F_{\text{micelle}}(P) = \gamma' P^{3/2} + \beta P^{2/3}$, with $\gamma' = 38$ and $\beta = 1.3$. Both the maximum, indicated by $F_a(\phi)$, and the minimum decrease rapidly with the unimer concentration ϕ_1



A typical time for micellization was found to be given by:

$$\tau_{\text{mic}} \sim \exp(F_a(\phi_1)) \quad (48)$$

where $F_a(\phi_1)$ is the height of the maximum of the $F(P, \phi_1)$. The values can be visualized more clearly in Fig. 5. This can be thought about as a barrier for micellization, similar to a nucleation barrier, that increases with decreasing ϕ_1 , reflecting an increasing entropic barrier closer to equilibrium. At $\phi_1 = \text{cmc}$, i.e., at equilibrium, the activation barrier scales with the interfacial tension and molecular weight: $F(P, \phi_1) \sim \gamma^{1.8} \cdot N_B^{1.2}$. This has the important consequence that the micellization time will be exceedingly long: the larger the polymer blocks and the higher the interfacial tension, the longer the equilibration of micelles will take. In a typical aqueous system with large $\gamma \approx 50 \text{ mN/m}$, the micellization time can easily reach literally astronomical times scales, e.g., 10^{10} s [68]. The dependence on the unimer concentration is also tremendous. This is shown in Fig. 6.

As seen, the typical equilibration time rapidly reaches extremely large values. This inspired Nyrkova and Semenov to define an apparent critical micelle concentration, cmc_{app} , corresponding an equilibration time of 3,600 s (1 h), i.e., $\tau_{\text{mic}}(\text{cmc}_{\text{app}}) \equiv 3,600 \text{ s}$. An important conclusion from this work is therefore that the measured cmc will always be much larger (in Fig. 6, by about a factor of 80–90) compared to the real cmc equilibrium value. A real cmc will not be measurable on a typical experimental time scale.⁴

In a given micellization process, $F_a(\phi_1)$ and of course also τ_{mic} will be time-dependent and lead to a broad distribution of relaxation times. Moreover, as $F_a(\phi_1)$ grows with time, the relaxation time becomes larger and the equilibration will slow down or even stop at longer times. However, in order to calculate this, the detailed time evolution needs to be developed. We show one example in the next section.

⁴ Such a definition is equivalent to what is customary in glass physics, where the transition from an equilibrium liquid to a non-equilibrium supercooled liquid (a glass) is characterized by a glass transition temperature, T_g , which is typically defined as the temperature at which the α -relaxation time scale approaches a certain laboratory time scale, typically 100 s.

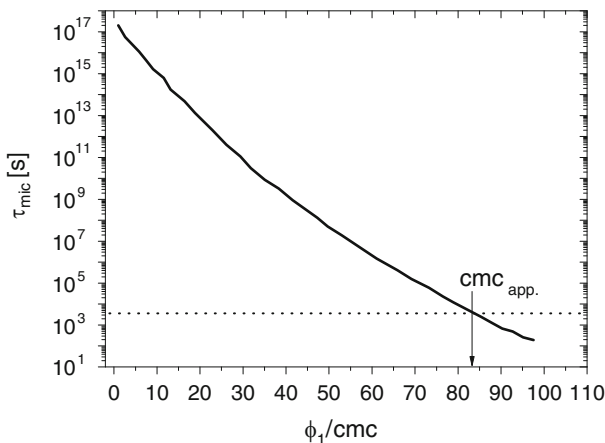


Fig. 6 Typical micellar equilibration time, τ_{mic} , as a function of the unimer concentration normalized by the equilibrium value (cmc). Dotted horizontal line corresponds to a time of 1 h and defines the apparent critical micelle concentration, cmc_{app} . Reproduced from [68]

2.3.3 Nucleation and Growth Approach

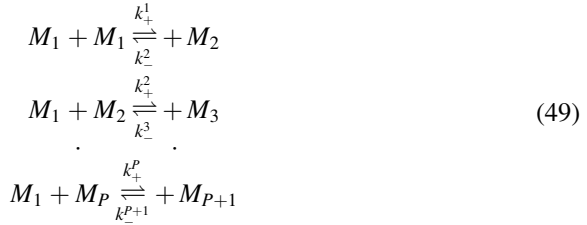
Nucleation and growth theories constitute a very attractive methodology in solid state physics to describe phenomena related to phase transitions. In this view, a new phase is pictured as growing out from a small finite-sized droplet. Typical examples are liquid bubbles formed from a gaseous phase (e.g., rain droplets), gas bubbles forming under close-to-critical liquids (e.g., boiling water), or crystallization in amorphous liquids (e.g., in silica-based semiconductors or organic polymers) [69].

Although micellization is not strictly speaking a phase transition phenomenon, nucleation and growth can also be used here. The micelles are then seen as droplets that can only grow up to limited size and will form a new continuous body (new phase). The next section reviews an example of such an approach.

Micellization Kinetics as a Nucleation Process

Considering the results of Halperin and Alexander [60] and of Nyrkova and Semenov [68] presented above, fusion and fission events between polymeric micelles appear to be rather rare. In any case, unimer exchange will always be an important if not completely dominating mechanism as a consequence of the low activation barrier of the process compared to other mechanisms.

Ignoring fusion and fission, the reaction scheme in Eq. 45 can be greatly simplified and we can write:



The growth rate of a given cluster of aggregation number P can be expressed via the flux, J_P , which describes the number created (or dissolved) per unit time and volume:

$$J_P = k_+^P \phi_1 \phi_{P-1} - k_-^P \phi_P \tag{50}$$

In order to simplify these equations, the basic principle of microscopic reversibility introduced by Onsager in the 1930s can be evoked [70]. According to this principle, used to derive the reciprocal relations in non-equilibrium thermodynamics, there is a local reversibility of all (sub-)processes even though the system is out of equilibrium. Hence, applying this principle, which is strictly speaking only likely to be valid close to equilibrium, we can write:

$$k_+^P \cdot \phi_P \cdot \phi_1 = k_-^{P+1} \cdot \phi_{P+1} \tag{51}$$

In other words, on a local scale the reaction is balanced, i.e., there is a microscopic reversibility. Note that this applies to locally defined variables and not to the mean (averaged) values. For an exchange-mediated growth process as we consider here, this means that the rate of individual unimer expulsion/insertion processes are much faster than the overall micelle formation.

Furthermore, the Boltzmann relation that describes the probability and stability of a given cluster can be used. From the theory of Nyrkova and Semenov this gives:

$$\phi_P = \phi_1 \exp(-F(P, \phi_1)) \tag{52}$$

where the chemical potential can be written as:

$$G(P, \phi_1) = k_B T (F_{\text{micelle}}(P) - P \cdot F_1 - (P - 1) \cdot \ln(\phi_1)) \tag{53}$$

Using Eqs. 52–53, one can eliminate one rate constant and express Eq. 50 in terms of the insertion rate constant k_+^P :

$$j_{P+1} = k_+^P \phi_1 [\phi_P - \phi_{P+1} \exp(G(P + 1, \phi_1) - G(P, \phi_1)/k_B T)] \tag{54}$$

thus, the flux is only determined by k_+^P and the chemical potential by $G(P, \phi_1)$.

Equivalently, the same scenario can be expressed mathematically in terms of the expulsion rate constant, k_-^P , which gives:

$$j_{P+1} = k_-^P [\phi_p \exp -(G(P+1, \phi_1) - G(P, \phi_1)/k_B T) - \phi_{P+1}] \quad (55)$$

The whole evolution of the micellar ensemble is then unambiguously given by the generic system of differential equations:

$$\frac{\partial \phi_P}{\partial t} = j_P - j_{P+1} \quad (56)$$

The stiff differential equation system can be solved numerically giving the concentration of the micellar entities/aggregates $\{\phi_1(t), \dots, \phi_P(t)\}$ as a function of time. In Sect. 5.1.2, a comparison between the theory and experimental TR-SAXS results will be presented.

3 Experimental Techniques

In this section we will go through the relevant details concerning experimental techniques, restricting ourselves to SANS and SAXS methods. Other relevant methods such as fluorescence spectroscopy and light scattering techniques will not be covered as these are considered out of the scope of this review article. Rather, we intend to give an overview of modern methodologies related to small-angle neutron and X-ray scattering.

3.1 *Small-Angle Scattering Methods*

In this section, the principles of small angle scattering and in particular the applications to micellar systems are briefly reviewed. We will later focus on the unique possibilities for resolving kinetic processes. For a more thorough review on small angle scattering in general, we refer to the textbook edited by Lindner and Zemb [71] or the classical books by Guinier and Fournet [72] and by Feigin and Svergun [73]. Detailed review articles on scattering of block copolymer and surfactant micelles have been published by Pedersen [74, 75].

3.1.1 Basic Principles of SAXS and SANS

The main differences between neutron and X-rays as probes in scattering experiments lie in their interaction with matter and their energy. While X-rays interact strongly with electrons in the (most frequently) outer shell of the atom and scatter through electromagnetic interactions, neutrons penetrate the core of the atom and scatter by

very short-range nuclear interactions. The energy for typical “cold” neutrons ($\approx \text{meV}$) differs strongly from that of typical X-rays ($\approx \text{keV}$), i.e., by factor of $\approx 10^6$.

The consequence is first of all that the scattering amplitudes are completely different in X-ray and neutron scattering, i.e., neutrons and X-rays “see” matter differently. As a consequence of their interaction with matter, neutrons can distinguish between isotopes and render even light elements visible. This can be exploited very efficiently to perform “contrast variation” studies, which are one of the main strengths of neutron scattering, in particular for organic matter with abundant hydrogen content. Secondly, because of their energy, neutrons are more suitable to detect slower motions in inelastic scattering experiments. Moreover, a photon carries no magnetic dipole moment whereas neutrons do, making neutron scattering also very useful for probing magnetic structures. The large energy of X-rays also causes difficulties for very high doses (from high flux sources). If the energy dissipation is slower than the impact rate, X-rays are able to provoke chemical changes as a consequence of free radical production, etc. However, this is only the case at high brilliance sources, such as synchrotrons, although there are ways to avoid or minimize these effects. For laboratory sources this is not an issue.

Despite the much higher energy, X-rays penetrate the material much less than neutrons due to their strong interactions with electrons. On the other hand, neutrons are only weakly scattering and, combined with the relatively low flux available at reactor sources (typically of the order of $\approx 10^8$ neutrons/(cm² s), this makes SANS an intensity-limited technique. Synchrotron sources, however, easily deliver $\approx 10^{12}$ – 10^{14} photons/s on the sample and thus improves the statistics issue dramatically. This opens up many exciting applications, as we will see later in Sect. 5.1, one of which is extremely fast time-resolved measurements.

Scattering Contrast and Scattering Intensity

In a scattering experiment, the intensity is most conveniently measured as the scattering cross-section, Σ per unit scattering volume divided by the solid angle Ω . This quantity is referred to as the macroscopic differential cross-section $d\Sigma/d\Omega(Q)$, which is measured as a function of the momentum transfer, $\mathbf{Q} = \mathbf{k}_f - \mathbf{k}_i$. Here, \mathbf{k} is the wave vector with modulus $|\mathbf{k}| = k = 2\pi/\lambda$ and λ is the wavelength.

Assuming that the scattering process is completely elastic, i.e., $\lambda = \lambda_i = \lambda_f$, the modulus of \mathbf{Q} can simply be cast into the following expression:

$$Q = 4\pi \frac{\sin(\theta)}{\lambda} \quad (57)$$

where 2θ is the scattering angle.

Within the assumptions usually valid for small angle scattering (Born approximation, Thomson scattering, single scattering events, etc.), the amplitude of scattering is given by:

$$A(\mathbf{Q}) = \sum_i^N b_i \cdot \exp(i\mathbf{Q} \cdot \mathbf{r}_i) \quad (58)$$

where b_i indicates the scattering length, i.e., the scattering amplitude of an atom i .

This important quantity is fundamentally different for X-rays and neutrons. For neutrons, the scattering length varies in a rather unsystematic fashion for the different elements across the periodic table, whereas the b_i values for X-rays vary monotonously with the amount of electrons,⁵ Z . This can be expressed as:

$$b_i(Z) = \begin{cases} b_i & \text{neutrons : irregular function of } Z \\ Z \cdot r_0 & \text{X-rays : linear with } Z \end{cases} \quad (59)$$

where $r_0 \approx 5.29 \times 10^{-13}$ cm is the so-called Bohr radius.

As seen for X-rays, the trend is clear: the larger the atom, the more it scatters. For neutrons, however, b_i depends on the nuclear interactions and is unrelated to its overall size. As an example, bromide ($Z = 35$) has a very similar value of $b \approx 6.8$ fm, as compared with carbon ($Z = 6$), $b \approx 6.6$ fm. For neutrons, these two elements are thus equally visible, whereas for X-rays Br is more dominant by a factor of $(35/6)^2 \approx (5.8)^2 \approx 30$ ($d\Sigma/d\Omega \approx b^2$) (more values can be found, e.g., at the NIST webpage, <http://www.ncnr.nist.gov/resources/n-lengths/>).

Moreover, for neutrons, b strongly depends on isotope. For example, the value for hydrogen, H (1 p⁺, 1 n) is -3.74 fm while that of deuterium, D (1 p⁺, 2 n) is 6.67 fm. Hence, not only are the values very different, but the value for hydrogen also has a negative sign because the phase is inverted during the scattering process. This is an extremely important aspect that allows contrast variation experiments by selectively labeling specific parts of the system in question through H/D exchange. As we will see later in particular in Sections 3.1.7, 3.1.8 and 3.2.2, this gives rise to very interesting possibilities in soft matter science.

The corresponding macroscopic differential scattering cross-section, $d\Sigma/d\Omega(\mathbf{Q})$ is of the general form:

$$\frac{d\Sigma}{d\Omega}(\mathbf{Q}) = \frac{1}{V_s} \langle |A(\mathbf{Q})|^2 \rangle = \frac{1}{V_s} \sum_{i,j=1}^N \langle b_i b_j \cdot \exp(i\mathbf{Q} \cdot (\mathbf{r}_i - \mathbf{r}_j)) \rangle \quad (60)$$

⁵ This is not strictly correct because the scattering length varies with energy and at certain energies there is absorption (near absorption edges) for certain energies and atoms. Strictly speaking, the scattering length should be written as: $b_i(E) = b'_i + i b''_i(E)$, where the latter imaginary part describes the absorption term. For X-rays, this is only important for rather high energy and large atoms, e.g., Br, which has one K-shell edge at 13.47 keV.

where V_s is the scattering volume.

In case there is a distribution in the scattering lengths for neutrons, e.g., because of a natural distribution of isotopes and spin states, the mean values and their spread must be considered. In this way Eq. 60 can be rewritten as:

$$\frac{d\Sigma}{d\Omega}(\mathbf{Q}) = \frac{1}{V_s} \langle b \rangle^2 \sum_{i,j=1}^N \langle |\exp(i\mathbf{Q} \cdot \mathbf{r}_i)|^2 \rangle + \frac{N}{V_s} (\langle b^2 \rangle - \langle b \rangle^2) \quad (61)$$

Equation 61 consists of a \mathbf{Q} -dependent and a \mathbf{Q} -independent part. The \mathbf{Q} -dependent part contains all structural information because it contains the phase factor $\exp(i\mathbf{Q} \cdot \mathbf{r}_i)$, which reflects the interference between pairs of scatterers. This is termed the coherent scattering. The last incoherent term contains no phase factor and is therefore not related to any interference and its cross-section is correspondingly isotropic. In a small-angle scattering experiment, where an elastic average is measured, the incoherent scattering represents an (inconvenient) constant background whereas for inelastic scattering experiments it opens up unique possibilities. We shall disregard such aspects in this contribution, where the focus lies on the coherent scattering giving direct access to the structure.

3.1.2 Scattered Intensity: Form and Structure Factors

Now considering the coherent scattering from particles (e.g., aggregates, micelles, etc.) dispersed in a solvent, the contrast relative to the solvent of scattering length, b_0 , must be considered, $b\langle b \rangle \rightarrow \langle b \rangle - b_0$. Furthermore, because small-angle scattering deals with scattering arising from entities significantly larger than the size of an atom, the spatial coordinates can be regarded as continuous coordinates and it is thus useful to use the following form:

$$\frac{d\Sigma}{d\Omega}(\mathbf{Q}) = \frac{1}{V_s} (\rho_p - \rho_0)^2 \int_{V_s} \int_{V_s'} g(\mathbf{r}, \mathbf{r}') \exp(i\mathbf{Q} \cdot (\mathbf{r} - \mathbf{r}')) d^3\mathbf{r} d^3\mathbf{r}' \quad (62)$$

where the scattering length density is defined as $\rho = \Sigma_i b_i / V_p$, V_p is the volume of the particle or solvent molecule, and $g(\mathbf{r}, \mathbf{r}')$ is the pair correlation function describing the probability for a correlation at a distance $\mathbf{r} - \mathbf{r}'$.

By decomposing the vector \mathbf{r} in intra- and interparticle contributions [76], it is possible to separate the scattering contribution according to:

$$\frac{d\Sigma}{d\Omega}(\mathbf{Q}) = \frac{N_p}{V_s} (\rho_p - \rho_0)^2 \cdot V_p^2 \cdot P(\mathbf{Q}) \cdot \left(1 + \frac{\langle |A(\mathbf{Q})| \rangle^2}{\langle |A(\mathbf{Q})|^2 \rangle} (S(\mathbf{Q}) - 1) \right) \quad (63)$$

Here, $P(\mathbf{Q})$ is the form factor, which relates to intraparticle correlations and gives information about the internal structure of a single particle. It can be defined as:

$$P(\mathbf{Q}) = \langle |A(\mathbf{Q})|^2 \rangle \quad (64)$$

and:

$$A(\mathbf{Q}) = \int_{V_p} n(\mathbf{r}) \exp(i\mathbf{Q} \cdot \mathbf{r}) dV_p \quad (65)$$

where $n(\mathbf{r})$ is the normalized density distribution of the particle and \mathbf{r} is now the vector from the center of mass to an arbitrary point located within the object or particle.

Note that in the case of polydispersity (i.e., a distribution in size, etc.) or anisotropic particles, $\langle |A(\mathbf{Q})|^2 \rangle \neq \langle |A(\mathbf{Q})| \rangle^2$ and each quantity must be evaluated accordingly.

The structure factor $S(\mathbf{Q})$ is defined as:

$$S(\mathbf{Q}) = \frac{1}{N_p} \sum_{i=1}^{N_p} \sum_{i'=1}^{N_p} \exp(i\mathbf{Q} \cdot (\mathbf{R}_i - \mathbf{R}_{i'})) \quad (66)$$

This describes the interparticle correlations and gives access to the interaction between the entities. \mathbf{R}_i is the vector to the centre of mass coordinate of particle i . The structure factor is close to unity at all Q values for dilute systems and, hence, Eq. 63 can be written as:

$$\frac{d\Sigma}{d\Omega}(\mathbf{Q}) = \frac{N_p}{V_s} (\rho_p - \rho_0)^2 \cdot V_p^2 \cdot P(\mathbf{Q}) \quad (67)$$

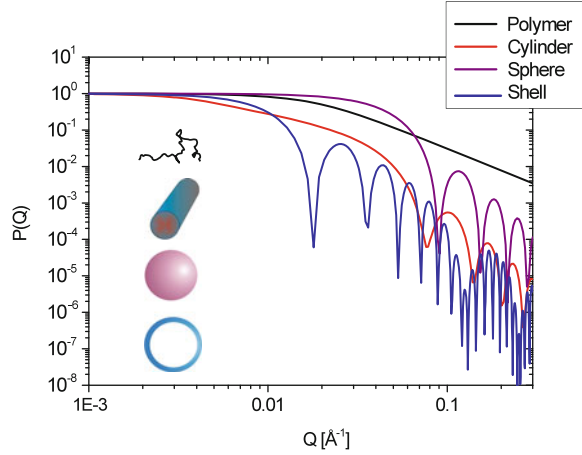
In this work we will mostly focus on dilute systems where interparticle interactions are negligible. A more detailed discussion concerning structure factors can be found in, e.g., [71, 75, 77].

3.1.3 Form Factors for Various Simple Geometrical Objects

In the remainder we will consider only isotropic systems, or isotropically averaged systems, and the momentum transfer vector will therefore be replaced with its absolute value, $|\mathbf{Q}| = Q$.

Eqs. 64–65 describe the theoretical scattering as a function of Q , which must be solved for each object or particle. Here, we will show some typical examples for different morphologies, the form factors for a sphere, cylinder, polymer chain, and a vesicle (hollow shell). The results for these structures are the following:

Fig. 7 The theoretical scattering form factor, $P(Q)$, from some common objects: (1) ideal polymer chain; (2) sphere; (3) cylinder; and (4) for vesicle/shell. See text for details. Note that the objects are for illustration only, and not to scale with respect to the depicted scattering curves



$$P(Q) = \begin{cases} \frac{2(\exp(-y)-1+y)}{y^2}, y = (QR_g)^2 & \text{Ideal Chain (Debye)} \\ (A_s(Q,R))^2, A_s(Q,R) = \frac{3(\sin(QR) - QR\cos(QR))}{(QR)^3} & \text{Sphere} \\ \left(\frac{R_2^3 A_s(Q,R_2) - R_1^3 A_s(Q,R_1)}{R_2^3 - R_1^3} \right)^2 & \text{Shell/Vesicle} \\ \int_0^{\pi/2} \left(\frac{\sin(Q \cdot L \cos(\alpha)/2)}{Q \cdot L \cos(\alpha)/2} \frac{2J_1(Q \cdot R \sin(\alpha))}{Q \cdot R \sin(\alpha)} \right)^2 \sin(\alpha) d\alpha & \text{Cylinder} \end{cases} \quad (68)$$

where α is the angle between the cylinder axis and the scattering vector, \mathbf{Q} of a cylinder with length, L .

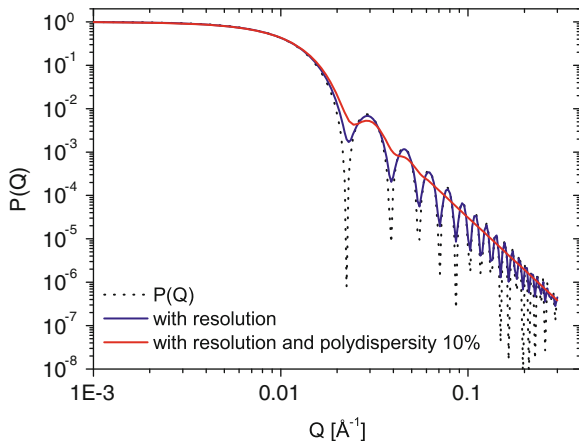
The results are calculated and depicted in Fig. 7 for a polymer chain with radius of gyration, $R_g = 80 \text{ \AA}$; a sphere with radius, $R = 50 \text{ \AA}$; an orientationally averaged cylinder with length $L = 1,000 \text{ \AA}$ and radius $R = 50 \text{ \AA}$; and a vesicle with outer radius $R_2 = 200 \text{ \AA}$ and inner radius $R_1 = 50 \text{ \AA}$.

3.1.4 Effect of Polydispersity

In real life, many systems are not monodisperse. For example, polymers prepared by synthetic methods are statistically distributed in molecular weight. Both synthetic and naturally occurring colloidal particles are polydisperse. The same applies to self-assembled systems constituted of surfactant and block copolymers. Owing to both the intrinsic polydispersity of the components and the statistical process of self-assembly, polydispersity in terms of aggregation number and size is evident.

This can be taken into account by considering a distribution function, $f(R)$, and averaging over the theoretically calculated intensity:

Fig. 8 Illustration of the effects of polydispersity and experimental smearing: Calculated scattering function of an ideal sphere with (a) experimental smearing and (b) both experimental smearing and polydispersity



$$\frac{d\Sigma}{d\Omega}(Q) = \frac{\phi_0}{\langle V_p \rangle} (\rho_p - \rho_0)^2 \int_R f(r) \cdot V_p(r)^2 \cdot P(Q, r) dr \quad (69)$$

where $\langle V_p \rangle = \int_r f(r) \cdot V_p(r) dr$

The normalized distribution function must be chosen according to the particular physical situation. A typical choice, suitable for many physical situations, is the Gaussian distribution:

$$f(r) = \frac{1}{\sqrt{2\pi\sigma_R^2}} \exp\left(-\frac{(r - R)^2}{2\sigma_R^2}\right) \quad (70)$$

Figure 8 shows the simulated scattering from an ideal sphere, with resolution convolution and both resolution and polydispersity included.

Another distribution function such as the Schulz–Zimm distribution is asymmetric with a tail toward larger values of r :

$$f(r) = \frac{(z+1)^{z+1} r^z}{r_0^{z+1} \Gamma(z+1)} \exp(-(z+1)r/r_0) \quad (71)$$

where $\Gamma(z)$ is the gamma function and z is a width parameter. The width of the distribution, σ_p , is given by: $\sigma_p = \frac{\langle R^2 \rangle - \langle R \rangle^2}{\langle R \rangle^2} = 1/(z+1)$

The choice of distribution function is best made on the basis of theoretical expectations, e.g., for the length distribution of cylindrical micelles an asymmetric distribution such as the Schulz–Zimm or log-normal distribution function is expected to be suitable [75].

3.1.5 Effect of Experimental Resolution

In practical situations, the scattering intensity is effectively “smeared” in Q because of the intrinsic finite beam divergence, distributed (neutron) wave lengths, finite size of detector pixels and so on. These issues are more important for SANS and laboratory SAXS equipments that use rather large apertures and/or are characterized by a significant wave length spread (for SANS, $\Delta\lambda/\lambda$ is typically 10–20%). This leads to a distribution of Q at each observed scattering angle that have to be incorporated when experimental results are compared with theoretical models.

This is described by the resolution function, $R(Q, \langle Q \rangle)$ describing the distribution of Q at a given mean value: $\langle Q \rangle$. Thus, the experimentally measured scattering cross-section takes the form:

$$\frac{d\Sigma}{d\Omega_{\text{exp}}}(\langle Q \rangle) = \int R(Q, \langle Q \rangle) \frac{d\Sigma}{d\Omega_{\text{theo}}}(Q) dQ \quad (72)$$

Following Pedersen [78], there are three main contributions that have to be incorporated when a typical diffractometer with a pin-hole geometry is used: wavelength spread, collimation effects, and the detector resolution. Using a Gaussian function for each effect, the resolution function is given by:

$$R(Q, \langle Q \rangle) = \frac{Q}{\sigma^2} \exp \left[-\frac{1}{2} \left(Q^2 + \frac{\langle Q \rangle^2}{\sigma^2} \right) \right] I_0 \left(\frac{Q \langle Q \rangle}{\sigma^2} \right) \quad (73)$$

where I_0 is the modified Bessel function of the first kind and zeroth order and σ is the smearing coefficient describing the resolution of the instrument. The effects summarized above can be related independently to the dispersion coefficient, σ , using:

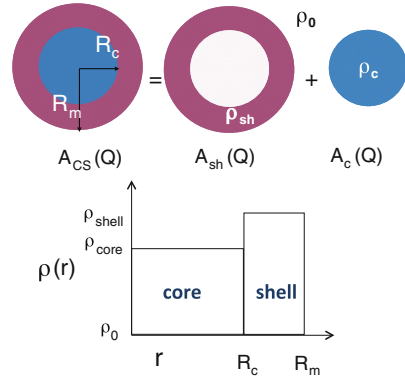
$$\sigma^2 = \sigma_W^2 + \sigma_C^2 + \sigma_D^2 \quad (74)$$

where σ_W is the dispersion of the wave length, σ_C describes the finite size of the beam due to the collimation and σ_D describes the detector resolution. For more details concerning the calculation of these quantities, we refer to the original work by Pedersen et al. [78]. For spallation sources, the calculation of the resolution function is a more complicated task. Here, ΔQ is, in addition to the divergence of the beam, also given by the uncertainty in the time of flight.

3.1.6 Scattering from Core–Shell Structures

For particles comprised of two or more types of materials, the scattered intensity needs to be calculated taking into account the interference between the different parts. For that it is more convenient to work in terms of scattering amplitudes defined in

Fig. 9 Scattering from a homogeneous core-shell system consisting of a core with scattering length ρ_c and a shell (ρ_{sh}) immersed in a solvent with ρ_0 . Please note that all relative values are chosen arbitrarily, i.e., $\rho_c > \rho_{sh}$ is equally possible. R_c core radius, R_m micelle radius



Eq. 65, correctly accounting for the volume and contrast for each part. A convenient and typical example is a sphere consisting of two layers: a core and a surrounding shell. Graphically, the scattering from such a particle can be constructed according to Fig. 9.

Compact Core-Shell Form Factor

Mathematically, the total amplitude can be written as:

$$A_{CS}(Q) = (\rho_c - \rho_0)V_c \cdot A_c(Q) + (\rho_{sh} - \rho_0)V_{sh} \cdot A_{sh}(Q) \quad (75)$$

Here we have introduced the mean scattering length density, ρ_i of solvent ($i = 0$), core ($i = c$) and shell ($i = sh$).

$A(Q)_i$ must be calculated by integrating over the volume of core and shell respectively resulting in:

$$A_i(Q) = \begin{cases} A(Q, R_c) & \text{Core} \\ \frac{R_m^3 A(Q, R_m) - R_c^3 A(Q, R_c)}{R_m^3 - R_c^3} & \text{Shell} \end{cases} \quad (76)$$

where $A(Q, R) = 3(\sin(QR) - QR\cos(QR))/(QR)^3$.

The total scattering is then given by (assuming a completely monodisperse system):

$$\frac{d\Sigma}{d\Omega_{CS}}(Q) = \frac{N}{V_s} \langle |A(Q)|^2 \rangle \quad (77)$$

where N is the number of particles and V_s the sample volume exposed to the beam. This can also be written as: $N/V_s = \phi_0/V_{tot}$ where ϕ_0 is the total concentration and V_{tot} is the volume of the particle.

In the case of micelles, the inner core is often compact and is constituted solely by hydrophobic (solvophobic) chain segments, whereas the outer shell is constituted by a hydrophilic (solvophilic) polymer swollen by solvent. In this case, the scattering length density of the shell must be averaged over the composition, i.e., polymer and solvent content according to: $\rho_{\text{sh}} = \Phi_p \cdot \rho_p + (1 - \Phi_p) \cdot \rho_0$. Here Φ_p is the (mean) polymer concentration.

In this case, it has been realized that the scattering from the internal polymer structure within the corona must also be taken into account [44, 74, 79–81]. This scattering results from the local contrast between corona-forming polymer and the solvent, which is not included in the calculation using a centro-symmetric mean density profile. Because these correlations are short-ranged compared to the overall micellar structure, interference terms with core and shell can be assumed to be negligible. Hence, to a first approximation this can be added to the overall intensity in Eq. 77:

$$\frac{d\Sigma}{d\Omega_{\text{CS-blob}}}(Q) = \frac{d\Sigma}{d\Omega_{\text{CS}}}(Q) + \frac{d\Sigma}{d\Omega_{\text{blob}}}(Q) \quad (78)$$

$\frac{d\Sigma}{d\Omega_{\text{blob}}}(Q)$ is the internal scattering from the individual polymer blobs adding up to the scattering. Inspired by correlations in semidilute polymer solutions [38, 82], Dozier et al. [83] calculated the scattering assuming the following:

$$g(r) \sim r^{1/(1-\nu)} \exp(-r/\xi) \quad (79)$$

A Fourier transformation of $g(r)$ and subsequent normalization then yields:

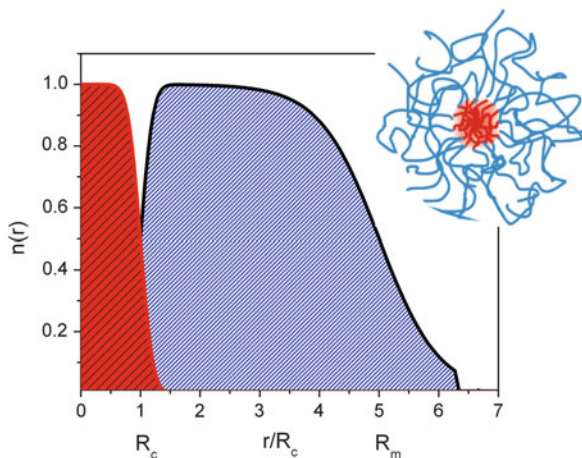
$$\frac{d\Sigma}{d\Omega_{\text{blob}}}(Q) = (\rho_p - \bar{\rho}_0)^2 \frac{4\pi\beta \sin(\mu \tan^{-1}(Q\xi))}{Q\xi(1 + Q^2\xi^2)^{\mu/2}} \Gamma(\mu) \quad (80)$$

where β is a prefactor, which should be proportional to the volume of polymer inside the blob, Γ the gamma function, ξ the average blob radius, and $\mu = 1/\nu - 1$ with the Flory exponent $\nu = 0.588$ for swollen chains.

Spherical and Cylindrical Core–Shell Form Factors Including Density Gradients

In reality, most micellar systems made up from polymers are not as perfect as depicted in Fig. 9. Instead, the micelles are expected to be more “fuzzy” and may more resemble the situation depicted in Fig. 10. In this case, the segmental distribution must be considered [44, 45, 48, 74, 79, 84–86] by calculating the scattering amplitude from a realistic density profile. In addition, the intrinsic polymer scattering must be incorporated by explicitly taking into account long-range excluded volume interactions.

Fig. 10 Illustration of density distribution in real block copolymer micellar systems. The data correspond to a core with a constant density profile convoluted by Gaussian function. The density profile of the corona grafted to the core is calculated using a Fermi–Dirac function $n(r) \approx (1 + \exp[(r - R_m)/(\sigma_m R_m)])^{-1}$. The parameters (see text for details) are $R_c = 30 \text{ \AA}$, $R_m = 150 \text{ \AA}$, $\sigma_m = 0.1$ and $\sigma_{\text{int}} = 5 \text{ \AA}$



In practical situations the interface of the micellar core may not be perfectly smooth due to chemical imperfections, packing restrictions of chains, thermal fluctuations, partial swelling of core with solvent, etc. To take into account smearing due to surface roughness, the ideal constant density can be convoluted with a Gaussian distribution:

$$n_c(r) \sim \int_0^\infty (1 - \Theta(r')) \frac{1}{\sqrt{2\pi\sigma_{\text{int}}^2}} \exp\left(-\frac{(r - r' - R_c)^2}{2\sigma_{\text{int}}^2}\right) dr' \quad (81)$$

Here, $\Theta(x)$ is the Heaviside step-function, i.e., $\Theta = 0$ for $x \leq 0$ and 1 otherwise. Likewise, for the corona density distribution:

$$n_{\text{corona}} \sim n_{\text{corona}}^0 \int_0^\infty \Theta(r') \frac{1}{\sqrt{2\pi\sigma_{\text{int}}^2}} \exp\left(-\frac{(r - r' - R_c)^2}{2\sigma_{\text{int}}^2}\right) dr' \quad (82)$$

where n_{corona}^0 is the inherent density profile of the corona, not taking into account the core–corona interface.

By virtue of the Fourier convolution theorem, this leads to a so-called Debye–Waller factor, $DW(Q)$ that modulates the scattering at high Q :

$$DW(Q, \sigma_{\text{int}}) = \exp(-Q^2 \sigma_{\text{int}}^2 / 2) \quad (83)$$

The scattering amplitude for the core including a graded core–corona interface (Gaussian distribution) can thus for a spherical or cylindrical core be written as:

$$A_c(Q) = \begin{cases} \frac{3(\sin(Q \cdot R_c) - Q \cdot R_c \cos(Q \cdot R_c))}{(Q \cdot R_c)^3} \cdot DW(Q, \sigma_{\text{int}}) & \text{Spheres} \\ \frac{\sin(Q \cdot L \cos(\alpha)/2)}{Q \cdot L \cos(\alpha)/2} \frac{2J_1(Q \cdot R_c \sin(\alpha))}{Q \cdot R_c \sin(\alpha)} \cdot DW(Q, \sigma_{\text{int}}) & \text{Cylinders} \end{cases} \quad (84)$$

where α is the angle between the cylinder axis and the scattering vector \mathbf{Q} , i.e., $\mathbf{QL} = QL \cos(\alpha)$.

For the shell, the corresponding expressions can be found by performing a Fourier transformation over the density profile, $n(r)$, using the appropriate geometry:

$$A_{\text{sh}}(Q) = \begin{cases} \int_{R_c}^{\infty} 4\pi r^2 n(r) \frac{\sin(Qr)}{Qr} dr \cdot DW(Q, \sigma) & \text{Spheres} \\ \int_{R_c}^{\infty} 2\pi r \cdot n(r) J_0(Q \cdot r \sin(\alpha)) dr \cdot DW(Q, \sigma) & \text{Cylinders} \end{cases} \quad (85)$$

J_0 is the Bessel function of zeroth order.

The density profile can be conveniently chosen to have the following generic form [44, 45, 48, 87]:

$$n(r) = \frac{1}{C} \frac{r^{-x}}{1 + \exp((r - R_m)/\sigma_m R_m)} \quad (86)$$

where x is a scaling exponent that for star-like micelles is predicted to be $x = 4/3$ [38], σ_m is the relative width of the micellar surface, and R_m is a mean (cut-off) radius of the micelle. C denotes a normalization constant obtained by integrating the density profile over the volume.

Generally, these expressions require numerical integrations. In the case of spherical symmetries, other approaches can be used such as hypergeometric [84] and spline functions [86] that reduce the problem to analytical functions. However, this might increase the number of fit parameters so extra care must be taken to ensure that the density profile is physically meaningful.

Pedersen and coworkers [74, 80, 81, 86] have modified Eq. 78 based on Monte Carlo simulation results from chains exhibiting excluded volume effects. Written in terms of a micelle constituted of a A-B block copolymer, this can be written independently of morphology (spherical, ellipsoidal, or cylindrical):

$$I(Q)_{\text{CS-acc.}}^{\text{calc}} = \frac{\phi}{PV_{\text{AB}}} (\Delta\rho_c^2 P^2 \cdot V_B^2 \cdot A(Q)_c^2 + \Delta\rho_{\text{sh}}^2 P \cdot (P - F(0)_{\text{blob}}) \cdot V_A^2 \cdot A(Q)_{\text{sh}}^2 + 2\Delta\rho_c \cdot \Delta\rho_{\text{sh}} P^2 \cdot V_A \cdot V_B \cdot A(Q)_c A(Q)_{\text{sh}} + V_A^2 \Delta\rho_{\text{sh}}^2 \cdot F_{\text{blob}}(Q)) \quad (87)$$

where $A_c(Q)$ and $A_{\text{sh}}(Q)$ are the scattering amplitudes of core and shell (corona), respectively; V_i is the molecular volume of the B- or A-block; $\Delta\rho_{\text{sh}} = (\rho_A - \rho_0)$; $\Delta\rho_c = (\rho_B - \rho_0)$; and $F(Q)$ is the effective scattering from the A-polymers

constituting the corona (“blob scattering”). ϕ_0 is the volume fraction of block copolymer.

As shown by Pedersen and Svaneborg, the scattering from the swollen PEO polymer chains in the corona (the blob scattering), can be written as [74, 80, 81, 86]:

$$F_{\text{blob}}(Q) = \frac{P(Q)_{\text{chain}}}{1 + \hat{v} \cdot P(Q)_{\text{chain}}} \quad (88)$$

where $P(Q)_{\text{chain}}$ is the form factor of a polymer chain, \hat{v} is an effective virial type parameter that scales with the effective concentrations of corona chains [74, 86].

The form factor of a polymer chain can be conveniently approximated by the following equation suggested by Beaucage [88] for arbitrary chain statistics:

$$P(Q)_{\text{chain}} = \exp\left(-Q^2 R_g^2/3\right) + \left(d_f/R_g^{d_f}\right) \Gamma(d_f/2) \left(\frac{(\text{erf}(QkR_g/\sqrt{6}))^3}{Q}\right)^{d_f} \quad (89)$$

where d_f is the fractal dimension and k is a numerical constant equal to 1.06. For mass fractals, $1 \leq d_f \leq 3$ and for polymers in a good solvent a typical value is 1.7. [88].

Alternatively, Pedersen and Schurtenberger have developed versatile expressions based on off-lattice Monte Carlo simulations that can be accurately used to describe almost any type of semiflexible polymer chain with and without excluded volume interactions [89].

3.1.7 Zero-Average Contrast in SANS

As previously mentioned, H/D substitution offers a great opportunity to perform contrast variation and thereby selectively highlight structural features in soft matter systems. Because of the abundance of hydrogen in soft matter systems and the relative easy access to deuterated materials,⁶ H/D substitution can easily be applied to a large range of systems. Contrast variation SANS played a key role in verifying the scaling approaches of de Gennes and others to chain conformation in semidilute and concentrated solution [90] and in establishing a Gaussian conformation of polymers in melts [91].

For structural characterizations, zero average contrast (ZAC) conditions can be used to eliminate structure factor effects. Here, we will briefly illustrate how this works by considering a very simple case consisting of two types of monodisperse

⁶ A large number of deuterated chemicals like solvents and monomers, particularly important in this context, are commercially available from standard chemical suppliers. In some cases, however, bottom-up organic synthesis is necessary, e.g., isoprene-d₈ or hexamethylcyclotrisiloxane-d₁₈ for deuterated PI and PDMS, respectively. This requires expertise from both polymer and organic chemistry.

particles where one is proteated (H) and the other deuterated (D). As before, the total intensity assuming identical volumes can be written as:

$$I(Q) = n_z V \left(f_H \Delta \rho_H^2 A(Q)_H^2 + f_D \Delta \rho_D^2 A(Q)_D^2 + 2 \cdot f_H f_D \Delta \rho_H \Delta \rho_D A(Q)_H A(Q)_D \right) \quad (90)$$

where $\Delta \rho_i = \rho_i - \rho_0$ ($i = H/D$) is the contrast for each component with respect to the solvent ($i = 0$). $A(Q)_i$ is the scattering amplitude, which can be split into two parts: one for all atoms belonging to the same particle, $A(Q)_{i,s}$, and one for the atoms belonging to two different particles, $A(Q)_{i,d}$, such that $A(Q)_i = A(Q)_{i,s} + A(Q)_{i,d}$. By definition, $P(Q) = A(Q)_{i,s}^2$ and $S(Q) = A(Q)_{i,d}^2$. Moreover, because there is no correlation term between internal structure and the arrangement of particles, we obtain:

$$I(Q) = n_z V^2 (f_H \Delta \rho_H^2 (P(Q)_H + S(Q)_H) + f_D \Delta \rho_D^2 (P(Q)_D + S(Q)_D) + 4 \cdot f_H f_D \Delta \rho_H \Delta \rho_D S(Q)_{HD}) \quad (91)$$

Now, if the H/D content of the solvent is adjusted such that $\Delta \rho_H = -\Delta \rho_D$, i.e., the scattering length density of the solvent is exactly between those for the deuterated and proteated particle $\rho_0 = (\rho_H + \rho_D)/2$ the system is at the zero average contrast condition. Furthermore, if the particles have identical form factors and the interactions between H -type and D -type particles as well as the mutual interactions are identical [i.e., $P(Q) = P(Q)_i$ and $S(Q) = S(Q)_i$] and for a 50% mixture of H/D -particles ($f_H = f_D = 0.5$), Eq. 90 reduces to:

$$I(Q) = n_z V^2 P(Q) \quad (92)$$

and hence the form factor can be measured even in a crowded environment with interparticle interactions. This very useful trick has been widely used to probe single chain or single particle structural properties in concentrated polymer systems by SANS [82, 90, 92–94]. In the following section, we shall see how contrast variation can be used to study micellar structures.

3.1.8 SANS Contrast Variation on Block Copolymer Micelles

For block copolymer micelles, a general strategy is to selectively deuterate one block while keeping the other proteated. In this way, by varying, e.g., the H_2O/D_2O composition (or other H - and D -type solvents), the core and shell can be selectively highlighted and studied in detail. As seen in Eq. 87, if the scattering length density of the solvent matches either that of block A or block B (i.e., $\rho_0 = \rho_A$ and $\rho_0 = \rho_B$), the pure corona ($\Delta \rho_{sh} = 0$) or core ($\Delta \rho_c = 0$) scattering can be obtained separately without any interference term. Hence in this way, the different scattering contribution of a multicomponent system can be extracted. The methodology is illustrated

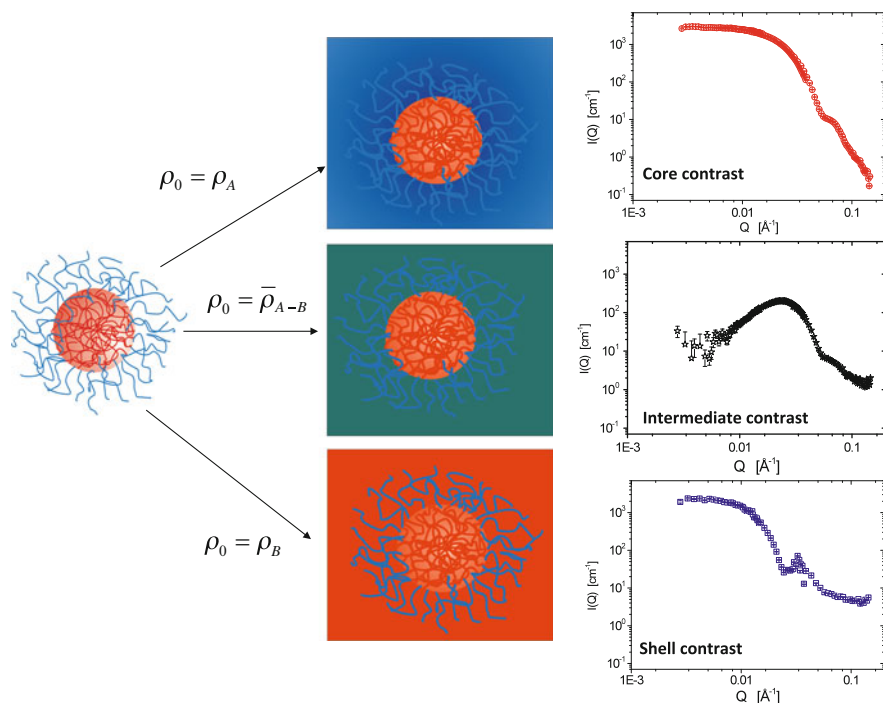


Fig. 11 Illustration of a SANS contrast variation study of block copolymer micelles (see text for details). Data to the right are reprinted with permission from [30]. Copyright (2009) American Chemical Society

more graphically in Fig. 11, where real results from a contrast variation study of proteated-polystyrene–deuterated polybutadiene (h-PS10–d-PB10) diblock copolymer micelles in heptane reproduced from [30] are also shown.

Moreover, by collecting data sets from different contrast situations and performing global fits (simultaneous fits) using a single scattering model, much more reliable and detailed structural results can be obtained. As an example, the scattered intensities from h-PS10–d-PB10 micelles in isotopic mixtures of various *n*-alkane solvents (selective for PB) are shown in Fig. 12. The different figures correspond to *n*-alkanes (C_nH_{2n+2}) with increasing length, from heptane ($n = 7$), decane ($n = 10$), dodecane ($n = 12$), and hexadecane ($n = 16$).

The different scattering patterns correspond to various isotopic solvent mixtures where the proteated PS core (h-PS) is matched: “shell” contrast; d-PB shell matched: “core” contrast and an “intermediate” contrast where the h-alkane/d-alkane mixture corresponds to a scattering length density in between that of the core and shell. Note that, in the latter case, the scattering at low angles ($Q \rightarrow 0$) almost disappears because the scattering contributions from core and shell are almost compensated by the interference term since $\Delta\rho_c = -\Delta\rho_{sh}$ and $V_A \approx V_B$ as can be rationalized from

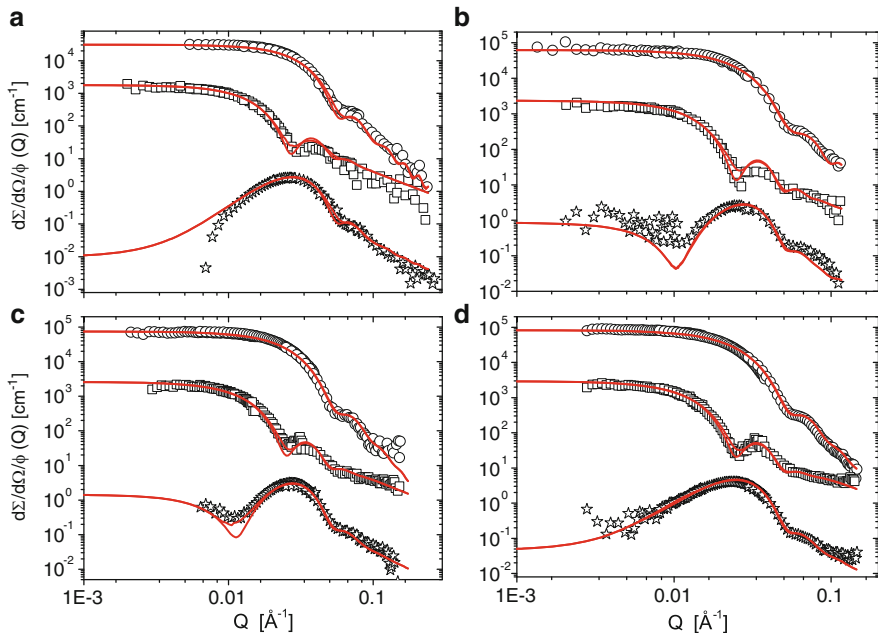


Fig. 12 Contrast variation results showing the absolute scattering cross-sections of h-PS-d-PB micelles in (a) heptane, (b) decane, (c) dodecane, and (d) hexadecane at $\phi = 0.25\%$ for different contrasts. The *solid lines* display simultaneous global fits using a core-shell model convoluted with the resolution function corresponding to the experimental settings. For better visibility, the data are shifted by a constant multiplication factor: core contrast (*circles*) 30; shell contrast (*squares*) 1; and intermediate contrast (*stars*) 0.02. Reprinted with permission from [30]. Copyright (2009) American Chemical Society

Eq. 87. At higher scattering vectors this is not the case because $A_c^2 \neq A_{sh}^2$, giving rise to scattering intensity at intermediate Q -values. The solid lines in Fig. 12 display simultaneous fits using the core-shell model above with an almost constant density profile, i.e., $x = 0$, a micellar smearing of about 10%, and $\sigma_m = 0.1$ in Eq. 86.

Thanks to the contrast variation and detailed model fitting, the internal structure could be obtained showing that the micelles are rather poorly segregated with a large quantity of solvent (approx. 30–50%) penetrating the core and a smaller compact corona. This important feature will be discussed in more detail in Sect. 4.3.

Other examples of such detailed analysis of the structure with the aid of contrast variation can be found for partially deuterated polystyrene–polyisoprene (PS-PI) diblock copolymer micelles in decane [86, 95]; “Pluronic” (PEO-PPO-PEO) micelles in water [96, 97]; PB-PEO micelles in water [85]; or PEP-PEO micelles in water [44] or in water/DMF mixture [98].

3.2 Time-Resolved Small-Angle Scattering as a Technique for Studying Micellar Kinetics

In addition to being a powerful tool for investigating the structural details of nanostructures, small-angle scattering methods are very useful techniques for following structural changes over time, i.e., to follow phase transitions, morphological transitions, etc. [13–15, 17, 18]. In addition to studying non-equilibrium kinetics associated with structural changes and transformations over time, the sensitivity of neutrons towards H/D, contrast variation, and SANS offers a study of subtle transport/diffusive processes and kinetics under equilibrium conditions [18, 19], i.e., kinetics can be probed without perturbing the system away from equilibrium.

Modern neutron instrumentation is an extensive subject that could cover a whole book alone. Here we will just review some basic concepts related to the more practical aspects and relevant principles related to studies of soft matter systems in general and micellar systems in particular. In this section, we briefly review recent modern methods used for time-resolved SAS studies.

3.2.1 Rapid Mixing Techniques: Stopped-Flow Methods

A versatile and classical method for studying kinetic reactions and other kinetic phenomena on short time scales is the use of a stopped-flow apparatus (SFA) for fast reproducible mixing and then to apply, e.g., spectroscopic methods for detection. In this technique, the reactants are rapidly mixed in a mixing chamber, usually under full turbulent flow that ensures fast homogenization on length scales down to nanometers [99]. Provided that short, synchronized acquisitions can be made, X-ray or neutron scattering can be used to probe kinetic transitions and other processes directly by measuring the temporal evolution of the intensity of the (mixed) sample.

The importance of a stopped-flow apparatus is to control the mixing of several solutions in a short time, achieve precise synchronization between the mixing process and the acquisition to ensure reproducibility of the experiment, and obtain a well-defined kinetic time [18, 99]. For fast measurements, it is important to use both fast mixing and short acquisition times while maintaining a reasonable statistics. This is more easily achieved with synchrotron sources, where the combination of small mixing volumes and high brilliance of the beam easily allow kinetic times of the order of a few milliseconds. However, with the more optimized neutron instrumentation and, in particular, with the advent of more powerful neutron sources such as spallation sources, there are a growing number of time-resolved SANS experiments investigating kinetic processes on a typical time scale of about 100 ms and upwards [18]. With more powerful spallation sources such as the planned European Spallation Source (ESS) in Lund, Sweden, time-resolved SANS measurements are expected to approach that of TR-SAXS at current synchrotron sources.

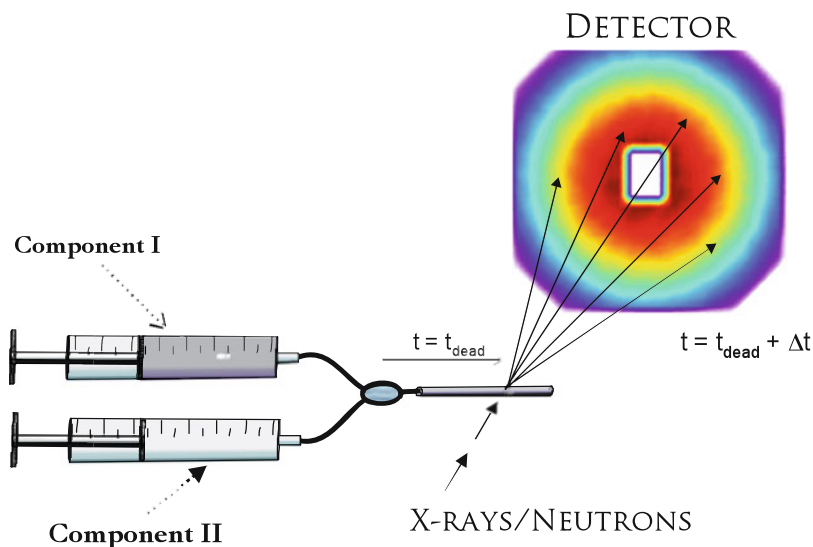


Fig. 13 Typical set-up of a small-angle scattering instrument coupled with stopped-flow apparatus. By synchronizing the mixing and transport of the solution to the observation chamber and the X-ray/neutron scattering acquisition, rapid processes occurring on a time scale down to a few milliseconds can be resolved

A crude scheme of a typical set-up for SAS combined with a stopped-flow apparatus is shown in Fig. 13. The idea is rather straightforward; the solutions are brought into contact by injecting the contents of two separate reservoirs into a “mixing chamber” that assures fast turbulent flow and homogeneous mixing. The solutions are thereafter transported to the observation cell (cuvette/capillary) through a stationary lamellar (non-turbulent/low Reynold number) flow. Although the homogenization time t_h , i.e., the time needed to completely mix the two liquids, itself is fast, there is a certain time lag associated with achieving lamellar flow, transport, and filling of the sample volume of the cuvette/capillary ($t_{\text{dead}} = V_{\text{dead}}/\mu$) where μ is the flow rate and V_{dead} is the volume that needs to be filled).

A typical measurement sequence is illustrated in Fig. 14. The reservoirs are continuously mixed by injection into the mixing chamber. Afterwards, the mixed solution is transported into the scattering volume. This transport time corresponds to t_{dead} . The flow of freshly mixed solution is maintained during a time t_{mix} , after which the flow is stopped by a hard-stop blocking the stream (hence the name “stopped-flow apparatus”). By varying the time for which the exposure/acquisition starts, defined by t_{delay} , and the duration t_{acq} , one may vary the kinetic times probed. Hence, placing an acquisition pulse within the duration of the mixing time would imply probing a fixed kinetic time $t = t_{\text{dead}}$ as fresh solution is continuously brought into the observation chamber. Placing the pulse outside the mixing duration, the kinetic time varies with

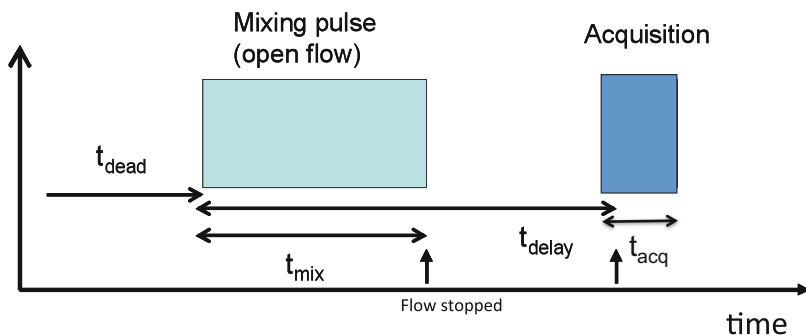


Fig. 14 Time sequence of a time-resolved small-angle scattering experiment. Using a stopped-flow apparatus, the data acquisition time, t_{acq} , can be synchronized with the mixing pulse time length, t_{mix} , giving access to fast kinetics. By varying the delay time, t_{delay} , high resolution stroboscopic measurements can be performed provided that the kinetics is reproducible. See text for details

the delay time t_{delay} . Hence, by synchronizing the SFA with the SAS instrument and varying the delay time, the kinetics can be probed stroboscopically by repeating several experiment with different time lags by varying t_{delay} , and thereby cover different initial kinetic times. The sequence of which subsequent kinetic time is probed is usually set by the detector of the instrument and the shutter. Here there is a difference between synchrotron X-rays and neutrons; whereas SAXS requires a shutter in order to avoid beam radiation damage, this is not required in SANS because such effects are absent. However, since many X-ray instruments use CCD-type detectors that require complete read-out and writing of data from each frame, the minimum lag time between frames is not set by the opening time of the shutter but rather by the readout time, which is typically between 100 and 300 ms. This is obviously only important for fast kinetics and limits the temporal resolution. However, provided that the kinetics is reproducible, this can be overcome by stroboscopic schemes whereby the kinetic is repeated with different lag times with respect to the acquisition, and can easily improve the resolution down to a few milliseconds. For SANS gas/scintillator detectors, the kinetic data can be stored in the different channels (typically 1,024 channels) and the minimal time is essentially set by the frame overlap in the wave packet and depends on the chopper speed (typically a few milliseconds for 1 m and an order of magnitude larger for 20 m).

Expressed mathematically, the first measured kinetic time in a stroboscopic experiment can be written as:

$$t_0 = \begin{cases} t_{\text{dead}}; & t_{\text{mix}} > t_{\text{delay}} \\ t_{\text{dead}} + (t_{\text{delay}} - t_{\text{mix}}); & t_{\text{mix}} \leq t_{\text{delay}} \end{cases} \quad (93)$$

The kinetic times at subsequent measurement frames numbered i are:

$$t_i = t_0 + \sum t_{i-1} + t_{\text{acq}}/2 \quad (94)$$

Often the delay time (X-rays), or the acquisition time (neutrons), is set to follow a geometrical progression to avoid oversampling and improve statistics at longer times (acquisition time). In the case, $t_{\text{delay/acq}}(i) = (t_{\text{delay/acq}}) \cdot f^i$ where f is a factor typically between 1.01 and 1.3 such that progressively slower processes can be followed. With this simple geometrical series, the kinetic time, Eq. 94, can conveniently be evaluated as: $t_i = t_{\text{dead}} + t_{\text{acq}}/2 + t_{\text{acq}} \frac{1-f^i}{1-f}$ and $t_i = t_{\text{dead}} + (i-1) \cdot t_{\text{acq}} + t_{\text{acq}}/2 + t_{\text{delay}} \frac{1-f^i}{1-f}$ for SANS and SAXS, respectively.

3.2.2 Contrast Variation and Time-Resolved SANS as a Method for Studying Exchange Kinetics

Time-resolved SAXS can be applied to the study of many types of kinetic processes. However, it must generally involve a transition from one state to another because the scattering signal only varies with changes in size, shape, etc. [14, 15]; in other words, the method is generally limited to non-equilibrium kinetics. Neutrons, however, may detect kinetics that do not necessarily alter the overall thermodynamic equilibrium state. This is essential for studying equilibrium processes such as chain exchange kinetics. Such kinetics can be studied by applying a H/D substitution scheme based on mixing H-type and D-type micelles made from block copolymers of identical volume and composition. By mixing these micelles in a solvent having an average scattering length density between the two, the contrast will decrease upon exchanging the chains between the micelles; hence, the molecular exchange kinetics is probed. The idea is schematically illustrated in Fig. 15.

This kinetic zero average contrast (KZAC) experiment [100–102] is an extension to the static zero average contrast (ZAC) described in Sect. 3.1.7. ZAC is used to effectively remove the structure factor such that interparticle correlations are eliminated and the single entities are visible, whereas in KZAC the trick is used to render mixing processes; hence, diffusion and transport become observable without perturbing the system in any substantial way.

In Fig. 16, experimental results of the time-dependent intensity after mixing proteated and deuterated PS-PB micelles in DMF under KZAC conditions [101] are shown. As can be seen the intensity decreases with time, directly showing that the micelles mix and kinetic processes are active. By analyzing the evolution of the scattered intensity and appropriate modeling, the mechanism and pathways can be determined from these experiments. In the following section, the technicalities will be described in more detail.

Model-Independent Evaluation of TR-SANS Kinetic Data

Mathematically, we might express this more precisely in the following way. The observed SANS intensity is determined by $I(t) \approx (\rho_m - \rho_0)^2$ where ρ_m is the effective scattering length density of the micelle given by the volume fraction of

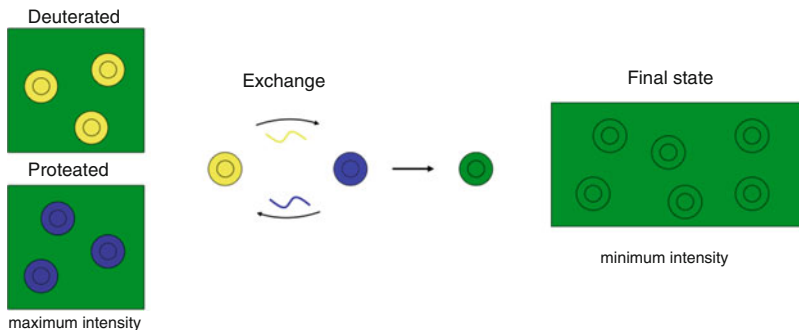


Fig. 15 Principle behind the KZAC experiment designed to measure chain exchange kinetics. Two populations of micelles, deuterated (*yellow*) and proteated (*blue*) are mixed at $t = 0$ in a solvent that matches the average color, *green* (about 50:50 deuterated/proteated solvent molecules). Upon molecular exchange of amphiphiles, the average contrast of the micelles decreases and thus the intensity in the TR-SANS experiment

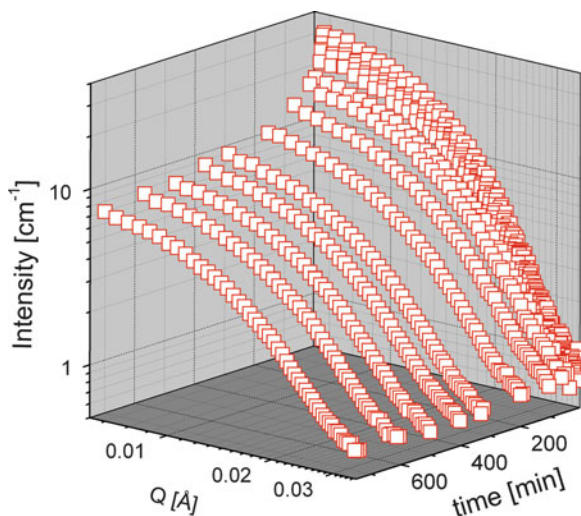


Fig. 16 Experimental curves showing a realization of the KZAC/TR-SANS technique applied to PS-PB block copolymers dissolved in DMF, which is a selective solvent for PS. At time zero, fully deuterated d-PS-d-PB micelles are mixed with fully proteated h-PS-h-PB micelles in a isotopic h-DMF/d-DMF solvent mixture exactly matching the average scattering length density. As the block copolymer chains exchange, an overall decrease in the intensity is observed while the form factor and hence the structure remains constant

proteated and deuterated chains, f and $1 - f$ respectively: $\rho_m = f\rho_h + (1 - f)\rho_d$ where ρ_h and ρ_d are the scattering length densities of the proteated and deuterated (in this section referred to as h- and d-) chains. Because in ZAC conditions we have $\rho_0 = (\rho_h + \rho_d)/2$, we see that the square root of $I(t)$ is linearly proportional to

the excess fraction of the h- or d-chains, i.e., $\sqrt{I(t)} \sim \Delta\rho(t) \sim (f(t) - 1/2)\rho_h + (1/2 - f(t))\rho_d = (f(t) - 1/2)(\rho_h - \rho_d)$. In this way, the analysis of the data is straightforward in comparison to other methods. Hence, using this method the information on the exchange kinetics is unambiguously given by the relaxation function, $R(t)$:

$$R(t) = \left(\frac{I(t) - I_\infty}{I(t=0) - I_\infty} \right)^{1/2} \quad (95)$$

where $I(t) = \int I(Q, t) dQ$ is the integral intensity at a given time and I_∞ denotes the intensity of the fully mixed sample at the final stage of the kinetic process (obtainable by randomly premixing the two block copolymers with $\phi_{hh} = \phi_{dd} = 0.5$). $I(0)$ is the arithmetic average of the two reservoirs (hh and dd samples) measured separately. The latter has to be measured at dilute concentrations, where no structure factor effects are present since $S(Q)$ vanishes under KZAC conditions.

$R(t)$ is the relevant function to be analyzed for extraction of the kinetics. However, in micellar systems where the micelles are not fully proteated/deuterated or there is residual contrast between core and shell, nonlinear interference scattering contributions are present. In order to take this into account, a more accurate description of the time-dependent scattering intensity is necessary. A scattering model, where the time-dependent hydrogen/deuterium composition of the core and shell of the micelles is built into a kinetic core-shell model, is described next.

Full Model Fitting Approach

The scattering function describing the time-dependent scattering intensity of micelles in a KZAC experiment involves a time-dependent core-shell model where the contrast is a function of the fraction of chains exchanged, f_{exc} . Here, we shall limit the discussion to cylindrical and spherical structures using simple A-B diblock copolymers as an example. Inclusion of other structures such as vesicles could be slightly more complicated because the microscopic composition might be potentially different in the inner and outer shells.

In the simple case of cylinders and spheres one can write:

$$I(Q, t)^i = \frac{\phi}{PV_{A-B}} \left(\Delta\rho_c^i(t)^2 P^2 \cdot V_B^2 \cdot A(Q)_c^2 + \Delta\rho_{\text{sh}}^i(t)^2 P \cdot (P - F(0)_{\text{blob}}) \cdot V_A^2 \cdot A(Q)_{\text{sh}}^2 + 2\Delta\rho_c^i(t) \cdot \Delta\rho_{\text{sh}}^i(t) P^2 \cdot V_A \cdot V_B \cdot A(Q)_c A(Q)_{\text{sh}} + V_A^2 \Delta\rho_{\text{sh}}^i(t)^2 \cdot F_{\text{blob}}(Q) \right) \quad (96)$$

where i denotes either proteated ($i = h$) or deuterated ($i = d$) species. $A(Q)_i$ is the scattering amplitude of core (c) and shell (sh), given in Eqs. 84 and 85, respectively.

The time dependence enters via the change of contrast of core and corona, $\Delta\rho_c^i(t)$, $\Delta\rho_{\text{sh}}^i(t)$ as a consequence of chain exchange between the differently labeled micelles.

Even though, after mixing and during the course of reaching a randomized mixture of h- and d-chains at equilibrium, a strict distinction between the originally proteated and deuterated micelles is lost, one can still write the contrast in terms of a surplus of either h- or d-chains $f(t)$ in the original micelles. We will use the convention $f(t=0) = 1$. Because the excess contrast is defined under ZAC conditions ($\rho_0 \approx (\rho_{hh} + \rho_{dd})/2$), $I(Q, t)^i$ must be symmetric around $f(t) \approx 0.5$, at least for low Q . For the situation where the micelles are completely randomized, $f(t) \approx 0.5$.

The contrast for the h- and d-cores made out of the h-B and d-B blocks, at time t is then given by:

$$\Delta\rho_c^i(t) = \begin{cases} \rho_{h-B} \cdot f(t) + \rho_{d-B} \cdot (1 - f(t)) - \rho_0 & \text{h-type micelle} \\ \rho_{h-B} \cdot (1 - f(t)) + \rho_{d-B} \cdot f(t) - \rho_0 & \text{d-type micelle} \end{cases} \quad (97)$$

and likewise for the corona:

$$\Delta\rho_{sh}^i(t) = \begin{cases} \rho_{h-A} \cdot f(t) + \rho_{d-PEO} \cdot (1 - f(t)) - \rho_0 & \text{h-type micelle} \\ \rho_{h-A} \cdot (1 - f(t)) + \rho_{d-PEO} \cdot f(t) - \rho_0 & \text{d-type micelle} \end{cases} \quad (98)$$

where the excess function is restricted to the range $0.5 \leq f(t) \leq 1$, assuming that the proteated and deuterated micelles are very similar and $V_h^{\text{mic}} \approx V_d^{\text{mic}}$.

The complete time-dependent scattered intensity can be calculated by taking the average of the two “types” of micelles in the following way:

$$I(Q, t) = \frac{1}{2} \left(I(Q, t)^h + I(Q, t)^d \right) + B \quad (99)$$

where $I(Q, t)^{h,d}$ is calculated according to Eq. 96 and B is a constant (time-independent) background reflecting the incoherent scattering of the sample.

As an example, Fig. 17 shows results [103] where the model is applied to describe the time-resolved SANS intensity in a KZAC experiment on n -alkane-PEO (C_{24} -PEO5k) micelles where only the PEO part was labeled (C_{24} -dPEO5k/ C_{24} -hPEO5k), i.e., the core-forming n -alkane block was proteated for both polymers and thus a net contrast between core and corona is always present during the course of the kinetic mixing process. As seen, both absolute values and the shape of the data are very well described at all times. At longer times, a shallow minimum at larger Q values evolves as a consequence of residual contrast between core and corona. This is also naturally described by the model. The results of this investigation are described in more detail in Sect. 4.4.

In analogy to the determination of $R(t)$ in Eq. 95, we can calculate $f_{\text{exc}}(t)$ for a better comparison of the kinetic data obtained by the two methods:

$$f_{\text{exc}}(t) = \frac{f(t) - f_{\infty}}{f(0) - f_{\infty}} \quad (100)$$

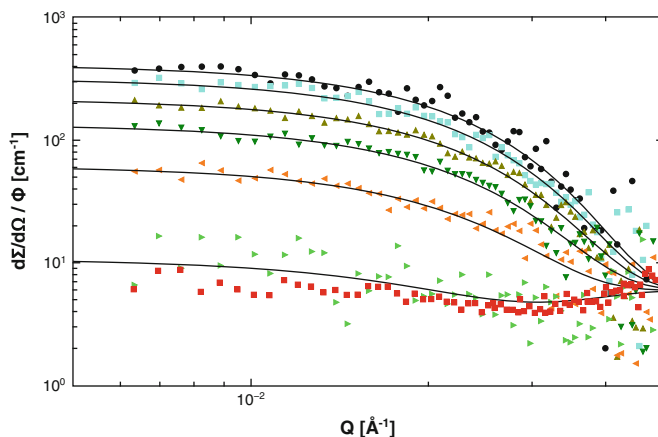


Fig. 17 Time-resolved SANS data showing the exchange process in *n*-alkyl-PEO micelles in water. *Solid lines* display fits of the core-shell model with $f(t)$ as free parameter. Time evolution from *top to bottom*: $t = 0.05, 5.6, 14.7, 25.2, 42.4$, and 95.0 s. [103] Reproduced by permission of The Royal Society of Chemistry

As shown in two recent studies [103, 104], both $f_{\text{exc}}(t)$ and $R(t)$ give essentially the same kinetic information and results. It should be mentioned, however, that the methodology described here only applies to rather low Q . At smaller scales, excess scattering is expected during the course of mixing as there might be local domains of either h- or d-type chains.

A similar approach could be used to describe hybridization kinetics after mixing two different micelles or for processes involving non-equilibrium relaxation experiments. However, in this case the time dependence of the structural parameters [$P(t)$, $R_m(t)$, etc.] as well as micellar composition must be taken into account.

Rate Constant From a Two-Component Labeling Experiment

Independently of the evaluation method, a KZAC TR-SANS experiment allows the kinetics to be evaluated through the decay of either $R(t)$ or $f_{\text{exc}}(t)$. The unimer exchange rate constant in simple labeling experiment will now be discussed.

A kinetic model for unimer exchange mechanism has been presented by Thilo [105] as well as by Cantú et al. [106]. According to Thilo [105], the following kinetic scheme can be used. Here, we use the terminology of proteated (H) and deuterated (D) chains or surfactants because in the present review the focus is on scattering experiments.

Starting from reservoir I where the micelles only contain proteated chains (H) and reservoir II with only deuterated chains (D), we define the initial conditions as $f_{\text{I}} = 1$ and $f_{\text{II}} = 0$ where the subscripts denote micelle I ($i = \text{I}$) or micelle

Π ($i = \Pi$), i.e., $f_I = N_H^I / (N_H^I + N_D^I)$ and $f_{II} = N_H^{II} / (N_H^{II} + N_D^{II})$ where N_H and N_D are the number of chains of type H or D inside the respective micelles. Considering proteated and deuterated unimers (number denoted by U_H and U_D , respectively) undergoing insertion/expulsion between the micelles, the rate equations can be written:

$$\frac{dN_H^I}{dt} = k_+^H U_H (N_H^I + N_D^I) - k_- N_H^I \quad (101)$$

$$\frac{dN_D^I}{dt} = k_+^D U_D (N_H^I + N_D^I) - k_- N_D^I \quad (102)$$

$$\frac{dN_H^{II}}{dt} = k_+^H U_H (N_H^{II} + N_D^{II}) - k_- N_H^{II} \quad (103)$$

$$\frac{dN_D^{II}}{dt} = k_+^D U_D (N_H^{II} + N_D^{II}) - k_- N_D^{II} \quad (104)$$

From mass-conservation we have:

$$\frac{dN_H^I}{dt} + \frac{dN_H^{II}}{dt} = 0 \quad (105)$$

$$\frac{dN_D^I}{dt} + \frac{dN_D^{II}}{dt} = 0 \quad (106)$$

It is useful to introduce the relative fraction of H-chains, r :

$$r = \frac{N_H^I + N_H^{II}}{N_H^I + N_H^{II} + N_D^I + N_D^{II}} \quad (107)$$

From Eqs. 101–107:

$$\frac{k_+^H}{k_-^H} = \frac{r}{U_H} \quad (108)$$

$$\frac{k_+^D}{k_-^D} = \frac{1-r}{U_D} \quad (109)$$

The time derivative of f_I and f_{II} are then obtained by direct derivation and yields:

$$\frac{df_I}{dt} = \frac{1}{N_H^I + N_D^I} \cdot \left[(1 - f_I) \frac{dN_H^I}{dt} - f_I \frac{dN_D^I}{dt} \right] \quad (110)$$

$$\frac{df_{II}}{dt} = \frac{1}{N_H^{II} + N_D^{II}} \cdot \left[(1 - f_{II}) \frac{dN_H^{II}}{dt} - f_I \frac{dN_D^{II}}{dt} \right] \quad (111)$$

Using Eqs. 101–109 and inserting into Eqs. 110 and 111 gives two second-order differential equations that can easily be solved using the above-mentioned boundary conditions:

$$f_I(t) = \frac{(1 - r)k_-^H \exp(-\lambda t) + rk_-^D}{(1 - r)(k_-^H - k_-^D) \exp(-\lambda t) + k_-^D} \quad (112)$$

and:

$$f_{II}(t) = \frac{1 - \exp(-\lambda t)}{1/r - (1 - k_-^D/k_-^H) \exp(-\lambda t)} \quad (113)$$

where $\lambda = rk_-^D + (1 - r)k_-^H$. In this work, all measurements have been performed by carefully balanced samples, i.e., $N_H \approx N_D$ consequently, since the fraction of free unimers is very small in these systems [31]: $r = N_H/(N_H + N_D) \approx 1/2$. Moreover, assuming that the labeled block copolymers are similar, $k_-^D = k_-^H = k_-$, Eqs. 112 and 113 can be cast to simple forms:

$$f_I(t) = \frac{1}{2} (\exp(k_- t) + 1) \quad (114)$$

$$f_{II}(t) = \frac{1}{2} (1 - \exp(k_- t)) \quad (115)$$

Hence, we see that for a simple unimer expulsion/insertion mechanism, the following expression holds:

$$\sqrt{I(t)} \sim (f_I(t) - 1/2)\rho_h + (1/2 - f_{II}(t))\rho_d \sim \exp(-k_- t) \quad (116)$$

In other words, $R(t)$ and f_{exc} would, in the case where the mechanism of unimer exchange is dominant, give rise to a simple exponential decay.

4 Equilibrium Kinetics in Block Copolymer Micelles

Experimental work on the equilibrium kinetics in block copolymer micelles is very rare in comparison with structural investigations. This is most likely due to the challenging problems in accessing the chain exchange by suitable experimental techniques or systems. Early experiments include studies using size-exclusion

chromatography [107–112] and ultracentrifugation [113, 114] as investigative tools. Since both techniques involve strong flow fields, the experiments yield information under quasi-static conditions rather than true equilibrium kinetics. Therefore, these works will not be further reviewed here. Kinetic studies have additionally been performed using ultrasonic absorption techniques [115–117] but after careful analysis it was concluded that the ultrasonic relaxation observed in micellar solution cannot be associated with the Aniansson and Wall mechanism of single chain exchange [117]. More relevant in the context of this chapter are relaxation experiments under quasi-equilibrium conditions, i.e., after small perturbations from equilibrium such as small temperature-jump (T-jump) experiments with light scattering detection in triblock copolymer micelles of the Pluronics type, PEO-PPO-PEO. Regarding this work, we will devote a small section (Sect. 4.1) to a brief summary of the main results. Other techniques like fluorescence quenching or nonradiative energy transfer [118–122] and transmission electron microscopy [123–125] have been used to assess micellar kinetics. However, strong perturbations or the incorporation of bulky labels are necessary to be able to monitor kinetic processes, which are often accompanied by reorganization of micellar structures. In any case these classical works have already been discussed extensively before in, e.g., the review of Zana [16]. Therefore, we will mainly restrict this section to the more recent results obtained by the H/D contrast variation/TR-SANS technique because this method was shown to access the chain exchange dynamics under true equilibrium conditions. By the combination of proper spatial and temporal resolution and by using suitable block copolymer/solvent systems, these experiments have given new insights into the mechanisms of chain exchange and allowed a profound discussion of the relaxation behavior within the framework of the existing theories.

This section on equilibrium kinetics is organized as follows: We will first focus on the T-jump experiments with light scattering detection on Pluronics polymers (Sect. 4.1). Thereafter, a chronological review of kinetic experiments on PEP-PEO block copolymers in aqueous solution is presented, including a summary of the morphological properties of this system (Sect. 4.2). A special focus is given on the tuning of kinetics by variation of mainly the interfacial tension. The main outcome of these experiments was the observation of an unexpected logarithmic time decay. This is discussed in more detail (Sect. 4.2.4). Further, we will review experiments obtained on block copolymers in organic solvents and discuss the dramatic effect of polydispersity on the kinetics, which finally allows an explanation of the log-time dependence (Sect. 4.3). Subsequently, a summary of kinetic experiments on *n*-alkyl-PEO block copolymers with monodisperse core blocks will be given, supporting the polydispersity effect by directly demonstrating the enormous influence of the *n*-alkyl chain length and the observed single exponential decay (Sect. 4.4). Finally, two special sections are devoted to the exchange kinetics at higher concentrations in ordered diblock copolymer micelles (Sect. 4.5) and to the influence of the morphology by comparing kinetics in spherical and cylindrical micelles (Sect. 4.6).

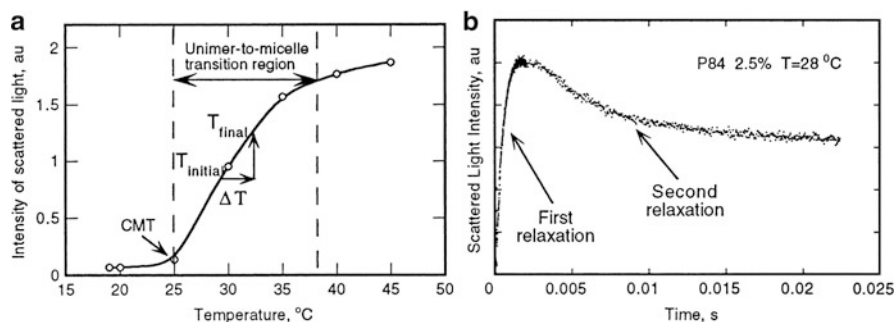


Fig. 18 Scattered light intensity (a) as a function of temperature in aqueous solution of PEO-PPO-PEO block copolymers, including the location of a typical temperature-jump; (b) as a function of time at the target temperature. Reprinted with permission from [127]. Copyright (1997) American Chemical Society

4.1 Quasi-equilibrium Kinetics of PEO-PPO-PEO in Temperature-Jump Experiments

The kinetics of poly(ethylene oxide)–poly(propylene oxide)–poly(ethylene oxide) (PEO-PPO-PEO) triblock copolymers have been intensively studied by T-jump experiments with light scattering detection [115, 126–130]. PEO-PPO-PEO triblock copolymers form micelles in aqueous solution, with PPO as the core forming hydrophobic block. Above the critical micelle concentration (cmc) and critical micelle temperature there exists a transition region of $\Delta T \approx 10\text{--}15^\circ\text{C}$ where single chains disappear in favor of micellar aggregates. The temperature jumps of typically $1\text{--}2^\circ\text{C}$ are performed in the transition region, leading to a change in the degree of aggregation and, consequently, to a variation in the scattered intensity. Fig. 18a shows the temperature dependent intensity of scattered light including the range and location of a typical jump experiment. Fig. 18b displays the response after the T-jump as a function of time, revealing two relaxation processes: a fast process that is accompanied by an increase in scattered light appearing on time scales in the micro- to millisecond range; and a second slow process with a negative scattering amplitude, i.e., a decrease in the light intensity with time, in the millisecond range. The fast process was assigned to the insertion of block copolymer chains into preexisting micelles, leading to aggregates, which are thermodynamically unstable. The second slow process was associated with formation–breakup processes to rearrange the micellar size distribution corresponding to thermodynamic equilibrium [115, 127]. The existence of two characteristic times is in agreement with the Aniansson and Wall picture [54–56] derived for low molecular weight surfactants. However, as the second slow process depends on concentration, fusion and fission as competing mechanisms for chain exchange need to be considered, as already proposed by Kahlweit et al. [52, 57]. Later, the T-jump experiments were extended by Kositzka et al. [128, 129] to higher temperatures close to the cloud point. At the cloud point, the solvent quality becomes bad enough such that a

macrophase separation into a block-copolymer-rich phase and a water-rich phase takes place. These experiments revealed the appearance of a third process with a positive amplitude. This was assigned to intermicellar interactions, indicating the onset of the macrophase separation. We note that in these cases PPO was the major compound in the triblock copolymer. The increasing hydrophobicity at higher temperatures may thus lead to the observed clustering and macrophase separation in water. In a subsequent paper by Waton et al. [130], it was argued that the second and third relaxation processes are identical and are both due to the formation and breakup of micellar entities at the point where the sign of the amplitude changes from negative to positive by increasing the temperature. This was shown to be a consequence of the relative size of the micelles after the fast initial growth and at equilibrium. If micelles are larger after the first process than at the end of the slow process, the scattered light decreases and vice versa. Because this changes with temperature, the change in the sign of the amplitude becomes obvious.

The above discussed experiments were performed under quasi-equilibrium conditions inherently showing a rather complex relaxation behavior that is governed by processes from equilibrium and non-equilibrium kinetics. Additionally, in light of the discussion above, the presence of an apparent third mode is controversial. With respect to the understanding of equilibrium kinetics in general, the outcome of these experiments is limited as it does not provide deep insight into the exchange mechanism and the dependence of system-specific parameters like the interfacial tension, core chain length, and polydispersity. A more thorough understanding was only possible after the advent of the TR-SANS technique, as will be shown in the subsequent sections.

4.2 PEP-PEO Block Copolymers in Aqueous Solution

The study of the structure and kinetics of hydrocarbon-PEO amphiphilic diblock copolymers in selective solvents has received increased attention within the last 25 years. For example, polystyrene-*block*-poly(ethylene oxide) (PS-PEO) was intensively investigated in the 1990s [3, 131–136]. More recently, the micellar properties of block copolymers containing either polydienes like 1,4-polyisoprene (PI); 1,2- or 1,4-polybutadiene (PB); or their saturated analogues poly(ethylene-*alt*-propylene) (PEP) and poly(ethyleneethylene) (PEE) as the hydrocarbon block have attracted the attention of many research groups because of their potential technical and biomedical applications. The micellar properties of PE-PEO block copolymers, with PE the saturation product of 1,4-PB, have only rarely been investigated [137, 138]. In particular, equilibrium kinetics have to the best of our knowledge not been studied so far most likely due to complications arising from unwanted coupling between crystallization of PE and chain exchange dynamics at moderate temperatures. The chemical design of amphiphilic block copolymers resembles that of the well-known low molecular weight oligo(ethylene oxide)-monoalkyl ether $[C_n(EO)_m]$ surfactants, with subscript n being the number of carbon atoms of the hydrophobic n -alkyl-moiety

and m of the hydrophilic EO units. Accordingly, amphiphilic block copolymers can form micelles in aqueous media as well as in nonpolar solvents.

In this part of the review we will focus on kinetics in aqueous dispersions because water-based systems have been more commonly investigated. Among the amphiphilic block copolymers mentioned above, PEP-PEO takes a prominent position because it possesses four main features that turn it into an ideal model system for studying fundamental aspects of block copolymer micellization: (1) The synthesis of narrowly distributed PEP-PEO with predefined molecular weight and composition is easily feasible by well-established living anionic polymerization techniques [139–141]. Importantly, as a prerequisite for TR-SANS studies, PEP-PEO can be synthesized fully deuterated. (2) Compared to polydienes, the aliphatic PEP block is chemically and thermally stable, which facilitates sample handling and preparation. The addition of stabilizing agents such as antioxidants is not necessary. (3) PEO is highly water-soluble and electrostatically neutral. (4) PEP is an amorphous material with a low T_g of -56°C . Specific influences from glassy or crystallized micellar cores need not be considered. (5) PEP is highly incompatible with water, as reflected by a large value for the interfacial tension, γ , of about 46 mN/m [45]. This high value of γ is the important physical quantity determining the aggregation behavior of PEP-PEO block copolymers in aqueous solutions. Moreover, the tuning of micellar structure and kinetics by varying γ through the addition of less incompatible co-solvents, e.g., DMF or ethanol becomes very effective. As the static properties are an important prerequisite for discussing exchange kinetics, the PEP-PEO micellar structure was characterized as a function of molecular weight, block composition, and solvent quality. A brief summary of the main structural features of these investigations is given in the beginning of Sect. 4.2.1.

The main part is then devoted to the equilibrium exchange kinetics of selected PEP-PEO micellar systems. We report on TR-SANS measurements in pure water that, independently of block copolymer molecular weight, composition, and temperature, revealed frozen micelles. This review further concerns the effect of tuning the kinetics by addition of co-solvents, i.e., reduction of γ . The relaxation behavior of some selected systems revealing chain exchange dynamics that can be resolved by TR-SANS will be presented, followed by a discussion of the main observation, namely, the unexpected appearance of a pseudo-logarithmic time decay of the relaxation function.

4.2.1 Morphological Behavior of PEP-PEO Block Copolymers in Aqueous Solution

The static structure of PEP-PEO block copolymer micelles in aqueous solution have been studied by small angle scattering techniques, primarily SANS [44, 45, 87, 104, 139, 142], and in one case by a combination of SAXS and static light scattering (SLS) [143]. In water, PEP-PEO block copolymers self-assemble into a variety of micellar structures depending on molecular weight and composition. A thorough structural characterization of micelles formed by a symmetric PEP5-PEO5 diblock

copolymer (numbers denote approximate molecular weight in kg/mol) was done by SANS using contrast variation and model fitting [87]. Fit results simultaneously obtained on four different contrasts revealed a spherical shape of the micelles, consisting of a compact solvent-free micellar core and a highly swollen PEO corona. It was found that the micelles have unusually large aggregation numbers of $P = 2,430$ and rather large dimensions. It was shown from thermodynamic calculations based on a mean-field model of Nagarajan and Ganesh [28] that this is a consequence of the large interfacial tension between PEP and water.

In a series of experiments, aqueous dispersions of symmetric PEP-PEO block copolymers were studied over a wide range of molecular weights, always keeping the ratio between the volumes of the blocks constant [142]. The scattering behavior of the solutions showed that a morphological transition takes place upon lowering the molecular weight. The high molecular weight materials all formed spherical, almost monodisperse, micelles with large aggregation numbers. At low molecular weights, however, cylindrical micelles were observed. An interesting intermediate case is represented by the PEP2-PEO2 system. Here spherical micelles were found at higher concentrations while cylinders occurred at larger dilutions.

The effect of a growing soluble block on the morphology of the micelles was investigated by varying the molecular weight of the PEO from about 5 to 120 kg/mol while keeping the PEP block constant at 5 kg/mol for all polymers [44]. Thus, a systematic study of the aggregation number and the corona shape became possible over a large range of compositional asymmetry ($1:1 \rightarrow 1:24$). Partial labeling of the block copolymers allowed highlighting corona structures individually by matching out core contributions using D_2O/H_2O mixtures. Data analysis using a spherical core-shell model with variable density profile indicated a crossover from a practically homogeneous corona profile for more symmetric diblocks to a star-like profile at larger asymmetries. Notably was the observation that PEP-PEO block copolymers aggregate into micelles even in a large compositional asymmetry, realizing thereby micelles with a star-like profile. It was concluded from free energy considerations that this is only possible because of the high interfacial energy as the main contribution.

In contrast to the study of Willner et al. [44], a cylinder-to-sphere transition was observed by Jensen et al. [143, 144] upon increasing the PEO block molecular weight in a similar molecular weight range. By SAXS and SLS it was found that PEP5-PEO5, PEP5-PEO10, and PEP5-PEO20 form cylindrical micelles whereas PEP5-PEO40 micelles are spherical. However, no explanation was given for the different molecular weight dependence of the morphology found in this work as compared to the work by Willner et al. [44].

The effect of interfacial tension γ on the micellar structure of a highly asymmetric PEP1-PEO20 block copolymer was examined using binary solvent mixtures of water and DMF as selective solvents [45, 145]. DMF and water are both good solvents for PEO and non-solvents for PEP, but exhibit a large difference in γ with respect to the insoluble core block. The micellar characteristics were obtained by SANS and subsequent fitting with a spherical core-shell form factor. Scattering curves together with model fits for selected water/DMF mixtures are depicted in Fig. 19a. As anticipated from the large asymmetry in block composition, the

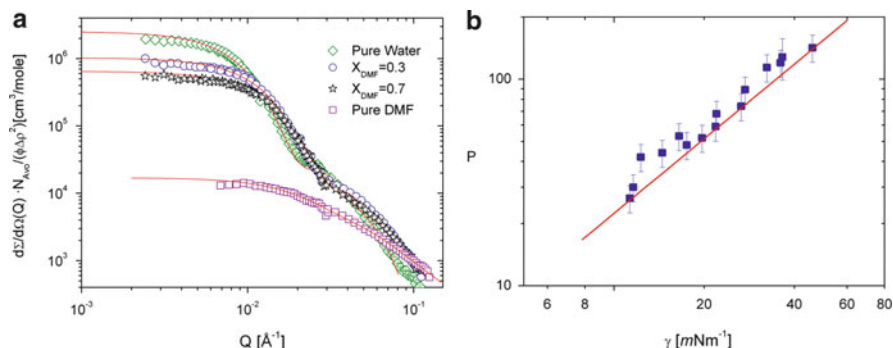


Fig. 19 (a) Normalized SANS curves in different $\text{D}_2\text{O}/\text{DMF-d}_7$ compositions at a polymer volume fraction of 0.25%. *Solid lines* represent fits with a spherical core shell model. Data in pure DMF-d_7 were fitted with a Beaucage form factor. (b) Aggregation number P plotted versus interfacial tension, γ . The *solid line* depicts the power-law dependence, $P \approx \gamma^{6/5}$, as predicted by Halperin for star-like micelles [40]. Reprinted with permission from [45]. Copyright (2004) American Chemical Society

scattering curves could be perfectly described using a hyperbolic density profile for the shell, $n(r) \approx r^{-4/3}$, indicative for star-like structures. The aggregation number of these micelles decreases from $P = 120$ in pure water to non-aggregated block copolymer chains in pure DMF. Corresponding interfacial tensions were measured by pendant drop tensiometry using a PEP homopolymer with similar molecular weight characteristics. In pure water, γ assumes a value of 46 mN/m, which decreases to 8.6 mN/m in pure DMF. A correlation of γ with P is shown Fig. 19b. The solid line indicates a power-law dependence of $P \approx \gamma^{6/5}$, revealing an excellent agreement of the data with the scaling prediction of Halperin [40] for star-like micelles.

The structural properties of micelles constituted of PEP1-PEO1 block copolymers were studied in DMF/water solvent mixtures [104]. Starting from cylindrical micelles in pure water, the addition of DMF (lowering of γ) leads to a morphological transition into spherical micelles at about 50% DMF mole fraction. By applying a detailed thermodynamic model, it was shown that both the dependence of the structural parameters with the interfacial tension as well as the morphological transition itself can be quantitatively understood. Interestingly, the cylinder-to-sphere transition, which is irreversible, can be also induced upon heating. This feature allowed the direct comparison of exchange kinetics in both morphologies without changing any other parameter of the system. Details of the kinetics will be discussed later in Section 4.6. Jensen et al. [143, 144] have used ethanol as co-solvent. Similar to the study of Lund et al. [48], they observed transitions from cylindrical to spherical micelles and from larger to smaller spherical micelles with increasing ethanol content.

A summary of the morphological behavior of PEP-PEO micelles is illustrated in Fig. 20a–d.

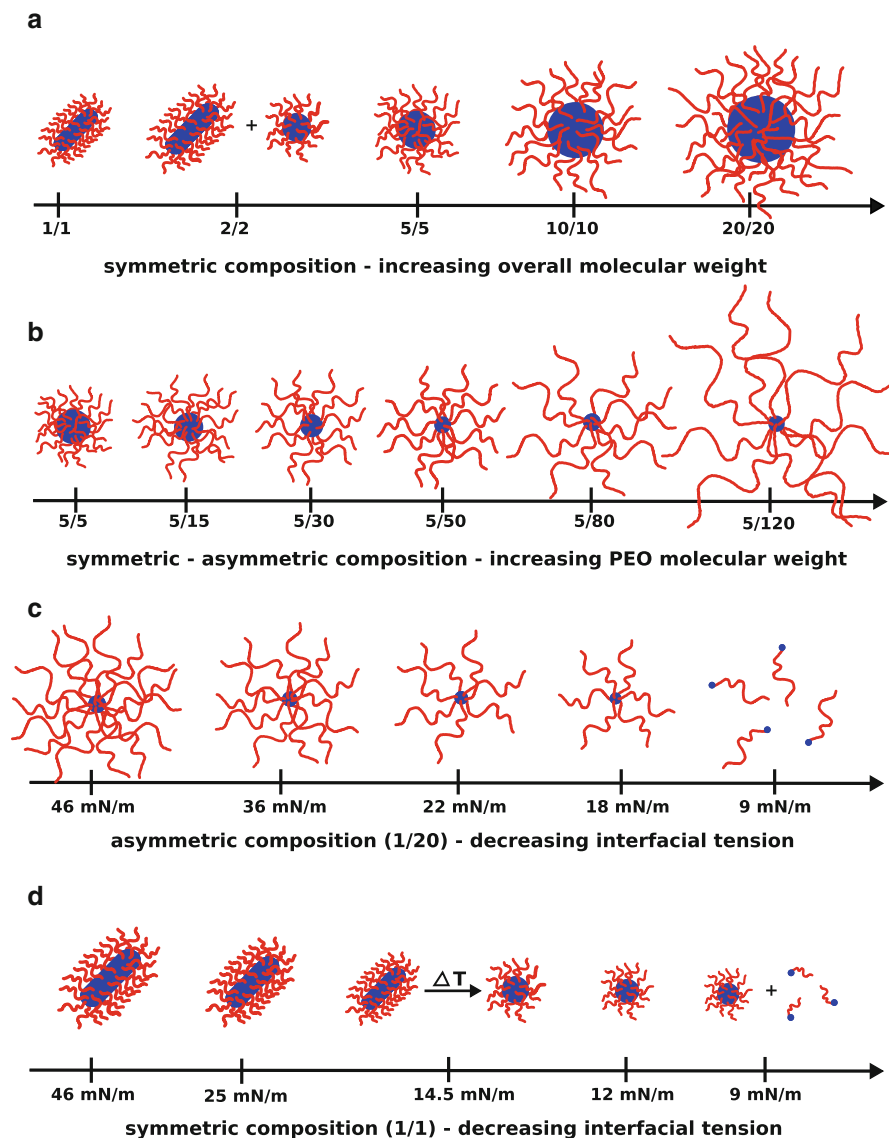


Fig. 20 Illustration of morphological behavior of PEP-PEO micelles in aqueous solution: Transition from (a) cylindrical to compact spherical micelles with increasing overall molecular weight at equal composition; (b) compact spherical micelles to star-like micelles with increasing PEO and constant PEP molecular weight; (c) star-like micelles to non-aggregated chains with decreasing γ by addition of DMF as co-solvent for PEP1-PEO20 block copolymers; (d) cylindrical to spherical micelles to coexisting spherical micelles/non-aggregated chains by adding DMF for a PEP1-PEO1 polymer

4.2.2 Equilibrium Kinetics in Pure Water: Frozen Micelles

Time-resolved SANS experiments using the H/D contrast scheme (KZAC) described in Sect. 3.1.7 were first carried out on a PEP5-PEO15 block copolymer in water for the determination of the unimer exchange kinetics [100]. However, there was no decrease in intensity observable even at high temperatures and long time scales, leading to the conclusion that the micelles are kinetically frozen due to the high interfacial tension between PEP and water. The kinetics of star-like micelles formed by a PEP1-PEO20 block copolymer with large compositional asymmetry and a short core-forming PEP block was investigated by Lund et al. [101, 102]. Analogous to the PEP5-PEO15 system, the TR-SANS experiment does not reveal any exchange of polymers over an extended period of time and increased temperature. This becomes obvious from Fig. 21 where SANS curves from the corresponding kinetic experiment are shown. Before mixing, typical form factors of star-like micelles were obtained. For better visibility, the arithmetic mean of the almost identical individual scattering curves of the labeled micelles are shown. This curve has a shallow maximum at low Q as a characteristic feature of a structure factor at 1% polymer volume fraction. After mixing the two differently labeled micellar solutions, the maximum disappears as a natural consequence of the ZAC condition. Details of the scattering behavior under ZAC are described in more detail in Sect. 3.2.2. However, the main result of this experiment is the fact that the intensity after mixing stays constant over an extended period of time, even at elevated temperatures. From this observation it was concluded that micelles are effectively frozen since due to chain exchange the intensity was expected to approach the intensity of the blend sample, depicted as black squares in Fig. 21. The blend sample consists of a random mixture of h-PEP1–h-PEO20 and d-PEP1–d-PEO20, providing the smallest contrast identical to the contrast of the final state of the kinetics after infinitely long time. A similar observation was made by Won, Davis, and Bates [146], who attempted to observe mixing kinetics or component exchange kinetics of PB-PEO micelles in water. Their experiment relied on differences in the SANS profiles of two block copolymers forming spherical or cylindrical micelles. Within a time period of 8 days, the scattering profile of a post-mixed specimen did not approach the profile of a premixed sample but rather resembled a superposition of the two micellar reservoirs. The structure of the premixed sample was expected to be the final structure in the case where chain exchange would lead to a reorganization of the micellar morphology. As this was not observed the authors concluded that the structure of the micelles that were initially formed upon dissolution were completely locked-in due to the effect of strong amphiphilicity. In a subsequent study, Jain and Bates [6] examined binary blends of PB-PEO block copolymers of different molecular weight and composition forming either spheres, cylinders, or bilayers using cryo-transmission electron microscopy (cryo-TEM). In agreement with the reorganization study by SANS, the cryo-TEM showed no perceptible chain exchange between aggregates over a long period of time, resulting in a non-ergodic state where equilibrium is never reached. The failure to globally equilibrate is already evident at molecular weights as small as

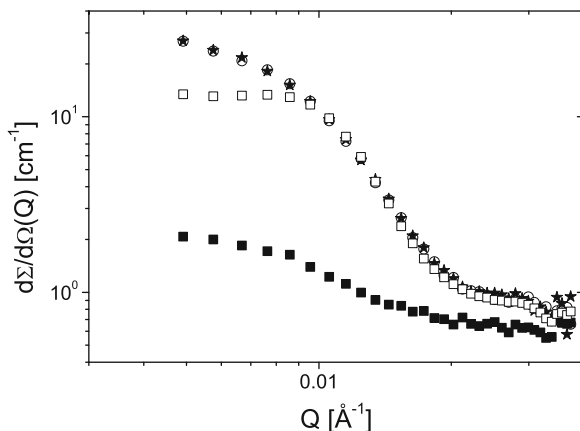


Fig. 21 SANS curves for the determination of chain exchange kinetics for h-PEP1–h-PEO20 and d-PEP1–d-PEO20 micelles in H₂O/D₂O at $\phi = 1\%$: *Open squares*, arithmetic mean of individual scattering curves before mixing; *open circles*, after mixing at $t = 0$; *filled stars*, after 24 h at 70°C; *filled squares*, final state obtained from a blend sample. Reprinted with permission from [102]. Copyright (2006) American Chemical Society

1–2 kg/mol of the core polymer. Hence, from the kinetic studies of both PEP-PEO and PB-PEO systems, it can be generally concluded that chain exchange dynamics in aggregates built from strong amphiphilic block copolymers, i.e., characterized with large interfacial tensions, is very likely to be frozen even at low molecular weights and elevated temperatures.

4.2.3 Tuning of Chain Exchange

As discussed above, chain exchange in micelles built from block copolymers with strong amphiphilicity, e.g., PEP-PEO or PB-PEO, is practically nonexistent. Consequently, such systems can be considered as effectively kinetically frozen. Therefore, in order to study such processes it is of great importance to adjust the rate of chain exchange such that it can be resolved within the time window of a typical scattering experiment. For instance, in a TR-SANS experiment using a stopped-flow apparatus for rapid mixing, the smallest achievable time resolution is about 50 ms. The longest accessible time is generally limited by the allocated beam time at neutron research facilities, which is typically 2–3 days. In order to identify effective tuning parameters we will briefly recall the Halperin and Alexander scaling approach outlined in Sect. 2.2.5. Within this theory, the exchange rate follows a single exponential behavior: $R(t) = \exp(-k_- t)$ with $k_- = (1/\tau_0) f(N_A, N_B) \exp(-E_a/k_B T)$ the expulsion rate constant. τ_0 denotes a characteristic diffusion time, k_B the Boltzmann constant, and T the absolute temperature. The activation energy, $E_a \sim \gamma \cdot l^2 \cdot N_B^{2/3}$ depends primarily on the degree of polymerization of core-forming B-block and the interfacial tension, γ , between selective solvent and block B.

We point out that the rate thus depends double exponentially on the interfacial tension, the temperature, and the degree of polymerization of the core block. Hence, these parameters are very effective for tuning the speed of chain exchange. The expression for the expulsion rate constant further contains a pre-exponential factor $f(N_A, N_B)$, which is determined by the micellar structure, i.e., crew-cut or star-like. Tuning by N_A will therefore be less effective because the rate depends only single-exponentially. Importantly, one should be aware that changing one or more of these parameters will also affect the underlying structure of the micelle. Therefore, a study of exchange kinetics requires a complementary structural characterization for each set of parameters.

Several strategies have been used to control the kinetics in polymeric micelles, including variation of temperature, change of the hydrophobic block size, and adjustment of the interfacial tension between core block and solvent [62, 63, 100–103, 114, 119, 120, 146–152]. We will review and discuss the effect of tuning on the kinetics by variation of γ because this parameter has been primarily used to control and to modify the exchange dynamics in micellar aggregates.

The interfacial tension can be effectively varied by modifying the incompatibility between core block and selective solvent. In general, for block copolymers with strong amphiphilicity in water, γ is very large such that even for short chains the micelles are kinetically frozen on experimental time scales. This applies especially for amphiphilic block copolymers with polybutadiene (PB), polyisoprene (PI), polystyrene (PS), poly(ethylene-*alt*-propylene) (PEP), or poly(butylene oxide) (PBO) as the hydrophobic block, having interfacial tensions against water typically larger than 30 mN/m. Several strategies have been employed to reduce γ in order to overcome the high barriers for chain exchange. One approach is the addition of small surfactant molecules. In the work of Jacquin et al. [151], the melting of kinetically frozen poly(butyl acrylate)-*block*-poly(acrylic acid) (PBA-PAA) micelles was investigated. They observed structural transitions from polymeric cylindrical micelles to spherical micelles as well as from large spherical to small spherical micelles upon addition of surfactant. Pendant drop tensiometry on PBA homopolymer in water and in surfactant solution revealed a drop in the interfacial tension from 20 mN/m to 5–8 mN/m. The low value of γ was explained by the incorporation of surfactant molecules into the interface, leading to the transition from frozen polymeric micelles to equilibrated surfactant/block copolymer mixed micelles.

Lejeune et al. [153] employed a chemical approach to lowering of interfacial tension in poly(*n*-butyl acrylate)-(polyacrylic acid) (PnBA-PAA). PnBA-PAA forms kinetically frozen micelles in water that are not able to reorganize over a month. By statistical incorporation of hydrophilic acrylic acid (AA) units into the hydrophobic PnBA block, P(nBA_{50%-stat}-AA_{50%})-PAA, they could moderate the hydrophobicity of the core block such that unimer exchange was promoted and thermodynamic equilibrium was reached at shorter times.

A more straightforward and facile way to tune the kinetics via reduction of the core-corona interfacial tension is by the addition of co-solvents. In the case of PEP-PEO micelles, the use of DMF/water mixtures as selective solvent for PEO

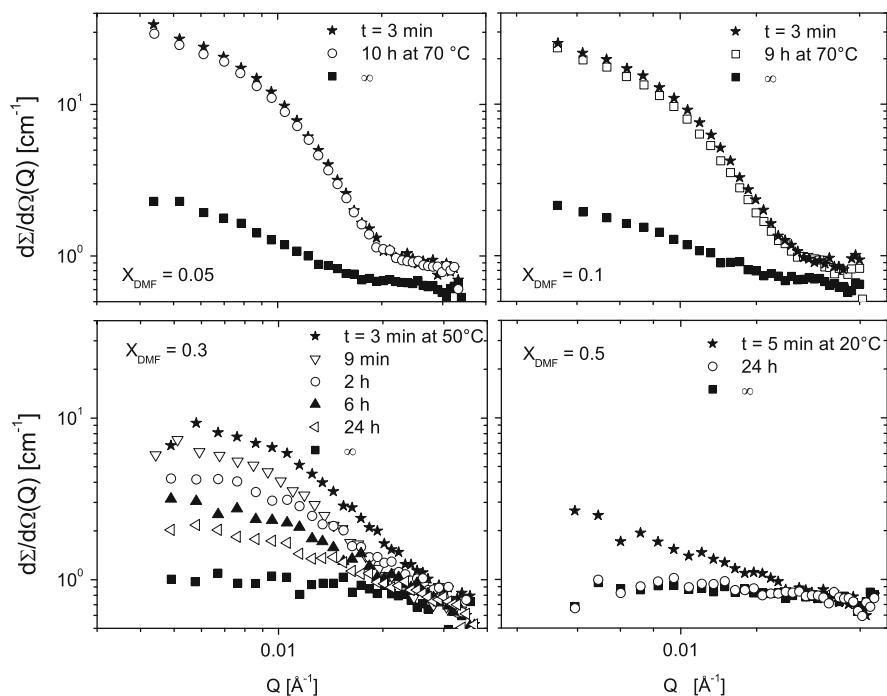


Fig. 22 Effect of the addition of DMF as co-solvent on the speed of chain exchange in aqueous PEP1-PEO20 micelles. Reprinted with permission from [102]. Copyright (2006) American Chemical Society

allows the adjustment of the rate of chain exchange from effectively frozen to accessible time scales of minutes or hours. The kinetics of a PEP5-PEO15 block copolymer was studied using pure DMF as selective solvent [100]. Although at room temperature the kinetics was still too slow, chain exchange became progressively faster at elevated temperatures between 65°C and 80°C . The influence of DMF on the kinetics of PEP1-PEO20 star-like micelles was studied by Lund et al. [102]. Figure 22 compares the time evolution of scattered intensity after mixing deuterated and proteated micelles at different DMF mole fractions in the water/DMF selective solvent mixture. At 5 and 10% DMF the intensity is only insignificantly reduced at 70°C after 9 and 10 h, respectively, revealing only slow kinetics. Upon increasing the DMF content to 30%, the scattered neutron intensity continuously decreases within a moderate time frame indicative of faster kinetics. At 50% DMF, $d\Sigma/d\Omega(Q)$ drops very fast and approaches the final state already after several minutes. For this solvent composition, the exchange dynamics was already too fast to be resolved by the TR-SANS technique. Finally, it turned out that the addition of 25 and 30% DMF, corresponding to a reduction in γ to 21.8 mN/m and 19.8 mN/m, respectively, moderates chain exchange such that the kinetic process could be conveniently followed. We note that mixing of the two micellar solutions was done by hand with a delay time of 1–2 min. A stopped-flow apparatus for rapid mixing in combination

with repetitive real-time data acquisition was not available at neutron research facilities at that time. Application of the stopped-flow mixing technique would most likely also allow resolving kinetics at 50% DMF by TR-SANS.

4.2.4 Equilibrium Kinetics in Water/DMF Mixtures: Logarithmic Relaxation

The relaxation functions, $R(t)$, of the TR-SANS experiments were quantitatively determined as described in Sect. 3.2.2. For the PEP5-PEO15 block copolymer micelles, $R(t)$ could be acceptably fitted by a sum of two exponentials. This was interpreted by the existence of two well-separated processes in time in strict conflict to the single exponential expected from the Halperin and Alexander [60] model. The activation energies of 29 KJ/mol for the slow and 12.2 KJ/mol for the fast process were deduced from Arrhenius plots. By estimation of the activation energy following the concepts of the scaling theory [60], the fast process was assigned to the unimer release. There was, however, no explanation for the existence of the second slow process. Different scenarios for the occurrence of two relaxation processes were discussed, including unimer diffusion between micelles, an isotope effect for the surface tension, the existence of two different species, and aggregation that supports fast exchange and slow rearrangement of the micelles. However, none of them could offer an explanation with a clear physical picture. Thus, the origin of the second slow process remained an open question. Double exponential time decays were also reported from TR-fluorescence measurements on various systems with characteristic rate constants well separated in time [118–120, 122]. This apparent bimodal distribution was either assigned to the presence of bulky labels [118, 122] or to competing chain transfer by micellar collision [120]. It should be pointed out that processes running in parallel, e.g., unimer exchange via micellar collision, just add to a single faster rate that still yields single exponential mixing: $R(t) \approx \exp(-(k_1 + k_2)t)$ and, consequently, cannot a priori be identified by the applied labeling techniques.

In continuation of the kinetic study of PEP5-PEO15 micelles, the relaxation functions of PEP1-PEO20 star-like micelles in water/DMF mixtures with 25 and 30% DMF were determined. Similarly to the PEP5-PEO15/DMF system, slow and heterogeneous kinetics were observed in this case but, in contrast, trial fits using a sum of two exponentials did not produce any satisfactory results. Therefore, it was more reasonable to assume a distribution of relaxation rates to describe the kinetics in PEP1-PEO20/water/DMF systems. Furthermore, as there was no explanation for the existence of two processes and no exclusive fits were performed, it was concluded that in the previous works the double exponential was more an approximation of a continuous distribution of relaxation rates. As a first obvious reason, a chain length distribution (polydispersity) of the core-forming polymer was taken into account since the rate constants exponentially depend on the activation energy, E_a , which in the Halperin and Alexander model is given by $E_a \sim N_B^{2/3} \cdot \gamma \cdot l^2$.

The PEP block was synthesized by living anionic polymerization with a rather small polydispersity (weight average molecular weight/number average molecular weight), $M_w/M_n = 1.06$. Accordingly, the effect of a distribution of chain length on the relaxation rates was taken into account by:

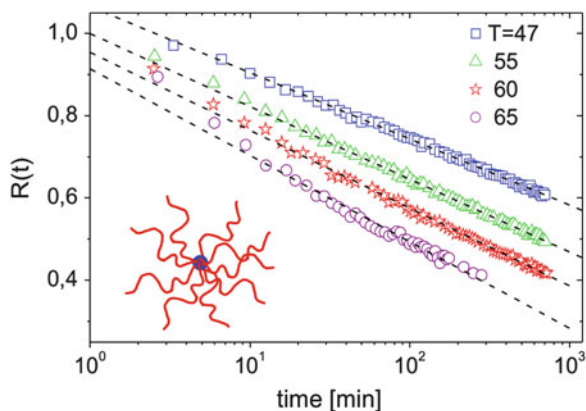
$$R(t) = \int_1^{\infty} f(N_B, \sigma) \exp(-k_-(N_B)t) dN_B \quad (117)$$

where:

$$f(N_B, \sigma) = \frac{(\langle N_B \rangle - 1)^{N_B-1} \exp(-(\langle N_B \rangle - 1))}{\Gamma(N_B)} \quad (118)$$

denotes the Poisson distribution, with $\Gamma(N_B)$ being the gamma function and k_- the expulsion rate constant. Polymers prepared by living anionic polymerization exhibit a Poisson-type chain length distribution where the width is directly given by the mean value of $\langle N_B \rangle$ by $\sigma = 1 + 1/\sqrt{\langle N_B \rangle}$. Nevertheless, the agreement with the data was still very poor and, hence, it was concluded that polydispersity alone is not sufficient to explain the broad relaxation pattern. It should, however, be noted that the prefactor α in the expression for the activation barrier [37] was neglected and simply set to 1. Further, in order to describe the data, a Gaussian distribution of activation energies has been used. This more general approach takes into account all factors that independently contribute to the relaxation. Although excellent fits could be obtained, the fitted mean activation energy, the attempt time, and the distribution all assumed unphysical values such that the Gaussian distribution was considered to be inapplicable for a reasonable explanation of the relaxation behavior. Similarly, a stretched exponential, $R(t) = \exp(-kt)^\beta$ has been applied, again with unsatisfactory fits because the parameters were not well defined and β assumes very low values ($\beta \approx 0.1$ – 0.2) that reflect a very broad distribution. A more close inspection of the relaxation data finally revealed an extremely broad and heterogeneous logarithmical decay over several decades in time $R(t) \approx -\log(t)$ that was independent of concentration and temperature. This is represented in Fig. 23, where $R(t)$ displays an almost straight line on a logarithmic time scale. The logarithmic relaxation a priori implies that no mean rate constant exists. At that point, the appearance of the logarithmic relaxation was interpreted as a consequence of uncharacterized hierarchical processes [154]. A more straightforward explanation for the existence of the broad relaxation was presented by Choi et al. [63], based on the polydispersity model already introduced earlier [101, 102] (Eq. 117). By taking into account prefactors and the temperature dependence of the diffusion coefficient previously ignored, it was argued that the observed hypersensitivity to core chain length was responsible for the logarithmic relaxation. This will be discussed in detail in the subsequent section.

Fig. 23 Ln-log representation of the relaxation function $R(t)$ of PEP1-PEO20 star-like micelles in water/DMF mixtures with 25% DMF at different temperatures. Dashed lines depict fits with a logarithmic time decay. Reprinted with permission from [101]. Copyright (2006) by the American Physical Society



4.3 Block Copolymer Micelles in Organic Solvents

In this section, we will focus on the kinetics of micelles built from diblock copolymers in organic solvents. Typical systems are polystyrene–polybutadiene (PS-PB), polystyrene–polyisoprene (PS-PI), or polystyrene–poly(ethylene-*alt*-propylene) (PS-PEP) block copolymers in hydrocarbon solvents like alkanes. Alkanes are poor solvents for PS and good solvents for the polydienes and PEP, respectively, such that in all cases PS forms the micellar core. A common feature of these systems is the fact that the thermodynamic interactions are significantly weaker than in water-based micelles, reflected by small χ parameters or correspondingly by low interfacial tensions. Accordingly, such systems are only weakly segregated, which may lead to micellar cores considerably swollen by the solvent. This has been observed, e.g., by SANS on PS-PI micelles in *n*-decane [74] and PS-PB micelles [30] in a series of *n*-alkanes (C_nH_{2n+2} , where $n = 7, 10, 12, 14$, or 16) by using contrast variation and detailed model fitting. For the PS-PI micelles in *n*-decane, the core was swollen with 15–25% solvent, depending on molecular weight. For micelles formed by a symmetric PS-PB block copolymer, the solvent fraction was even higher (35–55%) but decreased with increasing number of carbon atoms of the *n*-alkane solvent. The opposite trend was observed for the aggregation number, which increases with n although the interfacial tension stays constant or even slightly decreases from 5.7 mN/m for *n*-heptane to 4.8 mN/m for *n*-hexadecane. This unexpected behavior can be understood by applying a modified mean-field model that properly takes into account solvent entropy effects [30]. The chain exchange kinetics of the PS-PB system was studied in the different *n*-alkanes by TR-SANS [150, 155]. The study revealed that the exchange dynamics depend strongly on the choice of solvent. For instance, in *n*-decane exchange is very fast and outside the time window accessible by TR-SANS. This was still the case after lowering the temperature to 10°C. If the carbon length of the solvent is increased, the exchange dynamics decrease and is slowest for *n*-hexadecane where the time scale is optimal for TR-SANS measurements. It should be noted that the activation barrier, E_a , for unimer release

does not significantly change with the solvent size because γ stays almost constant. Therefore, in order to explain the effect of solvent chain length, it was considered that PS in the bulk state has a glass transition temperature (T_g) of 105°C but when swollen with *n*-alkanes, T_g is significantly reduced. The swelling ability and solvent quality, however, depend drastically on the number of carbons, *n*, of the *n*-alkyl solvent, which in turn also changes T_g . For example, for a bulk PS containing 18 vol% *n*-heptane, the glass transition is reduced from 105°C to −11°C whereas with 15 vol% *n*-octane T_g is only lowered to 40°C [156]. Quintana et al. [157, 158] have studied the micellization behavior of PS-PEP polymers in *n*-alkanes. They reported that the dependence of micellar properties on the temperature is decreased for longer *n*-alkanes. This was explained by a higher T_g of the PS core that is swollen to a lesser extent as *n* increases. This trend was further confirmed by structural studies of PS-PEP micelles in squalane by Choi et al. [159]. Squalane is a natural hydrocarbon with the molecular formula $C_{30}H_{62}$. Dynamic light scattering and SAXS experiments showed that below 100°C micellar cores are practically unswollen. Clear penetration of solvent into the PS core was observed only above 100°C close to the bulk T_g of PS. Nevertheless, the glass transition of PS-rich domains of PS-PI polymers in squalane was found to be considerably reduced as measured by Lai et al. [160]. They found that, depending on the PS weight fraction in solution, T_g is reduced to 70°C. Based on these findings it is reasonable to assume that the measured decrease in the exchange dynamics of PS-PB polymers in *n*-alkanes is directly related to the increase in T_g of the PS core.

In order to be independent of any feature related to the glass transition, the kinetics of PS-PB micelles formed in DMF were additionally studied by Lund et al. [101]. DMF is selective for PS such that the micelles consist of a melt-like PB core with a T_g of −95°C and a swollen PS corona. Structural studies by SANS have shown that the PB core is solvent-free and the corona has a compact structure with a constant polymer density distribution [155]. Hence, in DMF these micelles are inverted analogues to those in *n*-alkanes but with unswollen cores. Exchange kinetics could be conveniently measured by TR-SANS in a time range of 10 h until an almost statistical distribution of proteated and deuterated block copolymers across the micelles was reached. A thorough evaluation of the relaxation kinetics of the symmetric PS-PB block copolymer micelles in *n*-hexadecane and in DMF shows in agreement with the exchange kinetics in PEP-PEO micelles in water/DMF, i.e., a logarithmic time dependence indicating an extremely broad distribution of relaxation rates (Figs. 23 and 24).

Because this observation was obtained independently from three structurally different types of micelles, it was concluded that the broad relaxation is an inherent property of block copolymer micelles. Consistent with these findings is the almost linear dependence of $R(t)$ on a log-time scale of PS-PEP micelles in squalane presented by Choi et al. [63]. They used TR-SANS to study two pairs of PS-PEP micelles, d-PS-*h*-PEP-1/*h*-PS-*h*-PEP-1 and d-PS-*h*-PEP-2/*h*-PS-*h*-PEP-2 with different PS degrees of polymerization: pair 1, $N_{PS} \approx 255$ and pair 2, $N_{PS} \approx 412$. Each specimen was measured at three different temperatures. Individual master curves for $R(t)$ were obtained by time-temperature superposition principles. A comparison of $R(t)$ of the two PS-PEP samples was done at a reference temperature of 125°C and

Fig. 24 Logarithmic chain exchange kinetics of PS-PB block copolymer micelles (*top*) in DMF at 20°C (*stars*) and of inverted micelles (*bottom*) with swollen PS cores in *n*-hexadecane at 20°C (*circles*) and 30°C (*triangles*). *Lines* depict fits with a logarithmic time decay. Reprinted with permission from [101]. Copyright (2006) by the American Physical Society

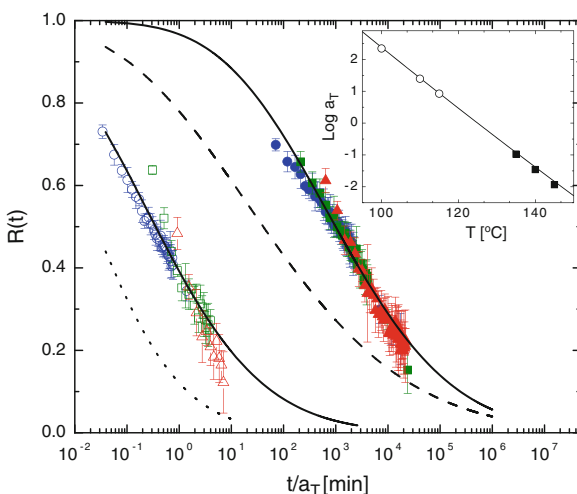
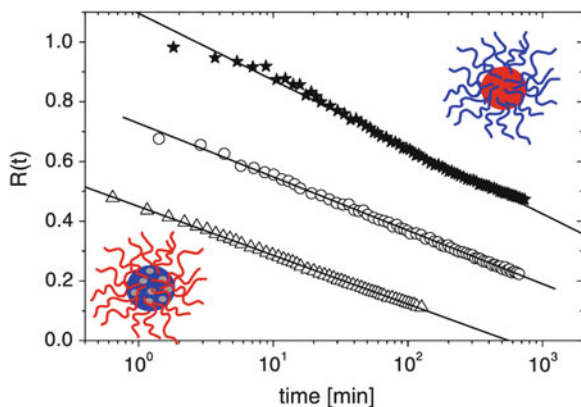


Fig. 25 Comparison of the master curves in dilute solution of PS-PEP-1 (*open symbols*: blue $T = 100^\circ\text{C}$; green $T = 110^\circ\text{C}$; red $T = 115^\circ\text{C}$); and PS-PEP-2 (*filled symbols*: blue $T = 135^\circ\text{C}$; green $T = 140^\circ\text{C}$; red $T = 145^\circ\text{C}$) in squalane at $T_{\text{ref}} = 125^\circ\text{C}$. The shift factors a_T used for generating the master curves are shown in the *inset*. *Solid lines* are fits of the theoretical model of Choi et al. [63, 152]. The dashed and dotted lines represent calculations with varying $\alpha\chi$ in order to demonstrate the high sensitivity of the fit to this parameter. Reprinted with permission from [63]. Copyright (2010) by the American Physical Society

demonstrated an extremely strong dependence on N_{PS} by approximately four orders of magnitude in time (Fig. 25).

In order to describe the data, Choi, Lodge, and Bates [63] based their model on theories of diffusion in block copolymer melts [161]. In their approach, the activation energy is written as:

$$E_a = \alpha\chi \cdot N_B \quad (119)$$

where α again is a free prefactor and χ the Flory–Huggins interaction parameter, χN denotes enthalpically unfavorable contacts between solvent and hydrophobic block segments. We note that the scaling is equivalent to that presented for E_a in Eq. 37 with $\beta = 1$.

Setting the time scale for the escape rate constant, Choi and colleagues used the longest Rouse time to replace the pre-exponential factor in Eq. 37⁷:

$$\tau_0 = \tau_R = \xi N_B^2 l_B^2 / (6\pi^2 k_B T) \quad (120)$$

with ξ being the monomeric friction for PS. The use of Rouse relaxation was justified by the fact that the short PS blocks are only weakly entangled. Motivated by the observed dramatic dependence on N_{PS} the authors anticipated that the distribution of core chain length must play an important role in the exchange dynamics. Hence, they modified the kinetics by using a Schulz–Zimm distribution for the core chain length:

$$f(N_B, \zeta) = \frac{\zeta^{\zeta+1}}{\Gamma(\zeta+1)} \cdot \frac{N_B^{\zeta-1}}{\langle N_B \rangle^\zeta} \cdot \exp(-\zeta \cdot N_B / \langle N_B \rangle) \quad (121)$$

Here $\zeta = 1/(N_w/N_n - 1)$, where N_w/N_n defines the polydispersity of the PS polymer. We note that the Schulz–Zimm distribution is a two parameter function where the width and the mean value can be adjusted independently. The use of the one-parameter Poisson distribution requires that the polymerization process occurs under ideal conditions, which in practical situations is not always guaranteed. By fitting with the above-described model, Choi et al. obtained an excellent agreement with the kinetic data using $\alpha\chi$ and N_w/N_n as free parameters. Optimal fitting was obtained for narrow polydispersities in close agreement with values received from standard polymer characterization. Variation of this fit parameter results in significant changes in the structure of $R(t)$, while on the other hand small changes in $\alpha\chi$ lead to a strong shift of $R(t)$ along the time axis, as demonstrated by the dashed and dotted lines in Fig. 25. By using two block copolymers with different core block molecular weights, the authors could finally uncover the hypersensitivity of chain length on the kinetics that, consequently, leads to the pronounced effect of polydispersity. In light of these results, Lund and coworkers [62] re-evaluated their data by considering the prefactor α as a free parameter. Moreover, to account for the temperature dependence, an attempt time $\tau = \tau_0 \cdot \xi(T) / \left(\xi(47) \cdot \left(\frac{N}{\langle N \rangle} \right)^{2/25} \right)$, with $\langle N \rangle$ being the mean number of repeat units, that scales with the friction coefficient $\xi(T)$ of PEP for a homopolymer melt was considered. Thus, a perfect reproduction of the logarithmic time decay was possible. However, a fit of β revealed $\beta = 2/3$, indicating a fully

⁷ In the original work by Halperin and Alexander (c.f. Eq. 33), τ is a function of N_B and N_A , i.e., $\tau = \tau_0 \cdot g(N_A, N_B)$, also taking into account the diffusion of the chain within the corona. Here, this is replaced by the Rouse time.

collapsed insoluble block during the expulsion process. The parameter $\alpha(36\pi)$ was fitted to be approximately equal to 3.3 instead of 4.8, as expected for spherical globules. This disagreement was thought to be due to deviations from the spherical conformation or to interfacial effects resulting from modifications of the surface energy by the other block. The best value for τ_0 was fitted to 2.4×10^{-7} s, which is comparable to a typical elemental time expected for polymer dynamics. In summary, the work of Choi et al. and, subsequently, the novel interpretation of the data of Lund et al. strongly corroborate that the pseudo-logarithmic time decay in the equilibrium kinetics is a consequence of core block polydispersity, which can be rationalized by a double exponential dependence of the exchange rate on chain length. In principle, both experiments essentially confirm the validity of the theory of Halperin and Alexander. However, there remain several contradictions concerning the exact mechanism, in particular the adopted chain conformation during the activated step of the exchange process. This still needs to be delineated in future experiments. These details of the mechanism can be more conveniently studied using a monodisperse system. Such a system will be discussed in the next section.

4.4 *n*-Alkyl-PEO Polymeric Micelles

The chain exchange kinetics of *n*-alkyl-PEO (C_nH_{2n-1} , where $n = 18, 24$, or 30) polymeric micelles in water was studied by Zinn et al. [103]. Structurally, the *n*-alkyl-PEO polymers can be considered as hybrids between amphiphilic block polymers (e.g., PEP-PEO or PEE-PEO) and nonionic $C_n(EO)_m$ surfactants. With respect to the exchange kinetics, these materials were taken as model system because the polydisperse hydrocarbon block is replaced by a relatively short but truly monodisperse ($M_w/M_n = 1$) aliphatic chain. Accordingly, if the above considerations were true, the relaxation kinetics was expected to follow a single exponential decay. Moreover, variation of n should directly reflect the dependence on chain length and thus the effect of polydispersity on the time decay of $R(t)$. In fact, the kinetic measurements reveal a strong dependence on the alkyl chain length, as depicted in Fig. 26, where the neutron detector count rates are plotted versus time after mixing the two differently labeled (H/D) micellar species at room temperature (22°C). The figure shows that within five orders of magnitude in time up to 1,000 s, the count rate of the $C_{30}H_{61}$ -PEO5 micelles (squares in Fig. 26) stays constant revealing no chain exchange. For the $C_{18}H_{37}$ -PEO5 micelles (triangles Fig. 26) on the other hand, full equilibration (depicted by the solid line in Fig. 26) was already obtained after a few milliseconds. Apparently, the relaxation process is too fast to be resolved by TR-SANS. Only for the $C_{24}H_{49}$ -PEO5 system (circles Fig. 26) could the full process of chain exchange be measured, indicated by the continuous decay of the count rate from initial to final state in a time frame of 100 s. Figure 27 shows the corresponding relaxation function on a logarithmic time scale. The linear decay in this representation perfectly revealed the theoretically expected single exponential decay: $R(t) = \exp(-t/\tau_0)$ with a characteristic time $\tau_0 = 44$ s. It should be mentioned that evaluation of the data using either the model-dependent, f_{exc} , or model-independent method, $R(t)$, (for details see Sect. 3.2.2)

Fig. 26 Detector count rates as a function of time after mixing oppositely labeled n -alkyl-PEO5 polymeric micelles: *squares* $n = 30$; *dots* $n = 24$; *triangles* $n = 18$; *solid line* final state. [103]. Reproduced by permission of The Royal Society of Chemistry

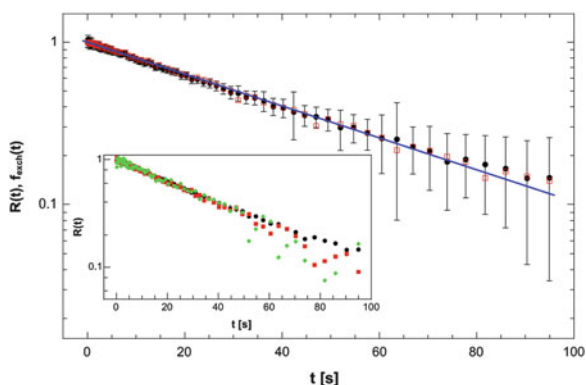
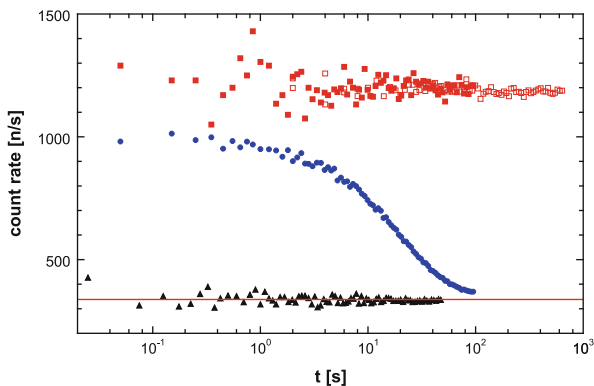


Fig. 27 Relaxation function $R(t)$ (filled circles) and $f_{\text{exch}}(t)$ (open squares) of $\text{C}_{24}\text{H}_{49}\text{PEO}5$ in a log-ln plot at room temperature. The line represents the single exponential fit for $R(t)$. Inset: Concentration dependence of $R(t)$ at 0.25% (diamonds), 0.5% (squares), and 1% (circles) polymer volume fraction. [103]. Reproduced by permission of The Royal Society of Chemistry

gave the same results, most likely due to the chosen small Q -range, where form factor differences of the two differently labeled polymers do not play a role. The inset of Fig. 27 shows relaxation curves measured at different polymer volume fractions of $\phi = 0.25\%$, 0.5% , and 1% . By normalization with ϕ , all curves fall on top of each other indicating single unimer exchange as the dominating mechanism. Fusion and fission as competing processes for chain exchange would lead to accelerated kinetics because the probability of micellar collisions is increased with concentration. A single exponential decay was also observed by dissipative particle dynamics simulation but, in addition to single unimer exchange, contributions from small aggregate fragmentation/merging and unequal size fusion/fission were found as additional kinetic mechanisms; however, all exhibit very similar relaxation times [162].

The observed strong dependence of the exchange rate on the n -alkyl chain length together with the single exponential relaxation found for the $\text{C}_{24}\text{H}_{49}\text{-PEO}5$ system supports the assumption of Choi et al. [63] that core block polydispersity leads to the

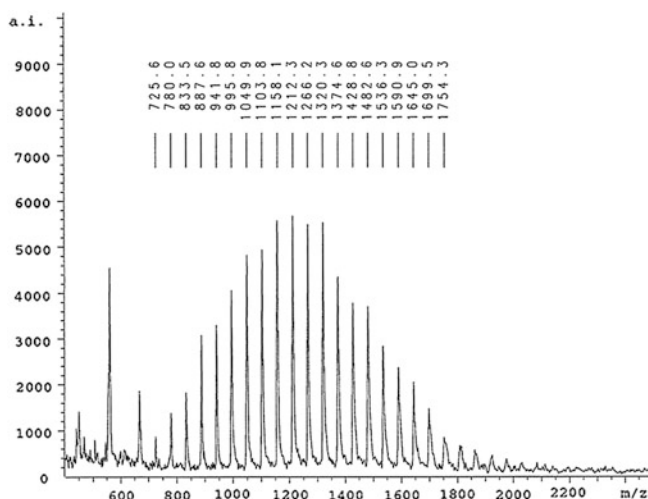


Fig. 28 MALDI-TOF measurement of a 1,4-PB with $M_n = 1.305$ kg/mol and $M_w/M_n = 1.05$

pseudo-logarithmic relaxation in polymeric micelles. This applies also for polymers with small polydispersities (M_w/M_n smaller than 1.1), usually obtained by living polymerization techniques. The actual distribution of chain length is demonstrated in Fig. 28, which shows the result of a MALDI-TOF measurement of a polybutadiene with $M_n = 1.305$ kg/mol and $M_w/M_n = 1.05$, similar to the molecular weight characteristics of PEP1 used as hydrophobic block in the kinetic study of the PEP1-PEO20 water/DMF system. In the MALDI spectrum, the individual chains with different mass constituting the PB polymer are resolved. If one considers that each of these chains has its own activation energy, the measured broad relaxation pattern becomes obvious. It further leads to the conclusion that many block copolymer micellar systems can only partially equilibrate since long chains with high activation energies will not exchange on finite time scales. Therefore, the strict distinction between dynamic polymeric micelles versus frozen nanoparticles, as recently suggested by Nicolai et al. [163], cannot be made a priori. This presumes on the one hand that the exchange rate is either very fast, such that even the long chains will equilibrate, or on the other hand is very slow so that short chains are also frozen on experimental time scale. However, in order to be certain, a kinetic study for each individual block copolymer solvent system is required.

4.5 Chain Exchange in Soft Solids: Effect of Concentration

Kinetic experiments reviewed so far were all made in dilute solution at less than 2% polymer volume fraction. In this concentration range the measured relaxation curves were found to be independent of concentration, revealing single unimer

exchange as the dominant mechanism for chain exchange in agreement with the theoretical picture of Halperin and Alexander. Exchange due to other mechanisms, e.g., fusion/fission or fragmentation/defragmentation, if at all existent can play only a minor role because they would show a clear concentration dependence.

Recently, Choi et al. [152] measured the molecular exchange in ordered diblock copolymer micelles, employing the same PS-PEP micelles in squalane as already studied before in dilute solution by TR-SANS. At 15% polymer volume fraction, the spherical micelles are packed on body centered cubic (bcc) lattices. Individual micellar solution with 15 vol% of h-PS-PEP or d-PS-PEP were annealed far above T_g , resulting in soft solids after cooling to room temperature. Blending of the soft solids on a nanoscale level with a complete statistical arrangement of micelles was achieved by a special cup-rotor mixer device [94]. The efficiency of this technique was demonstrated by a combination of SANS and SAXS measurements. While the SAXS data confirmed the bcc structure of the mixture, the SANS data showed the single micellar form factor since intraparticle contributions were canceled out due to the applied ZAC. Notable was the observation that in comparison to dilute solution, individual micelles had increased aggregation numbers and core radii. This was attributed to the system's tendency to avoid energetically unfavorable corona overlap by reducing the number density of micelles, as discussed in the mean-field model of Grason [164]. The kinetic studies were carried out at different temperatures above the glass transition of PS in an isotopic mixtures of squalane ($T_g \approx 70^\circ\text{C}$). In order to account for the temperature dependence, individual master curves were derived by the principle of time-temperature superposition. A comparison of the master curves at dilute solution and at 15% polymer volume fraction are shown in Fig. 29 at a reference temperature $T_{\text{ref}} = 110^\circ\text{C}$ for PS-PEP-1 and $T_{\text{ref}} = 145^\circ\text{C}$ for PS-PEP-2. We note that time-temperature superposition for the higher concentrations does not work as well as for the dilute solutions. The data do not exactly superimpose by using the shift factors, a_T , shown in the inset of Fig. 29. Nevertheless, the obtained curves show the typical logarithmic time decay consistent with the finding at dilute solution. The relaxation curves obtained for the soft solids are, however, shifted to longer times by more than one order of magnitude. Because of the logarithmic form of $R(t)$, the molecular exchange kinetics could be described by the same theoretical model as already used for the dilute solutions (see Eqs. 119, 120, and 121). Reasonable fits were obtained by increasing the activation barrier through an increase in the parameter $\alpha\chi$ and by slightly adjusting the polydispersity of the core block.

The authors postulated several reasons for the slowing down of the exchange rate at higher concentrations. These include weaker mobility arising from a higher glass transition of the core polymer. A higher T_g was assumed because the tendency of solvent to penetrate the core is reduced at higher block copolymer concentration. However, this effect was considered to be too small to account for the dramatic change observed for the chain exchange dynamics. It was also suggested that increased core chain stretching arising from increased micellar sizes in the bcc state could lead to altered Rouse dynamics. It was, however, estimated that core block stretching cannot be so significant in the low entanglement regime to reasonably explain the slowdown of the kinetics. As the most probable explanation,

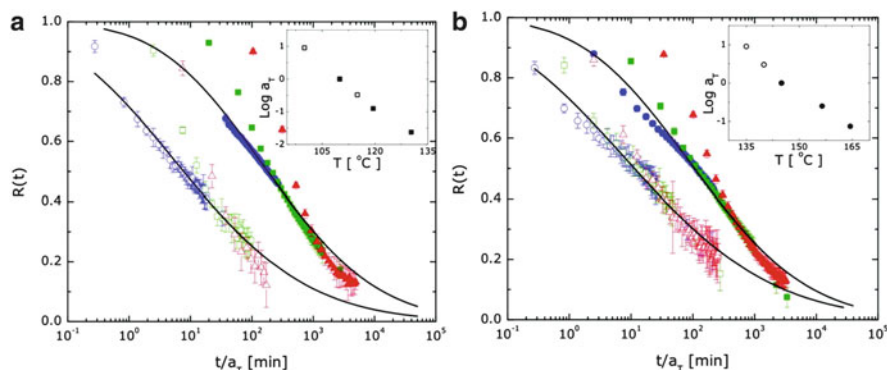


Fig. 29 Comparison of the relaxation curves at dilute solution (*open symbols*, already shown in Fig. 25) and of soft solids at 15% polymer volume fraction (*filled symbols*) in squalane for (a) PS-PEP-1 at $T_{\text{ref}} = 110^\circ\text{C}$ [originally measured at 110°C (*filled circles*), 119.5°C (*filled squares*) and 130.3°C (*filled triangles*); and (b) PS-PEP-2 for $T_{\text{ref}} = 145^\circ\text{C}$ [originally measured at 144.5°C (*filled squares*), 156.5°C (*filled circles*), and 165.5°C (*filled triangles*)]. The shift factors a_T used for generating master curves are shown in the *inset*. *Solid lines* are fits of the theoretical model of Choi et al. [63, 152]. Reprinted with permission from [152]. Copyright (2011) American Chemical Society

the authors proposed that the deceleration in chain exchange might arise from considerable corona overlap of neighboring micelles at higher concentration. Crowding of corona polymer should generate an additional contribution to the activation barrier because a single polymer would be more easily soluble in dilute solution than in semidilute solution.

Based on this experimental observation, Halperin extended the original scaling model to higher concentrations by introducing an additional penalty term that takes into account an increase in the osmotic pressure due to coronal screening. This was outlined in Sect. 2.2.7. Halperin further suggested that for a systematic investigation, coronal screening can also be obtained by the addition of soluble corona homopolymer while keeping a dilute solution of micelles. This would facilitate the interpretation because other possible mechanisms like fusion and fission, which are expected from computer simulation and theory, occur at higher concentrations and need not to be discussed.

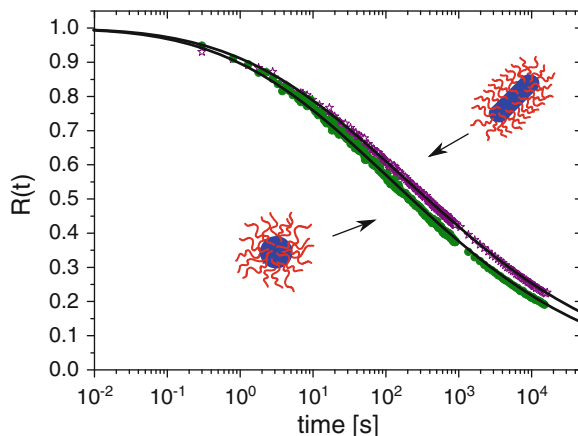
4.6 Cylinders Versus Spheres: Effect of Morphology

The influence of micellar morphology on the exchange kinetics in diblock copolymer micelles has been investigated by Lund et al. [104]. The studied system was a short chain PEP1-PEO1 copolymer with symmetric block composition in water/DMF mixtures as selective solvents for PEO. The morphological behavior of this system has already been described. The main features are illustrated in Fig. 20d.

It can be seen that cylinders are formed in water and in water/DMF mixtures with low DMF fractions, i.e., high interfacial tensions, whereas spherical micelles occur above ~ 50 mol % DMF at low interfacial tensions. TR-SANS experiments were performed at different DMF/water compositions for both cylindrical and spherical geometries at 41%, 47%, 60%, and 75% DMF mole fraction. As already observed for PEP1-PEO20 micelles [102], chain exchange became increasingly faster with growing DMF content due to lower interfacial tensions (see Fig. 22). In order to access the initial part of the relaxation, a stopped-flow apparatus for rapid mixing was used. Technical details of the stopped flow method are given in Sect. 3.2.1. However, with 75% DMF in the selective solvent mixture, chain exchange was already too fast to be resolved even with the stopped-flow fast mixing technique. The relaxation curves obtained for the other solvent compositions showed an extended decay over several orders of magnitude in time, which for intermediate and long time scales was again quasi-logarithmic. Accordingly, the data were analyzed using Eq. 117 by taking into account the polydispersity of the PEP block by a Schulz–Zimm distribution (Eq. 121). In accord with the model of Choi, Bates, and Lodge [63], the longest Rouse time was used as pre-exponential factor as defined in Eq. 120. Independent of the morphology, good fits were only obtained by taking $\beta = 1$ implying a stretched conformation of the insoluble block during the expulsion process (see Sect. 2.2.6.).

The parameter α assumed values that were about a factor of three smaller than expected from the geometrical estimate. Parallel to the transition from cylinders to spheres, α slightly decreases. However, this does not clearly reflect any influence of the morphology because the fits are very sensitive to α and other influences (e.g., arising from experimental uncertainties) cannot be fully excluded. Therefore, in order to delineate any factors arising from the different morphologies, Lund et al. have exploited the fact that at 50% DMF fraction the transition can be also induced by heating. Dissolution of the polymer at room temperature leads first to stable cylindrical micelles, which transform into spherical entities after annealing for several hours at 70°C. Importantly, the transition is irreversible, meaning that the spherical shape is preserved at low temperatures. The exchange kinetics was then measured in both morphologies on the same specimen by TR-SANS under exactly the same conditions. The authors found that the kinetics in spherical morphology is slightly but unambiguously faster than for cylinders, as shown in Fig. 30. With respect to the fit parameters, the faster kinetics is reflected by a slightly smaller α while $\beta = 1$ was kept constant. This was found to be in accordance with the slightly more pronounced decrease in α for varying DMF composition. The value of $\beta = 1$ was in contrast to $\beta = 2/3$ found for PEP1-PEO20 star-like micelles in which the PEP1 chain assumes a completely segregated spherical bud. It was argued that a stretched conformation facilitates passage through the more dense corona of the spherical and cylindrical crew-cut type micelles obtained from PEP1-PEO1 block copolymers. An interpretation of the small differences in α is, however, difficult. It was speculated that this has its origin in small variances in the local coronal structure, which may be different for the cylindrical and spherical morphologies.

Fig. 30 Comparison of exchange kinetics in spherical and cylindrical morphology of PEP1-PEO1 block copolymers in water/DMF mixture before and after the thermally induced transition. Solid lines represent model fits as described in the text. Reprinted with permission from [48]. Copyright (2011) American Chemical Society



4.7 Summary

In general, the experimental results obtained by the TR-SANS technique strongly indicate that the component exchange kinetics of all the micellar systems investigated occurs solely via the Aniansson and Wall mechanism, i.e., the insertion/expulsion of only single chains at a given time even for elevated concentrations. The involved activation energy for chain expulsion scales with the core block degree of polymerization and the interfacial tension: $E_A \sim \alpha \gamma N_B^\beta$, thus determining the relaxation rate double exponentially. The observed strong dependence on the core block degree of polymerization finally allowed explanation of the logarithmic time decay by the finite polydispersity of the insoluble block, even for chains with a narrow chain length distribution. Thus, from theoretical and experimental points of view one can conclude that the equilibrium kinetics in block copolymer micelles in dilute solution is essentially understood. Solely the value of the exponent β and of the numerical prefactor α remain unclear. For $\beta = 2/3$, the activation energy is determined by the interfacial tension arising from surface contacts between the fully collapsed insoluble block and the solvent in the corona of the micelle. For $\beta = 1$, the expelled insoluble block is still swollen with solvent and E_a is determined by monomer–solvent contacts via the Flory–Huggins interaction parameter, χN . A visualization of the two discussed possibilities for chain expulsion is shown in Fig. 31.

Deviations of the parameter α from the theoretical value may be due to small variations in local structural properties of the “activated complex” during the expulsion process. Here, factors like screening of solvent/core polymer contacts by the corona block and ill-defined core–corona interfaces might come into play. However, discrepancies could also arise from small uncertainties in the determination of polymer characteristics. However, these discrepancies are obviously system-specific and depend on selective solvent, type of block polymer, temperature, and degree of polymerization and are thus of minor relevance for the general understanding of equilibrium kinetics. From the experimental point of view, a more systematic study

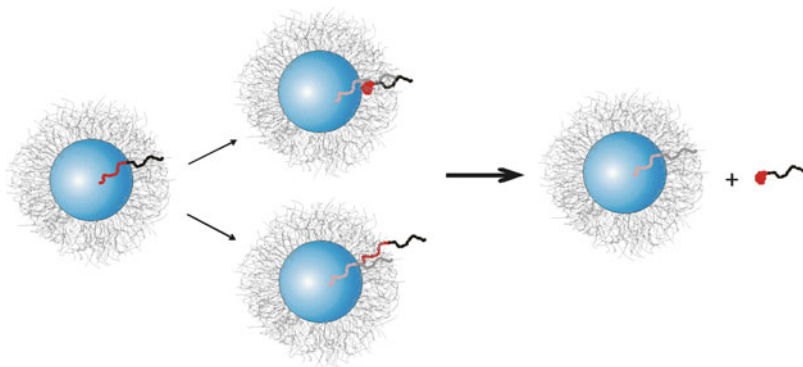


Fig. 31 Scheme for two possible scenarios for chain expulsion determining the activation energy: core chain forms a bud in the corona (*top*) or adopts a linear conformation (*bottom*) leading to an exponent $\beta = 2/3$ or 1, respectively. Reprinted with permission from [104]. Copyright (2011) American Chemical Society

of the concentration dependence is desirable in order to scrutinize in more detail the slowing down of chain exchange observed in ordered diblock copolymer micelles. Moreover, the diffusion process through the corona should be investigated. Thus, variation of the corona chain length needs still to be explored although this might only be a minor factor and perhaps mostly relevant for star-like micelles. Motivation for such a study can be found in recent computer simulation results [162], where a quicker exchange rate was found by increasing the corona block length, which is in conflict with the slower rate predicted by theory. The double exponential dependence of γ and N could effectively be used to tailor micellar properties for applications such as the production of frozen nanoparticles, for tuning rheological properties of transient networks built from telechelic polymers, or the control of release from micellar cores for biomedical purposes.

5 Non-equilibrium Kinetics in Block Copolymer Micelles

5.1 Formation and Micellization Kinetics

Non-equilibrium kinetic processes typically involve monitoring a change in micellar structure or morphology over time, or following the formation of micelles from a molecular solution (unimers), i.e., micellization kinetics. Thus, in contrast to equilibrium processes a perturbation is required. Typically this is achieved by abruptly altering the thermodynamic conditions, which can be achieved either via extensive parameters like temperature and pressure, or by changing intensive parameters such as salt concentration or pH.

Classically, studies of micellization kinetics involve monitoring the time-resolved response of micelles using either fluorescence spectroscopy or light scattering methods. SAX/SANS techniques have not been used very extensively so far but are becoming increasingly popular because the technical feasibility has increased significantly over the last few years due to more advanced instrumentation and more powerful sources. The main limitation of light scattering and fluorescence spectroscopy methods is the lack of relevant structural resolution. Consequently, the structural evolution of micellar systems, whose typical sizes are of the order of 1–50 nm, cannot be followed during the course of the kinetic process. An exception is large particles of the order of several hundreds of nanometers, which thus enter into the window of light scattering. Consequently, most studies discuss relaxation times, which cannot be straightforwardly related to specific kinetic processes.

As mentioned in the Introduction, there is some unclear terminology related to kinetics of micelles: often the terms “micelle dynamics” or “micelle kinetics” are used interchangeably for equilibrium kinetics (exchange kinetics), relaxation kinetics (micelle–micelle relaxation kinetics) and micellization kinetics (unimer–micelle transition). We will focus on results related to micellization kinetics of block copolymers starting from unimers, although in some cases we will also mention results more related to re-equilibration kinetics. The term “dynamics” will be associated with molecular level diffusion, rotations or elemental rotations/vibration, etc. and will be left out of this review.

5.1.1 Temperature-Jump Experiments

As in experiments related to equilibrium or near-equilibrium kinetics, micellar growth can be induced using larger amplitude T-jumps, thereby perturbing the system from a unimer to micellar state. This requires temperature-sensitive polymers that undergo micellization upon heating or cooling. A particularly well-studied block copolymer system is poly(ethylene oxide)–poly(propylene-oxide)–poly(ethylene oxide) (PEO-PPO-PEO; Pluronics) triblock copolymer in aqueous dispersions. PPO exhibits a LCST and is generally not water soluble at ambient temperature. PEO-PPO-PEO undergoes a unimer–micelle transition in a range of approximately 10–35°C, depending on molecular weight, composition, and concentration [165]. The transition temperature is referred to as the critical micellization temperature (cmt), which is equivalent to the cmc at constant temperature.

The first applications of the T-jump method to study kinetics related to micelles is due to Kreschek et al. [166] and Eyring and coworkers [167, 168] in the late 1960s to early 1970s. The rate of dissociation of various ionic surfactants was measured by suddenly increasing the temperature using electrical resistance heating and capacitor discharge following the change in time using scattered light. While the experiments showed qualitatively that the kinetics occurred on a typical milli-second timescale, not much more information could be obtained due to a lack of angular resolution. Block copolymer systems are generally more robust towards environmental changes than surfactants. Consequently, polymer systems where at

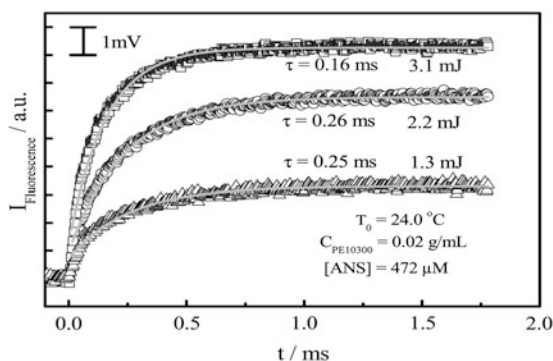
least one block is thermosensitive are used and micellization is induced by crossing the cmt via a sudden temperature jump or quench. A disadvantage is, however, that systems are usually in the proximity of the microphase boundary and thus typically not well segregated, complicating comparisons with theories that often assume strong segregation.

Honda et al. [169, 170] employed a thermosensitive poly(α -methylstyrene)–poly(vinyl phenethyl alcohol) (P α MS-PVPA) block copolymer system with two molecular weights that micellize in benzyl alcohol below 24°C and 50°C, respectively. In the experiments, the system was completely dissolved into unimers at 60°C and subsequently abruptly quenched to various temperatures in the micellar region of the phase diagram using a pre-thermostated sample and measuring cells. Subsequently, the system was monitored in real time using simultaneously time-resolved static and dynamic light scattering. By investigating two molecular weights and various temperatures, a thorough and systematic investigation of the system was made. Interestingly, the micellization process was found to be very slow and occurred on a time scale of hours. For the lowest molecular weight (8.1 kg/mol), a single exponential growth was found whereas for the higher molecular weight block copolymer (12.5 kg/mol) the kinetics was slower and could be fitted with a double exponential decay. This behavior was interpreted in terms of nucleation and growth type kinetics and a clear distinction was made with respect to the Aniansson and Wall-type kinetics that predicts a double exponential behavior close to equilibrium. By comparing the information obtained from both dynamic and static light scattering, it was observed that the radius of gyration and the hydrodynamic radius increase more rapidly in the beginning compared to the molecular mass. The polydispersity, obtained using a cumulant expansion, appeared to decrease towards the end of the micellization process. The micellization process was therefore pictured as having a rapid initial process that bears some similarity to a nucleation and growth process and is characterized by an increase in the number of micelles. The time constant of the first process was observed to decrease with increasing concentration. This process is followed by a slower reorganization process, independent of concentration, reflecting an equilibration mechanism where the number of micelles decreases but the micelles increase in overall size.

Small Temperature-Jump Studies of Pluronics

Hecht and Hoffman [126] investigated the kinetics of Pluronics micelles using a capacitor discharge in the micellar solution containing electrolytes to increase the conductivity and amplify the temperature jumps. Using this method, T-jumps ranging from 0.05 to 2.4 K were obtained. The micellization was followed using light scattering at a fixed angle of 90°. T-jumps were performed both below and above cmt at different concentrations without any clear distinction between the nature of the kinetic process. In other words premicellization, micellization and micelle–micelle equilibration kinetics were investigated, leaving a theoretical comparison difficult. This study thus indicates the existence of “pre-critical” micelles. Interestingly, the

Fig. 32 Time-dependent fluorescence intensity of a hydrophilic fluorescent probe (ANS) in a Pluronic aqueous solution under different laser powers. *Solid lines* display fits of a single exponential growth law. Reprinted with permission from [171]. Copyright (2007) American Chemical Society



time evolution of the scattered signal was found to be close to exponential in all cases. Typical time constants ranged from 1 s to a few milliseconds; however, no clear physical interpretation of the results was presented.

Later studies of Pluronics have similarly been performed without a clear distinction between micellization kinetics and micelle–micelle relaxation kinetics [115, 127–129]. Contrary to the study of Hecht and Hoffmann, these studies reveal the presence of two [115, 127] or three time constants [128, 129]. The first two were interpreted in terms of the Aniansson and Wall theory and attributed to unimer absorption and unimer exchange-mediated reorganization kinetics. The third relaxation time constant was proposed by Kositz et al. [128, 129] on the basis of an infrared laser-induced T-jump and attributed to “clustering of micelles into larger aggregates” and was observed with increasing amplitude close to the cloud point of the sample, i.e., a micellar fusion mechanism related to a macrophase separation. In one of the works by Kositz et al. [128], the effect of impurities, inherently present in industrial grade Pluronic samples, was investigated by fractionation and purification. The results showed that although the first (fast) process was not appreciatively affected by impurities, the second and third processes were slowed down, suggesting that these processes are dependent on the structural composition. It was also found that addition of hydrophobic compounds led to much larger clusters, especially around the cmt.

In the experiments of Goldmints et al. [127] and Kositz et al. [128, 129] mentioned above, an iodine-based laser heating was used, which provides a faster heating as compared to a traditional resistance-based heating apparatus (“Joule heating”). Using Joule heating, a certain thermal inertia may be important and cause a time-lag as opposed to the instantaneous perturbation often assumed in theories. Consequently, if the heating time is slow, the process may be regarded as a gradual thermal equilibration process rather than a deep non-equilibrium quench, which would lead to a nucleation-like process. Using an intense laser operating in the infrared region, Ye et al. [171] obtained a much faster heating (typical time of 10 ns) and a tunable T-jump by fine-tuning the laser output power. However, because of thermal loss, the temperature relaxed back to its initial value after only about 100 ms. The fluorescence intensities of a dilute Pluronic solution containing a hydrophilic fluorophore after several ultrafast heating runs with different laser power are displayed in Fig. 32.

Interestingly, the study showed that both the fluorescence and light scattering signals exhibited a similar single exponential growth law, with a relaxation time of about 0.1–1 ms after a temperature jump $\Delta T \approx 1$ K close to the cmt. A single time constant was interpreted in terms of the unimer insertion rate constant, k_+ , and discussed within the Aniansson and Wall theory (c.f. Sect. 2.2.5). The absence of a slower relaxation process could be related to a restricted total time interval of only 100 ms.

Other Temperature-Jump Studies

The temperature jumps achieved by lasers and capacitor discharge Joule heating are usually very small; of the order of some few degrees Kelvin, limiting the techniques to marginally segregated systems close to cmt. In addition, the temperature will typically follow a pulse-like time dependence and will decay to the initial temperature after a relative short time (typically 100 ms [171]) due to energy dissipation. An alternative method can overcome this problem by using a stopped-flow apparatus with a rapid mixing temperature jump system (mT-Jump from BioLogic Scientific Instruments, France). This set-up achieves temperature changes by mixing two solutions of different initial temperatures T_1 and T_2 . The final temperature of the mixture (T_3) is calculated from the initial temperatures and the mixing ratio of the two solutions and can be kept stable over a long period after mixing. In this way, the initial solution can be quenched rapidly through fast mixing to a different temperature with relatively large temperature jumps, ΔT .

Liu and coworkers employed this method to study the micellization kinetics of a double hydrophilic diblock poly(*N*-isopropylacrylamide)–poly(2-diethylamino ethyl methacrylate) (PNIPAM-PDEA) in aqueous solution [172]. The results obtained after a temperature jump from 20°C (unimers) to different final temperatures are shown in Fig. 33.

As seen in Fig. 33, the micellization occurs increasingly rapidly with the amplitude for moderate ΔT , reflecting deeper quench and thus increasingly unstable unimers. For the largest ΔT , the intensity is smaller and the terminal relaxation is actually slower than for the lower temperatures. This might indicate that the micelles are trapped in smaller aggregates and the terminal kinetics is slower at higher temperatures where the segregation between the core PNIPAM block and the solvent is larger. Interestingly, at intermediate ΔT the size of the initial micelles are larger than the terminal ones. The resulting intensity curves (reflecting both a change in aggregation number and number of micelles as well as distribution) could be tentatively fitted to a double exponential growth model. The fit results show that the fast relaxation time (τ_1) decreased with the micellar concentration while the second, slower relaxation time, τ_2 , was found to be virtually independent of the concentration, in line with the observations by Honda et al. [169]. The results were discussed in terms of a dominating unimer exchange mechanism.

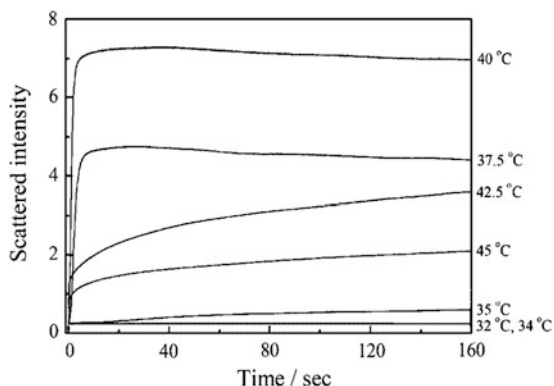


Fig. 33 Time evolution of the scattered intensity upon different temperature jumps of the poly (*N*-isopropylacrylamide)–poly(2-diethylamino ethyl methacrylate) (PNIPAM-PDEA) block copolymers undergoing micellization in water. The temperatures shown indicate the final temperature after a jump from 20°C. Reprinted with permission from [172]. Copyright (2007) WILEY-VCH Verlag GmbH & Co. KGaA, Weinheim

5.1.2 Stopped-Flow Experiments

As seen from the results from the T-jump experiments described above, there is a tendency in the literature to analyze the data in terms of two relaxation constants, even for highly non-equilibrium processes such as micellization kinetics. This is not obvious because micelle formation kinetics involves a distribution of many types of intermediate aggregates and will not necessarily behave in the way Aniansson and Wall predicted for small perturbations away from equilibrium (“linear regime”). Perhaps a more convenient way of inducing micellization is by adding a component that selectively precipitates one of the blocks. Fast kinetic measurements in the order of microseconds can be achieved with modern instruments by using a stopped-flow apparatus for rapid mixing, as described in Sect. 3.2.1. Because micellization is induced very rapidly, this technique is in principle very suitable for comparing experimental data with theory.

The earliest measurements using stopped-flow and light scattering to study kinetics of block copolymer micelles were done by Bednar et al. [173]. In their work, both the micellization kinetics and dissociation kinetics of two commercial block copolymers (“Kraton”) were studied: an A-B poly(styrene-*b*-ethylene/propylene) (SEP) diblock and an A-B-A poly(styrene-*b*-ethylene/butylene-*b*-styrene) (SEBS) triblock copolymer. The polymers were molecularly dissolved in mixtures of 1,4-dioxane and heptane that were poor solvents for either EP/EB or S blocks. Micelle formation with EP or EB as core block was then studied by rapidly adding additional pure 1,4 dioxane to the solution. Dissociation of the micelles could be observed by adding heptane to the mixture. Although heptane is a good solvent for the EP or EB blocks it is a marginally bad solvent for PS and thus dissolution of the system is only possible in a solvent mixture and the micelles are likely to have partially swollen

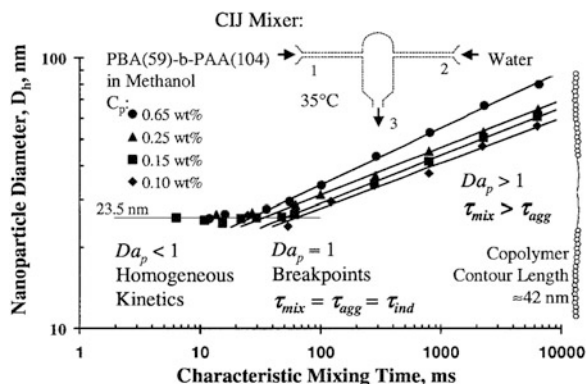
cores. The kinetics was observed using a light scattering instrument at a fixed angle $\theta = 90^\circ$, thus limiting the experimental outcome to a net scattered intensity without structural resolution in terms of the radius of gyration, R_g , or similar quantities. For micelle formation, the data were best fitted with a sum of two simple exponential decay functions. The individual relaxation time constants, τ_1 and τ_2 , were not given but an “average” value was defined by $\tau = a_1\tau_1 + a_2\tau_2$ where a_1 and $a_2 = 1 - a_1$ are the normalized amplitudes. The mean relaxation time was found to be about 40 and 70 ms for the diblock and triblock copolymer micelles, respectively. For the decomposition kinetics, the process was observed to be too fast for the diblock copolymer (< 1 ms) whereas for the triblock copolymer micelle a mean relaxation time of about 140 ms was found. Although a theoretical analysis was not performed, the authors speculate that the finding of two relaxation times probably reflects a continuous spectrum of relaxation times.

In a study by Kositz et al. [129] on Pluronic micelles, the kinetics was investigated using both the laser temperature jump and a stopped-flow method. The results after adding salt to a solution originally below cmc showed that micellization could be induced. The associated intensity was characterized by a double or single relaxation time constant depending on concentration. Despite the fact that the initial conditions were completely different, the stopped-flow results seem to indicate a terminal relaxation time similar to the T-jump experiments (τ_2) for certain temperatures. No quantitative correspondence was found for the fast process. A similar dependence, where τ_2 decreased with concentration, was observed and interpreted as a redistribution process by which the micelles might undergo fusion or fission.

Johnson and Prud'homme [174] investigated the micellization kinetics indirectly by applying an analytical confined impinging (CIJ) mixer to induce micelles and studied the effect of the mixing speed on particle size (a process coined “flash nanoprecipitation”). By using poly(butyl acrylate)–poly(acrylic acid) (PBA-PAA) diblock copolymers, the system could be molecularly dissolved in methanol. By adding water, which is selective towards the PPA block, micelles can be induced. Once formed, the micelles were expected to be kinetically frozen, i.e., further ripening of the micelles was inhibited by the high interfacial tension and the aggregates could be regarded as stable particles. By applying various mixing times, τ_{mix} , the supersaturation as well as the so-called Darmköhler number were varied. The latter is defined here as $Da \equiv \text{mixing time/micellization time}$, $\tau_{\text{mix}}/\tau_{\text{mic}}$. The dependence of Da on concentration and mixing time is given in Fig. 34.

As can be seen from Fig. 34, below certain mixing times of between 20 and 60 ms, depending on concentration, the micellar dimensions were independent of both mixing time and concentration. At the breakpoints, the characteristic time was taken as the micellization time, hence $Da \equiv 1$. For $Da > 1$, the measured radii were found to be a function of concentration [generally $R = R(\text{conc})$], as well as to depend on τ_{mix} . The latter regime is characterized by large inhomogeneities in the solvent mixture that homogenize at time scales longer than the time it takes to form the particles, i.e., the system can fuse and exchange unimers for a long time, leading to larger particles. It is also likely that the particles in this regime would be much

Fig. 34 Hydrodynamic diameter of the particles formed in a CIJ mixer induced by a selective solvent to a stream of soluble copolymer. The mixing time and aggregation time are equivalent at the breakpoint, where $Da \equiv 1$. [174]. Copyright (2003) by the American Physical Society



less defined and more polydisperse. The characteristic micellization times deduced from the breakpoints were found to increase with decreasing concentration. From this fact it was speculated that the micellization process follows a two-step mechanism, characterized by a nucleation event almost independent of concentration, followed by a concentration-dependent fusion/fission event. It should be mentioned, however, that a nucleation process followed by unimer exchange should also depend on concentration (see Sects. 2.3.2 and 2.3.3). Thus, a definitive conclusion cannot be reached from these data alone without measuring the actual time evolution.

In a series of publications, Liu and coworkers employed a sophisticated experimental design using a stopped-flow apparatus combined with both light scattering and fluorescence techniques to study a range of block copolymer systems ranging from responsive A-B diblock [8, 175–177], A-B-C triblock [47, 178], and miktoarm star block copolymers [179]. We will briefly go through results related to diblock copolymers. In a study from 2007, Zhang et al. [176] investigated a pH-responsive double-hydrophilic poly(2-diethylamino ethyl methacrylate)–poly(dimethylamino ethyl methacrylate) block copolymer system end-labeled with a pyrene group, allowing fluorescence spectroscopy to be used in parallel with light scattering. The time dependence after pH-jumps qualitatively indicated that the growth curve of the fluorescence intensity displays a more “stretched behavior”, i.e., the process is characterized by the existence of several, or perhaps a distribution, of rate constants. The fits performed showed that although the time evolution of the scattered light displayed a double exponential behavior, the fluorescence intensity, characterizing the association of pyrene groups into excimers, demanded three rather than two discrete relaxation constants for reasonable fits. The initial increment of the intensity was assigned to the formation of oligomeric aggregates that cannot be detected with light scattering. Although the second process observed with fluorescence spectroscopy showed a similar time scale as the initial process in light scattering, the slow process (τ_3) was much slower than that observed with light scattering. All time constants were found to decrease with increasing concentration.

Chain Length Dependence

In a study by Zhang et al. [177], the effect of hydrophobic chain length on the micellization kinetics was investigated in a series of poly(ethylene oxide)–poly(2-diethylamino) ethyl methacrylate) (PEO-PDEA) block copolymers with varying PDEA molecular weight. Again, the time dependence of the scattered light was approximated by a growth function consisting of a sum of two exponentials. Interestingly, the time constant of the second, slow process slightly decreases with increasing hydrophobic block length. This was accompanied by a tendency for increasing concentration dependence as well as a decreasing apparent activation energy with chain length. These rather unexpected results were interpreted as an increasing dominance of fusion and fission processes because of an increasing suppression of pathways involving unimer exchange (increasing hydrophobicity). The activation energy, E_a , varied from about 8 to 3 kJ/mol, which seems rather low for a fusion process. However, the measurements were performed on time scales from some milliseconds to seconds and it is not clear whether the terminal relaxation reflects the final equilibration to the true equilibrium state. As the final relaxation may be exceedingly slow, it might be that the measured τ_2 only reflects an apparent value.

“Schizophrenic” Block Copolymer Micelle Systems

In a series of studies [8, 175], so-called schizophrenic systems were investigated. These are diblock copolymers that may undergo micellization with either one block or the other to form the micellar core, depending on pH and/or salt concentration. In one study, for micelles formed by poly(4-vinylbenzoic acid)–poly(N-morpholino ethyl methacrylate) (PVBA-PMEMA), the results show that the micellization process induced by a pH-jump exhibited a fast initial growth and a slow terminal growth, where the latter could not be described by a simple relaxation constant. Consequently, only the initial part of the data was fitted to a two-exponential growth function. With this description, the initial process was found to accelerate upon increasing the concentration whereas the second process remained roughly constant. Salt-induced micellization, however, led to a τ_1 that was roughly independent of concentration while τ_2 decreased. Interestingly, the micellar dissolution kinetics induced by dilution or an inverse pH-jump led to a very fast decay that could be described with a single exponential. Also, the remicellization kinetics (“inversion kinetics”), whereby the systems are transformed from micelles with one core-forming block to the other, was investigated. The associated kinetics exhibited in some cases an initial decay followed by a slower growth characterizing the re-equilibration of the micelles.

In a work on a double stimuli-responsive PNIPAM-PDEA block copolymer, micellization was triggered by either precipitating the PDEA upon a pH-jump or by performing a T-jump to selectively precipitate the PNIPAM block. The kinetics upon T-jumps has already been discussed above and was found to be represented by two relaxation constants: τ_1 was found to decrease with concentration while τ_2 was

essentially independent of concentration. However, for the pH-induced micellization process, both τ_1 and τ_2 were found to decrease with concentration. This difference was attributed to electrostatic charges present in the corona during the thermally induced micellization process, leading to a prevention of corona overlap and hence a decreased probability of micellar fusion. Moreover, activation energies for both processes were found to be very similar (about 35 and 38 kJ/mol, respectively) and the time scales differed by a factor of about five. This was taken as an indication of a predominant fusion/fission mechanism in both processes, although in this case these time constants might reflect a continuum.

Influence of Salt Addition

Liu and coworkers investigated a series of A-B-C triblock copolymers, where the C-block is selectively precipitated upon a pH-jump to alkaline conditions [47]. The results showed very similar results as for the A-B diblock copolymers and was again analyzed in terms of two relaxation constants, the first decreasing with concentration and the second being concentration independent. Again, two very similar apparent activation energies were found, where E_a for the second, slower process was even smaller than for the faster process. This indicates a larger entropic barrier for the second process, leading to $\tau_2 > \tau_1$. In a second paper [178], the effect of addition of salt was studied. It was found that upon addition of salt, a gradual increase in the concentration dependence of the second process was found. The obtained results for τ_2 as a function of concentration are given for different added salt amounts in Fig. 35. The results were interpreted as a signature of an increased occurrence of fusion/fission due to screening of electrostatic interactions between corona blocks. Interestingly, the micellization rate was faster at lower salt contents, indicating that, although the fusion might occur in addition to unimer exchange, the terminal process is slower, possibly due to higher interfacial energies and more stable micelles. The latter may occur because addition of electrolytes is well known to induce larger interfacial tensions between hydrocarbons and aqueous solutions [180].

Ge et al. [179] investigated the formation kinetics of vesicles by pH-jumps in a system consisting of a zwitterionic diblock copolymer, poly(2-(methacryloyloxy)ethyl phosphorylcholine)–poly(2-(diisopropylamino)ethyl methacrylate) (PMPC-PDPA) using a combination of stopped-flow and light scattering. The kinetics of pH-induced formation was shown to be tentatively described by three distinct relaxation processes for the early stages of vesicle self-assembly (0–40 s). The kinetics of vesicle formation in the later stage (for times longer than some minutes) was investigated using dynamic light scattering. It was found that both the hydrodynamic radius and the polydispersity decrease approximately exponentially with a single characteristic relaxation time. The observed multiple time constants were interpreted in terms of theoretical considerations, where the unimer-to-vesicle transition is proposed to proceed via a series of four steps: spherical micelles to cylindrical micelles to lamellae platelets that are finally wrapped-up into vesicles [10, 181, 182]. Such a

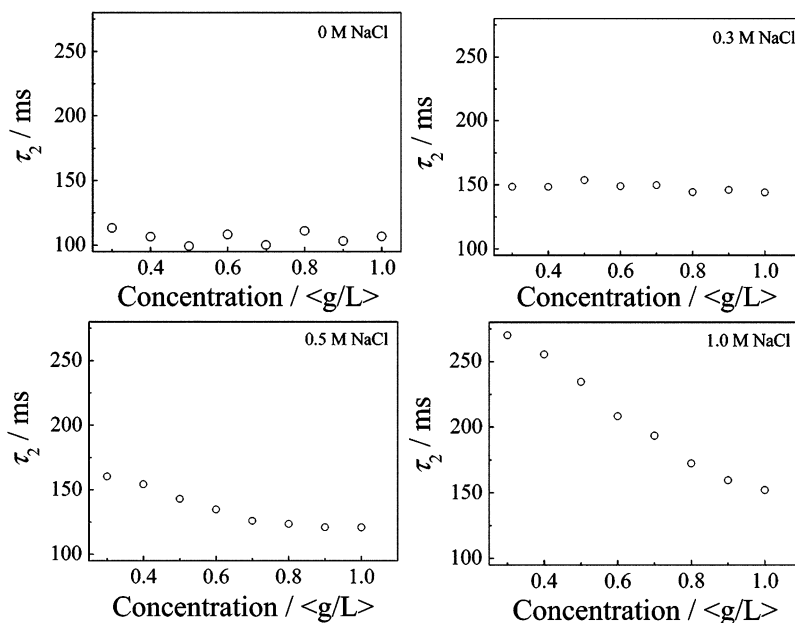


Fig. 35 Concentration of the slow terminal relaxation constants observed for the micellization kinetics of pH-sensitive A-B-C triblock copolymers with different amount of added salts. Reprinted with permission from [178]. Copyright (2007) American Chemical Society

pathway could be more rigorously verified using time-resolved SAXS or SANS whereby the intermediate nanostructures can be observed directly. An example using this technique is given in the next section.

5.1.3 Time-Resolved SAXS with Millisecond Resolution

Most of the works mentioned so far have used light scattering or fluorescence spectroscopy to follow the kinetics, hence the experiments provide little or no structural resolution. In a recent work by Lund et al. [183], synchrotron SAXS was coupled with a stopped-flow apparatus in order to study micellization kinetics with a millisecond time resolution and nanometer structural resolution. In this study, an amphiphilic model system consisting of a well-defined PEP1-PEO20 block copolymer in DMF/water mixtures was used. As previously mentioned, both DMF and water are bad solvents towards PEP but good solvents for PEO. The PEP1-PEO20 system is very useful for studying micellization because in pure DMF only single chains (unimers) are present, but the block copolymers aggregate into well-segregated micelles as soon as some water is added. Hence, micellization can be induced by rapidly mixing a solution of PEP1-PEO20 in DMF with water in a

stopped-flow apparatus. Typical time-resolved scattering curves were obtained using a high-brilliance synchrotron SAXS instrument (ID02, at the European Synchrotron Radiation Facility, ESRF) and show the increase in scattered intensity associated with the formation of micelles (see Fig. 36a). The scattering could be described with a core-shell micellar scattering model (c.f. Sect. 3.1.6), thereby allowing the extraction of detailed parameters of the internal structure of the micelles at all times.

Fig. 36b shows the aggregation number, P_{mean} , plotted against the corresponding thickness of the micellar corona, $R_{\text{corona}} = R_{\text{m}} - R_{\text{c}}$ for three concentrations in a double logarithmic representation. The data agree well with the prediction [38, 40]: $R_{\text{corona}} \sim P_{\text{mean}}^{1/5}$ expected for star-like micelles. The results thus show that the micelles grow like well-defined star-like micellar entities. No regime where the size grows faster than the molecular weight, which was observed on a less segregated system by Honda et al. [169], were observed in this case. This probably reflects the fact that the initial time range of the micellization in this is too fast to be captured ($t < 2\text{--}3$ ms). Also, for star-like micelles only a few chains are necessary to achieve a star-like structure [38].

The time dependence of the aggregation number, P_{mean} , deduced from the core-shell model fits (Sect. 3.1.6) for three concentrations, is given in Fig. 37.

The observed growth behavior shown in Fig. 37 could be approximately fitted using a phenomenological model in the form of a stretched exponential $P_{\text{mean}} \approx 1 - \exp[-(kt)^\beta]$. This yields in all cases an exponent β of about 0.2. A trial fit to a sum of two exponentials did not give satisfactory fits, in contrast to other results [169, 171, 176]. The broad relaxation suggests an intrinsically broadly distributed kinetic growth process that cannot be described with a finite number (typically 1–3) of relaxation times. An approximate two-exponential behavior is expected for micelle relaxation kinetics after a sudden external disturbance, but only very close to equilibrium [55, 60] that is not the case for micellization kinetics observed deep in the micelle region. The data at the shortest times suggest the existence of a fast initial aggregation ($t < \approx 5$ ms) that cannot be entirely resolved experimentally. This process seems to become exhausted at intermediate times leading to a “shoulder” of P_{mean} that changes with concentration. The terminal relaxation towards a common equilibrium then appears to slow down with time, the overall rate increasing with concentration.

The concentration dependence of the terminal relaxation has been observed earlier in light scattering experiments and sometimes qualitatively attributed to fusion/fission processes [176]. In [183], however, the relaxation curves could be described using the nucleation and growth model highlighted in Sect. 2.3.3 where growth was only allowed to occur unitarily through unimer exchange kinetics. The corresponding size distribution extracted from the fits are displayed in Fig. 38.

The size distribution of micelles gives a very detailed view of the micellization process. Extracted parameters such as the unimer concentration and the Gaussian width are correlated with the mean aggregation number, giving a complete view of the process in Fig. 38b. The results reveal the following scenario: First, the initial free unimers are consumed rapidly in a nucleation-like event that leads to the formation of

Fig. 36 (a) Scattered intensity at different kinetic times during the micellization of a 0.25 vol% PEP1-PEO20 block copolymer in a 90 mol% DMF/water solution.

Solid lines display fit results using the scattering model functions (see text for details). (b) Scaling of the thickness of the corona, R_{corona} , with the aggregation number of the micelles, P_{mean} , both deduced from the core-shell fits for the 0.125% (stars), 0.25% (squares), and 0.5% (triangles) solutions, in double logarithmical representation. The linear fits (solid lines) almost perfectly reproduce the theoretically expected scaling law for star-like micelles:

$$R_{\text{corona}} \sim P_{\text{mean}}^{1/5} \text{ [183].}$$

Copyright (2009) by the American Physical Society

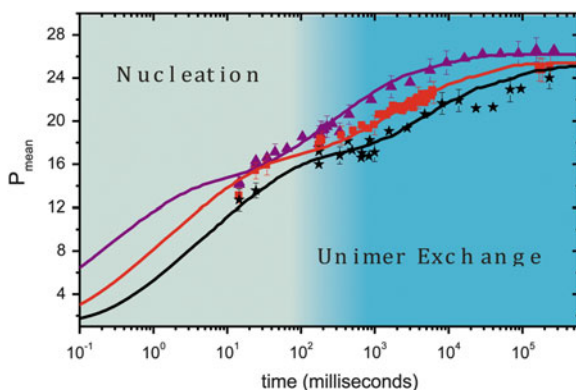
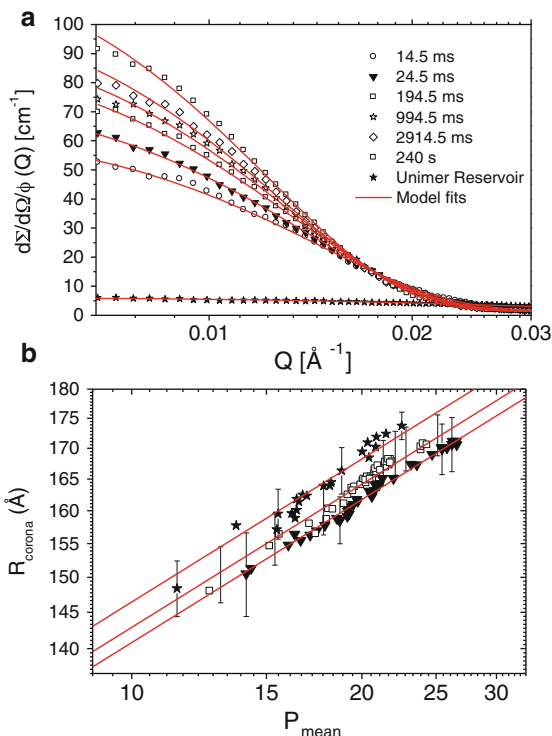


Fig. 37 Experimentally determined growth behavior and comparison with a unified nucleation and growth model. Time dependence of the aggregation number, P_{mean} , extracted from the fits for all three total volume fractions on a logarithmical time scale: 0.125% (stars), 0.25% (squares), and 0.5% (triangles). Solid lines represent a fit using the nucleation model described in the text. Typical error bars are shown [183]. Copyright (2009) by the American Physical Society

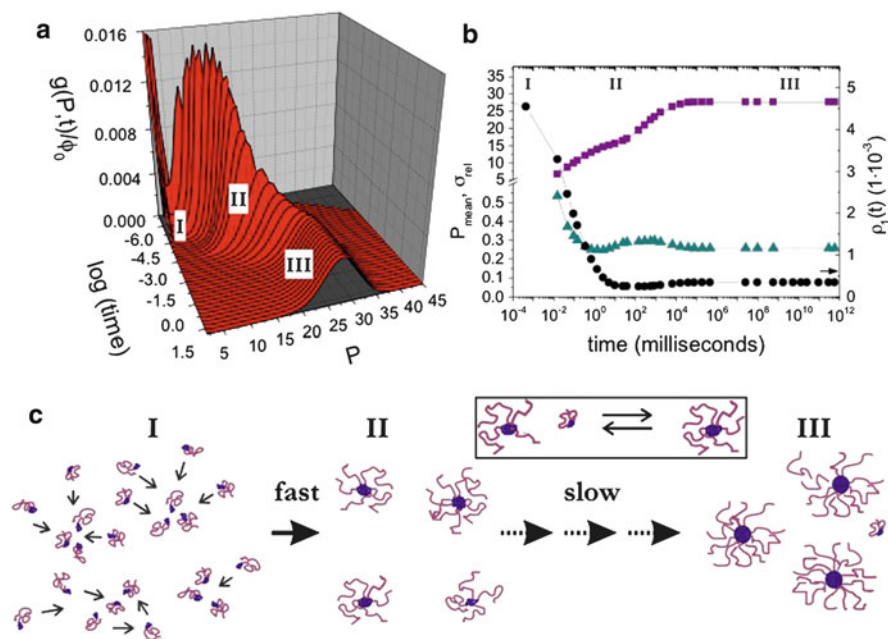


Fig. 38 Nucleation and growth view of the micellization process. (a) The time evolution of the distribution of the micellar ensemble in terms of the aggregation number, P_{mean} , corresponding to the fit results of the 0.5% micellar system. (b) Time evolution of the unimer concentration (circles) compared to the associated increase in P_{mean} (squares). Also shown is the relative Gaussian width of the micellar distribution $\sigma_{\text{rel}} = \sigma/P_{\text{mean}}$ (triangles). (c) Illustration of the micellization process showing the fast nucleation event, which essentially consumes all the unimers (region I), followed by a region where the micellar growth slows down and is temporarily nearly frozen due to the lack of available unimers (region II). The terminal slow growth towards the final equilibrium is governed by the amount of free unimer and thus effectively limited by the unimer expulsion/insertion process between the metastable micelles (region III). [183]. Copyright (2009) by the American Physical Society

metastable micelles (region I in Fig. 38c). In analogy with Ostwald ripening for macrophase separation, the microphase separated micelles can only grow further if other micelles dissolve. However, an important distinction here is that while in Ostwald ripening the system in principle grows to macroscopical scales, the micelles are limited to the equilibrium size set by the thermodynamics of the micelle itself. In this model, this “coarsening mechanism” occurs through unimer exchange (region II in Fig. 38c). This continues until the micelles achieve their equilibrium size (region III in Fig. 38c). These results show that nucleation and growth including only unimer exchange kinetics is sufficient to describe the kinetics. This does not necessarily exclude the presence of other mechanisms such as fusion and fission but, in the sense of a physical minimum model, unimer exchange is sufficient to describe all data. In order to further advance understanding, systematic TR-SAS studies in which molecular parameters such as molecular weight, composition, etc. are varied

would be very helpful. Complementary, more theoretical modeling is necessary in order to fully understand the mechanisms and kinetic pathways. Here computer simulations are particularly useful. A summary of existing works on this topic will be covered in the next section.

5.1.4 Computer Simulations

The central questions occupying theoreticians and experimentalists are the mechanism and kinetic pathways of self-assembly. To answer these questions, computer simulations are particularly useful because the coordinates of each molecule can be traced individually and pathways can be observed directly. The challenge for computer simulations is to access the relatively long time scales needed to observe micellization kinetics, which can only be done using coarse-grained models, relatively few particles, and/or by excessively long computation times.

An early simulation work was presented by Mattice and coworkers [184] in which A-B diblock copolymers consisting of 5–45 monomers for each block were studied. The simulations were performed in cubic simulation cells with 44^3 – 88^3 lattice sites. The total concentration of the polymers were found to be in the range of 0.5–6%. Results obtained after starting from typically a few hundred chains revealed a rapid initial step that essentially consumed all single unimers, followed by a very slow coarsening process that was not fully equilibrated within the simulation time. In the work, no direct detailed analysis or evaluation of the kinetic pathway was performed. Nevertheless it was observed that upon increasing the interaction strength between the hydrophobic block and the solvent or increasing the insoluble block length, smaller trapped metastable micelles were detected. These micelles were found to essentially “freeze” the self-assembly process, at least on the time scale of the simulations.

Using full atomistic force field-based molecular dynamics simulations, Marrink et al. [185] simulated the micellization process of 54 dodecylphosphocholine (DPC) surfactant molecules in water on short time scales from some picoseconds to some tenths of nanoseconds. The results showed that the process is diffusion limited but that the surfactant aggregation still occurred on time scales much faster than expected from theoretical calculations. It was speculated that long-range interactions could enhance the aggregation rate. However, upon varying the interaction potential, it was concluded that this did not influence the results. Instead, water-mediated long-range hydrophobic interactions were suggested as a possible alternative explanation for the observed behavior. Interestingly, the simulation runs revealed that the micelles aggregate into larger cylindrical micelles at higher DPC concentration, whereas smaller spherical micelles are formed at lower concentrations. The difference was attributed to finite size effects and a small number of particles.

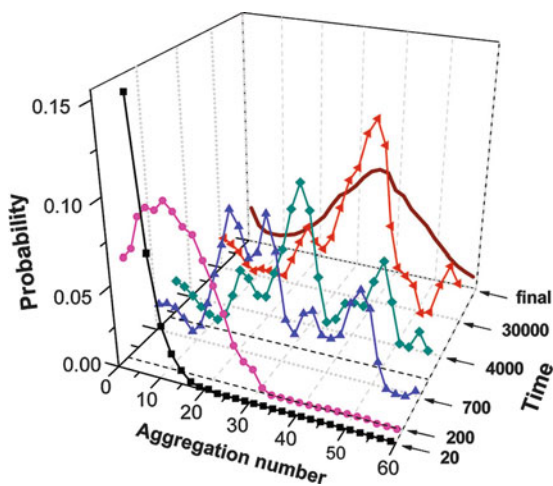
In a work by Chen et al. [186], Brownian dynamics was used to simulate the formation of micelles constituted of PS-PEO in water, with the particular aim of investigating the processes involved in “flash nanoprecipitation”. The effective (coarse-grained) potential was carefully mapped to experimentally determined

quantities of the system in order to obtain as realistic simulations as possible. In that way, the authors were able to reproduce the structural and thermodynamic properties of the system. Still, instead of changing the interaction parameters associated with the abrupt change in solvent composition experienced by the diblock copolymer under the experimental conditions, micellization was induced by quenching the temperature. Thus, the quenching time, corresponding to the mixing time in experiments, is controlled by the cooling rate. The results showed that the block copolymers aggregated into micelles with similar sizes and dimensions as observed experimentally. However, the time scale (a few milliseconds) was found to be considerably faster than that experimentally determined, which ranged from 20 to 60 ms. Also, although previous experiments showed that the micellar size decreases with increasing mixing time until the break (20–60 ms), the simulations showed the opposite trend; the micellar size increases with mixing time until a breakpoint that occurs at lower times than in experiments. This discrepancy was attributed to the different time scales probed in simulations ($t \leq 5$ ms) and that in the experiments the system was allowed to grow further through fusion/fission, although the mechanisms were not analyzed in detail in this work.

The mechanism and pathways of self-assembly were investigated in great detail in a work by Li and Dormidontova [162], who analyzed a system consisting of oligomeric block copolymers, A_2-B_3 and A_4-B_x (the numbers indicate the numbers of beads, $x = 4, 6$, or 8) using dissipative particle dynamics. This simulation technique combines molecular dynamics and Brownian dynamics-type simulations, giving the advantage of accessing relatively large temporal and spatial time scales. The growth curve associated with the weight and number average molecular weights of the aggregates (M_w and M_n respectively), was found to be significantly different. Here M_n was found to stabilize to an equilibrium size more rapidly than M_w , indicating that the number of micelles assumes a constant value earlier but the micelles are increasingly polydisperse in size with time. By tagging different micelles as a function of time, it was found that the aggregation numbers exhibited discrete jumps with amplitudes much larger than 1, indicating fusion events during the course of the reaction. It was also found that unimer exchange was primarily important in the first part of the micellization process (nucleation event); at later stages processes involving fusion/fission of micelles were more dominating. The latter was manifested in a bimodal character of the distribution function of M_w , where two peaks were clearly visible at intermediate stages during the micellization process. Increasing oligomer concentrations were found to speed up the whole micellization process, which was attributed to increased probabilities of micellar collision and fragmentation. The distribution function in terms of the aggregation number is plotted as a function of time in Fig. 39.

In order to understand the interactions controlling the mechanisms behind self-assembly, the interaction energy between the hydrophobic core chains and the solvents as well as the corona chain length were also varied. The results show that the effect of incrementing the hydrophobic energy is threefold: First, the initial nucleation-like event appears to be essentially unaffected; second, the time window of micellization expands, i.e., the time for completion increases; and third, the

Fig. 39 Time evolution of the aggregation number distribution for A_2B_3 oligomers undergoing micellization. Note the bimodal character of the distribution function at intermediate time stages. Reprinted with permission from [162]. Copyright (2010) American Chemical Society



importance of unimer exchange increases during the final stage of micellization. Also, fusion/fission events appear to be virtually unaffected upon an increase in the interaction energy although events involving small aggregates were found to be less likely to occur. The effect of increasing corona length was, perhaps surprisingly, found not to affect the relative contributions from the different mechanisms; instead, the overall rate of events decreased. It should be mentioned that the range of molecular weights studied by Li and Dormidontova corresponds to oligomers and that there might be a significant difference for polymers. This is still to be studied and compared to experimental results, providing a significant challenge for future studies.

5.2 Morphological Transition Kinetics

Most of the works related to the kinetics of morphological transitions have been performed in systems of regular (low molecular weight) surfactant micelles. Examples include micelle-to-vesicle transitions [187–189] studied by TR-SANS coupled with stopped-flow or with time resolved small-angle static and dynamic light scattering [190, 191]. Such morphological transitions have also been observed using TR-SAXS in other systems [192–194], where the processes can be resolved on time scales of only a few milliseconds. Since morphological transition kinetics of surfactant micelles have been extensively reviewed elsewhere [14, 15, 189, 195], this will not be covered in more detail here because we are mainly dealing with block copolymer systems in this review.

For block copolymer systems, most studies are related to ordering kinetics and morphological transition in melts or concentrated solutions. Examples include disorder-to-order [196], lamella-to-cylinder [197], cylinder-to-sphere [198], and

cylinder-to-gyroid [199] transition kinetics. Because we are dealing here with micellar solutions, these examples fall out of the scope of this review.

It has been widely reported that amphiphilic diblock copolymers can self-assemble into various nanoscale morphologies such as spheres, cylinders, and vesicles [46, 200]. The type of morphology that is obtained in a certain block copolymer solvent system was found to depend on the hydrophilic fraction of the block copolymer [201, 202], the overall molecular weight [142], solvent quality [48, 203], and temperature [204, 205]. Also, the polymer concentration was found to affect the morphology and the size of the aggregates [203]. The transitions between different morphologies of strong amphiphilic block copolymer aggregates in water are generally irreversible. In particular, vesicles are non-equilibrium structures in a trapped metastable state analogous to frozen spherical micelles [46]. The kinetics of the morphological transitions can be accelerated by the use of co-solvents with higher compatibility to the insoluble block or by variation of temperature such that the transitions are reversible [203–205]. Hence, it was argued that the speed of single chain exchange also determines the reversibility of the transition process. However, in a recent work by Lund et al. [48], it was shown that the transition from cylinders to spheres is very fast whereas the reverse process will not take place on finite time scales, although the single unimer exchange was measured to be very fast in the transition region. We note that both morphologies are thermodynamically stable within their range of existence, as was explicitly shown from model calculations taking into account the variation of structural parameters with the interfacial tension [48]. The irreversibility of the cylinder-to-sphere transition is thus due to a kinetic hindrance, which generally implies that for morphological transitions mechanisms other than pure chain exchange are active.

Unfortunately, kinetic studies of morphological transitions in block copolymer micellar systems are very rare. Most important in this context is the work of Eisenberg and colleagues, who explored the kinetics and mechanisms of various transitions of polystyrene₃₁₀-*b*-poly(acrylic acid)₅₂ (PS₃₁₀-*b*-PAA₅₂) block copolymer in water/1,4-dioxane mixtures. A morphological phase diagram of the ternary system, PS₃₁₀-*b*-PAA₅₂/water/1,4-dioxane was elaborated by Shen and Eisenberg [203] employing freeze-drying transmission electron microscopy (TEM), turbidity measurements, and static and dynamic light scattering. Starting from molecularly dissolved block copolymer chains in 1,4-dioxane they found upon addition of water the following sequence of morphologies: spheres, coexisting spheres and rods, rods, coexisting rods and vesicles, and vesicles at all polymer concentrations. It was found that in this system the appearance of the morphologies is reversible. The formation of the coexisting mixtures of morphologies is thermodynamically controlled, as concluded from the fact that they are identically formed independent of the pathway. Burke and Eisenberg [206] studied the kinetics and mechanisms involved in the sphere-to-rod and rod-to-sphere transitions of this system by TEM and turbidity measurements. The transition was induced by adding small amounts of water close to the morphological boundary for the forward transition and 1,4-dioxane for the reverse transition. Analysis by double exponential equations revealed two relaxation steps in both directions. The observed time scales in

forward and backward directions were found to be comparable to each other. In the forward direction, the evaluation of TEM micrographs showed the formation of an irregular pearl necklace structure by adhesive collision of spheres, which reorganize in a second slow step into smooth rods. The inverse transition starts with the formation of bulbs at the end of the rods, which in the rate-determining second step are released from the ends of the cylindrical body. The kinetics of both transitions was found to depend on the initial solvent composition, the magnitude of the solvent jump, and the initial polymer concentration. Systematic studies have shown that the kinetics are mostly affected by the initial conditions, i.e., location in the morphological phase diagram.

Using the same techniques as described above, Chen et al. [207] studied the rod-to-vesicle transition by adding water to the ternary system, PS₃₁₀-*b*-PAA₅₂/water/1,4-dioxane in the corresponding region of the phase diagram. Similar to the observation in the sphere-to-rod transition, the kinetics were governed by two consecutive steps. The first step involves the flattening of short rods to circular lamellae followed by the second step, which is the closing of the vesicles. The rates of the shape transformation crucially depend on the initial water content. The studies revealed that the larger the initial water content, the slower the relaxation times. This was also the case for increasing polymer concentration, while the size of the jump did not change the relaxation times significantly.

The corresponding vesicle-to-rod transition was investigated by Burke and Eisenberg [208]. The transition, monitored by turbidity measurements, could be described by a single relaxation step. The TEM micrographs revealed that the reorganization to rods proceeds through a sequence of intermediate structures: first the deformation of a vesicle to a “bowtie” shape structure was seen, which afterwards develops into dumbbells. Elongation of the long axis finally leads to the formation of thin rods. It was argued that the driving force is the increase in the curvature energy due to the change in the bilayer thickness. The instability is then relaxed by the transformation to thinner rods which, apparently, is the energetically favorable morphology for the final solvent composition. In summary, the work by Eisenberg and colleagues impressively demonstrates that the transition between different morphologies proceeds via different pathways, including the formation of different irregular intermediate structures. Thus this work reveals that, besides single chain exchange, other mechanisms are important for a shape transformation. However, reorganization of structures will not take place whenever unimer exchange is not existent, i.e., aggregates are in a frozen metastable state. We note that, except for the studies of Eisenberg and colleagues, there is a lack of systematic studies on the kinetics and mechanisms of morphological transitions. Time resolved small angle scattering on suitable block copolymer/solvent systems may help to obtain a clear picture of the general mechanisms governing morphological transitions in block copolymer micelles.

6 Concluding Remarks and Future Challenges

In this review, we have provided a selective overview of theoretical and experimental studies on kinetic processes in block copolymer micellar systems. We have demonstrated the strengths of time-resolved small-angle scattering techniques by highlighting recent examples from the literature. Most of the available literature in this field is either related to equilibrium exchange kinetics or micellization kinetics.

Although limited in number, the examples given illustrate impressively the potential and strength of these techniques. Primarily, as a common feature of both methods, TR-SAXS and TR-SANS provide a structural resolution of the kinetic processes of self-assembled systems on the nanometer scale. Individually, the strengths of TR-SAXS for studying kinetic processes is the high flux available at synchrotron sources, which allows experimenters to resolve fast kinetic processes such as block copolymer micellization in the millisecond range on small sample volumes. The advantage of TR-SANS on the other hand is the ability to exploit H/D contrast variation, which makes this technique unique for studying fundamental aspects of equilibrium kinetics like the influence of temperature, interfacial tension, and chain length. Even fine details like the chain conformation during the expulsion process or contributions from “hidden” processes like diffusion or fusion/fission are accessible.

Time-resolved techniques show promise for the future as improved technical capabilities and more powerful neutron and X-ray sources emerge. For neutrons, particularly promising is the planned construction of the powerful European Spallation Source (ESS), which will allow time resolutions approaching submilliseconds as well as the use of smaller and more dilute samples. Although the flux at synchrotron sources will still be significant larger, H/D contrast variation provides enhanced contrast over X-rays as well as a playground for performing studies of equilibrium kinetics in soft matter systems that cannot easily be achieved by other techniques. Additionally, neutrons may provide a significant advantage because beam radiation damage, which is a concern in particular for synchrotron studies of aqueous systems, is not an issue with SANS.

Increased flux and more powerful sources will also be particularly useful for the study of biological or biohybrid materials, which often are only available in small quantities. This demands a significant quality in terms of both flux and background as biomaterials often are characterized by weak signals and/or low contrast. Combining time-resolved wide-angle and small-angle scattering techniques can be expected to be particularly useful to bridge mesoscopic and microscopic scales, providing full structural information and information on correlations between local and global motions. This places an additional demand for low background and accurate background subtraction that constitutes a significant challenge to instrumentation development in terms of stability and optimization.

Despite its rather short history, TR-SAS techniques have helped to resolve many aspects of kinetic processes in micellar systems, in particularly the equilibrium kinetics. However, many challenges remain for the future. For block copolymer micelles, these include studies of morphological transitions, drug encapsulation and

release, etc. For the kinetics of biological systems, such as membranes and assemblies involving secondary and tertiary structures of proteins, TR-SAS is still to be exploited on a wider scale. In a notable example, the KZAC/TR-SANS technique was used to study and understand the equilibrium exchange kinetics in phospholipid vesicle structures [209, 210], showing the existence of both intermicellar exchange processes and “flip-flop” motions. In the future, studies are likely to be related to conformational changes, diffusion, and structural transitions that can be investigated in great detail using the combined structural and temporal resolution of TR-SAS techniques. Other applications likely to come are investigations of kinetics in drug delivery carrier systems, where stability as well as diffusion processes can be investigated.

For surfactant micelles, studies on the micellization kinetics and equilibrium kinetics are still to come although, for the latter, results from a hybrid system consisting of a short *n*-alkyl head group and a polymer tail were presented in Sect. 4.4. Studies of such systems constitute significant challenges for the instrumentation as the time scale of these systems approaches ranges of a few milliseconds and even submilliseconds. With improved and increased availability of neutron and X-ray sources, the next decade is likely to see a significant increase in the application and continued success of time-resolved scattering techniques in soft matter, material, and biological sciences.

Acknowledgements The authors are thankful to all colleagues on the beamlines, in particular Dr. Peter Lindner, Dr. Isabelle Grillo, Dr. Vitaliy Pipich, Dr. Aurel Radulescu, Dr. Theyencheri Narayanan, and Dr. Jeremie Gummel for fruitful collaborations. We are also indebted to Dr. Michael Monkenbusch, Dr. Jörg Stellbrink, and Thomas Zinn for numerous fruitful discussions.

References

1. Israelachvili JN (1985) Intramolecular and surface forces- with applications to colloidal and biological systems. Academic, London
2. Hamley IW (1998) The physics of block copolymers. Oxford University Press, New York
3. Yu K, Zhang L, Eisenberg A (1996) *Langmuir* 12(25):5980
4. Zhang L, Eisenberg A (1999) *Macromolecules* 32(7):2239
5. Jain S, Bates F (2003) *Science* 300(5618):460
6. Jain S, Bates FS (2004) *Macromolecules* 37:1511
7. Cui H, Chen Z, Zhong S, Wooley KL, Pochan DJ (2007) *Science* 317(5838):647
8. Wang X, Guerin G, Wang H, Wang Y, Manners I, Winnik MA (2007) *Science* 317(5838):644
9. Hayward RC, Pochan DJ (2010) *Macromolecules* 43(8):3577
10. He X, Schmid F (2008) *Phys Rev Lett* 100(1):137802
11. Cabral H, Matsumoto Y, Mizuno K, Chen Q, Murakami M, Kimura M, Terada Y, Kano MR, Miyazono K, Uesaka M, Nishiyama N, Kataoka K (2011) *Nat Nanotechnol* 6(12):815
12. Patist A, Oh S, Leung R (2001) *Colloids Surf A Physicochem Eng Asp* 176:3
13. Bras W, Ryan AJ (1997) *Adv Colloid Interface Sci* 75(1):1
14. Gradzielski M (2003) *Curr Opin Colloid Interface Sci* 8:337
15. Gradzielski M, Grillo I, Narayanan T (2004) *Prog Colloid Polym Sci* 129:32

16. Zana R (ed) (2005) Dynamics of Surfactant Self-assemblies Micelles, Microemulsions, Vesicles, and Lyotropic Phases. Surfactant science series, vol 125. Taylor and Francis, London
17. Narayanan T (2009) *Curr Opin Colloid Interface Sci* 14(6):409
18. Grillo I (2009) *Curr Opin Colloid Interface Sci* 14(6):402
19. Lund R (2010) *Stud Kinet Neutrons* 161:213
20. Hill TL (1964) Thermodynamics of small systems. Benjamin, New York
21. Hall DG, Pethica BA (1967) In: Schick MJ (ed) Nonionic surfactants. Arnold, London, ch. 16
22. Tanford C (1972) *J Phys Chem* 76(21):3020
23. Tanford C (1974) *Proc Natl Acad Sci USA* 71(5):1811
24. Tanford C (1974) *J Phys Chem* 78(24):2469
25. Flory PJ (1953) Principles of polymer chemistry. Cornell University Press, Ithaca
26. Leibler L, Orland H, Wheeler JC (1983) *J Chem Phys* 39(7):3550
27. Hong K (1983) *Macromolecules* 14:727
28. Nagarajan R, Ganesh K (1989) *J Chem Phys* 90(1):5843
29. Balsara N, Tirrell M, Lodge TP (1991) *Macromolecules* 24(8):1975
30. Lund R, Willner L, Lindner P, Richter D (2009) *Macromolecules* 42(7):2686
31. Nagarajan R (1991) *Langmuir* 7:2934
32. Landau LD, Lifshitz EM (1976) Statistical physics. Nauka, Moscow
33. Kadanoff L (2000) Statistical physics: statics, dynamics and renormalization. World Scientific Publishing, London
34. de Gennes PG (1979) Scaling concepts in polymer physics. Cornell University Press, Ithaca
35. des Cloizeaux J, Jannink G (1990) Polymers in solution: their modelling and structure. Claradon, Oxford
36. De Gennes PG (1976) *Journal de Physique* 37(12):1445
37. Alexander S (1977) *Journal de Physique* 38(8):977
38. Daoud M, Cotton JP (1982) *Journal de Physique* 43(3):531
39. Semenov A (1985) *Zhurnal Eksperimentalnoi I Teoreticheskoi Fiziki* 88(4):1242
40. Halperin A (1987) *Macromolecules* 20(11):2943
41. Halperin A, Tirrell M, Lodge TP (1992) *Adv Polym Sci* 100:31
42. Izzo D, Marques CM (1993) *Macromolecules* 26:7189
43. de Gennes P (1980) *Macromolecules* 13(5):1069
44. Willner L, Poppe A, Allgaier J, Monkenbusch M, Lindner P, Richter D (2000) *Europhys Lett* 51(6):628
45. Lund R, Willner L, Stellbrink J, Radulescu A, Richter D (2004) *Macromolecules* 37:9984
46. Förster S, Borchert K (2005) Polymer Vesicles. *Encyclopedia of Polymer Science and Technology*, pp. 1–52
47. Zhulina EB, Adam M, LaRue I, Sheiko SS, Rubinstein M (2005) *Macromolecules* 38(12):5330
48. Lund R, Pipich V, Willner L, Radulescu A, Colmenero J, Richter D (2011) *Soft Matter* 7(4):1491
49. Haliloglu T, Bahar I, Erman B, Mattice WL (1996) *Macromolecules* 29(13):4764
50. Muller N (1972) *J Phys Chem* 76(21):3017
51. Lang J, Zana R, Bauer R, Hoffmann H, Ulbricht W (1975) *J Phys Chem* 79(3):276
52. Lessner E, Teubner M, Kahlweit M (1981) *J Phys Chem* 85:1529
53. Lessner E, Teubner M, Kahlweit M (1981) *J Phys Chem* 85:3167
54. Aniansson E, Wall S, Almgren M (1976) *J Phys Chem* 80(9):905
55. Aniansson E (1974) *J Phys Chem* 78(10):1024
56. Aniansson E (1975) *J Phys Chem* 79(8):857
57. Kahlweit M (1982) *J Colloid Interface Sci* 90:92
58. Lang J, Zana R (1987) In: Zana R (ed) Surfactant solutions. New methods of investigation. Marcel Dekker, New York
59. Atkins PW (1988) *Physikalische Chemie*. VCH Verlagsgesellschaft GmbH, Weinheim

60. Halperin A, Alexander S (1989) *Macromolecules* 22:2403
61. Kramers H (1940) *Physica* 7:284
62. Lund R, Willner L, Stellbrink J, Lindner P, Richter D (2010) *Phys Rev Lett* 104:049902
63. Choi SH, Lodge TP, Bates FS (2010) *Phys Rev Lett* 104:047802
64. Halperin A (2011) *Macromolecules* 44(13):5072
65. Dormidontova EE (1999) *Macromolecules* 32(22):7630
66. Doi M, Edwards SF (1986) *The theory of polymer dynamics*. Oxford University Press, Oxford
67. Hadjiivanova R, Diamant H, Andelman D (2011) *J Phys Chem B* 115(22):7268
68. Nyrkova IA, Semenov AN (2005) *Macromol Theory Simul* 14(9):569
69. Shchekin AK, Grinin AP, Kuni FM, Rusanov AI (2005) Nucleation in micellization processes. In: Schmelzer JWP (ed) *Nucleation theory and applications*. Wiley-VCH, Weinheim
70. Onsager L (1931) *Phys Rev* 37:405
71. Lindner P, Zemb T (eds) (2002) *Neutrons, X-ray and light scattering methods applied to soft condensed matter*. Elsevier, Amsterdam
72. Guinier A, Fournet G (1955) *Small angle scattering of X-rays*. Wiley, London
73. Feigin L, Svergun D (1987) *Structure analysis by small-angle X-ray and neutron scattering*. Plenum, New York
74. Pedersen JS, Svaneborg C (2002) *Curr Opin Colloid Interface Sci* 7:148
75. Pedersen JS (2008) *Small-Angle Scattering from Surfactants and Block Copolymer Micelles*. In: Borsali R, Pecora R (eds) *Soft-Matter Characterization*. Springer, Berlin 1:191–234
76. Sheu E (1992) *Phys Rev A* 45(4):2428
77. Pedersen JS (1997) *Adv Colloid Interface Sci* 70:171
78. Pedersen JS, Posselt D, Mortensen K (1990) *J Appl Cryst* 23:321
79. Richter D, Schneiders D, Monkenbusch M, Willner L, Fetters LJ, Huang JS, Lin M, Mortensen K, Farago B (1997) *Macromolecules* 30:1053
80. Svaneborg C, Pedersen JS (2001) *Phys Rev E* 64(1):010802
81. Svaneborg C, Pedersen JS (2002) *Macromolecules* 35(3):1028
82. Daoud M, Cotton JP, Farnoux B, Jannink G, Sarma G, Benoit H, Duplessix C, Picot C, De Gennes PG (1975) *Macromolecules* 8:804
83. Dozier WD, Huang JS, Fetters LJ (1991) *Macromolecules* 24:2810
84. Förster S, Burger C (1998) *Macromolecules* 31:879
85. Won YY, Davis HT, Bates FS, Agamalian M, Wignall GD (2000) *J Phys Chem B* 104(30):7134
86. Pedersen JS, Svaneborg C, Almdal K, Hamley IW, Young RN (2003) *Macromolecules* 36(2):416
87. Poppe A, Willner L, Allgaier J, Stellbrink J, Richter D (1997) *Macromolecules* 30:7462
88. Beaucage G (1996) *J Appl Cryst* 29:134
89. Pedersen JS, Schurtenberger P (1996) *Macromolecules* 29:7602
90. Cotton J (1996) *Adv Colloid Interface Sci* 69:1
91. Wignall G, Hendricks R, Koehler W, Lin J et al. (1981) *Polymer* 22:886
92. Willner L, Jucknischke O, Richter D, Roovers J, Zhou LL, Toporowski PM, Fetters LJ, Huang JS, Lin MY, Hadjichristidis N (1994) *Macromolecules* 27:3821
93. Benmouna M, Hammouda B (1997) *Prog Polym Sci* 22(1):49
94. Choi SH, Lee S, Soto HE, Lodge TP, Bates FS (2011) *J Am Chem Soc* 133(6):1722
95. Pedersen JS, Hamley IW, Ryu CY, Lodge TP (2000) *Macromolecules* 33(2):542
96. Yang L, Alexandridis P, Steytler DC, Kositz MJ, Holzwarth JF (2000) *Langmuir* 16(23):8555
97. Goldmints I, Yu G, Booth C, Smith KA, Hatton TA (1999) *Langmuir* 15(5):1651
98. Laurati M, Stellbrink J, Lund R, Willner L, Zaccarelli E, Richter D (2007) *Phys Rev E* 76:041503
99. Panine P, Finet S, Weiss TM, Narayanan T (2006) *Adv Colloid Interface Sci* 127(1):9
100. Willner L, Poppe A, Allgaier J, Monkenbusch M, Richter D (2001) *Europhys Lett* 55(5):667

101. Lund R, Willner L, Stellbrink J, Lindner P, Richter D (2006) *Phys Rev Lett* 96:068302
102. Lund R, Willner L, Richter D, Dormidontova EE (2006) *Macromolecules* 39(13):4566
103. Zinn T, Willner L, Lund R, Pipich V, Richter D (2012) *Soft Matter* 8(3):623
104. Lund R, Willner L, Pipich V, Grillo I, Lindner P, Colmenero J, Richter D (2011) *Macromolecules* 44(15):6145
105. Thilo L (1977) *Biochim Biophys Acta* 469(3):326
106. Cantú L, Corti M, Salina P (1991) *J Phys Chem* 95(15):5981
107. Price C, Stubbersfield R, Elkafrawy S, Kendall K (1989) *Br Polym J* 21(5):391
108. Booth C, Naylor TD, Price C, Rajab NS, Stubbersfield RB (1978) *J Chem Soc, Faraday Trans 1* 74:2352
109. Malmsten M, Lindman B (1992) *Macromolecules* 25(20):5440
110. Špaček P, Kubin M (1985) *J Appl Polym Sci* 30(1):143
111. Špaček P (1986) *J Appl Polym Sci* 32(3):4281
112. Holmqvist P, Nilsson S, Tiberg F (1997) *Colloid Polym Sci* 275(5):467
113. Procházka K, Glöckner G, Hoff M, Tuzar Z (1984) *Die Makromolekulare Chemie* 185(6):1187
114. Tian MM, Qin AW, Ramireddy C, Webber SE, Munk P, Tuzar Z, Procházka K (1993) *Langmuir* 9(7):1741
115. Michels B, Waton G, Zana R (1997) *Langmuir* 13(12):3111
116. Waton G, Michels B, Zana R (1999) *J Colloid Interface Sci* 212(2):593
117. Thurn T, Couderc-Azouani S, Bloor DM, Holzwarth JF, Wyn-Jones E (2003) *Langmuir* 19(10):4363
118. Procházka K, Bednář B, Mukhtar E, Svoboda P, Trněná J, Almgren M (1991) *J Phys Chem* 95(11):4563
119. Procházka K, Kiserow D, Ramireddy C, Tuzar Z, Munk P, Webber S (1992) *Macromolecules* 25(1):454
120. Wang Y, Kausch C, Chun M, Quirk RP, Mattice WL (1995) *Macromolecules* 28(4):904
121. Smith C, Liu G (1996) *Macromolecules* 29(6):2060
122. Underhill R, Ding J, Birss V, Liu G (1997) *Macromolecules* 30(26):8298
123. Zhang L, Shen H, Eisenberg A (1997) *Macromolecules* 30(4):1001
124. Esselink FJ, Dormidontova EE, Hadzioannou G (1998) *Macromolecules* 31(9):2925
125. Esselink FJ, Dormidontova EE, Hadzioannou G (1998) *Macromolecules* 31(15):4873
126. Hecht E, Hoffmann H (1995) *Colloids Surf A Physicochem Eng Asp* 96:181
127. Goldmints I, Holzwarth JF, Smith KA, Hatton TA (1997) *Langmuir* 13:6130
128. Kositzka MJ, Bohne C, Alexandridis P, Hatton TA, Holzwarth JF (1999) *Langmuir* 15(2):322
129. Kositzka MJ, Bohne C, Alexandridis P, Hatton TA, Holzwarth JF (1999) *Macromolecules* 32(17):5539
130. Waton G, Michels B, Zana R (2001) *Macromolecules* 34(4):907
131. Xu R, Winnik MA, Hallett F, Riess G, Croucher M (1991) *Macromolecules* 24(1):87
132. Wilhelm M, Zhao C, Wang Y, Xu R, Winnik MA, Mura J, Riess G, Croucher M (1991) *Macromolecules* 24(5):1033
133. Xu R, Winnik MA, Riess G, Chu B, Croucher M (1992) *Macromolecules* 25(2):644
134. Calderara F, Hruska Z, Hurtrez G, Lerch J, Nugay T, Riess G (1994) *Macromolecules* 27(5):1210
135. Hickl P, Ballauff M, Jada A (1996) *Macromolecules* 29(11):4006
136. Jada A, Hurtrez G, Siffert B, Riess G (1996) *Macromol Chem Phys* 197(11):3697
137. Yin L, Hillmyer MA (2011) *Macromolecules* 44(8):3021
138. Li T, Wang WJ, Liu R, Liang WH, Zhao GF, Li Z, Wu Q, Zhu FM (2009) *Macromolecules* 42(11):3804
139. Allgaier J, Poppe A, Willner L, Richter D (1997) *Macromolecules* 30:1582
140. Hillmyer M, Bates F (1996) *Macromolecules* 29(22):6994
141. Förster S, Krämer E (1999) *Macromolecules* 32(8):2783

142. Kaya H, Willner L, Allgaier J, Stellbrink J, Richter D (2002) *Appl Phys A Mater Sci Process* 74:s499
143. Jensen G, Shi Q, Hermansanz M, Oliveira C, Deen G, Almdal K, Pedersen JS (2011) *J Appl Cryst* 44: 473–482
144. Jensen GV, Shi Q, Deen GR, Almdal K, Pedersen JS (2012) *Macromolecules* 45(1):430
145. Lund R, Willner L, Stellbrink J, Radulescu A, Richter D (2004) *Physica B: Condens Matter* 350(1–3):E909
146. Won YY, Davis HT, Bates FS (2003) *Macromolecules* 36:953
147. van Stam J, Creutz S, De Schryver FC, Jérôme R (2000) *Macromolecules* 33(17):6388
148. Bronstein LM, Chernyshov DM, Vorontsov E, Timofeeva GI, Dubrovina LV, Valetsky PM, Kazakov S, Khokhlov AR (2001) *J Phys Chem B* 105(38):9077
149. Nordskog A, Fütterer T, von Berlepsch H, Böttcher C, Heinemann A, Schlaad H, Hellweg T (2004) *Phys Chem Chem Phys* 6(12):3123
150. Lund R, Willner L, Richter D, Iatrou H, Hadjichristidis N, Lindner P (2007) *J Appl Crystallogr* 140:S327
151. Jacquin M, Muller P, Cottet H, Crooks R, Théodoly O (2007) *Langmuir* 23(20):9939
152. Choi SH, Bates FS, Lodge TP (2011) *Macromolecules* 44(9):3594
153. Lejeune E, Drechsler M, Jestin J, Müller AHE, Chassenieux C, Colombani O (2010) *Macromolecules* 43(6):2667
154. Palmer RG, Stein DL, Abrahams E, Anderson PW (1984) *Phys Rev Lett* 53(10):958
155. Lund R (2004) Chain exchange kinetics and structure of polymeric micelles – a comprehensive study of three model systems. Ph.D. thesis, Mathematisch-Naturwissenschaftliche Fakultät der Westfälischen Wilhelms-Universität Münster, Germany
156. Kambour R, Gruner C, Romagosa E (1973) *J Polym Sci B Polym Phys* 11(10):1879
157. Quintana J, Villacampa M, Munos M, Andrio A, Katime I (1992) *Macromolecules* 25(12):3125
158. Quintana J, Villacampa M, Andrio A, Munos M, Katime I (2001) *Macromolecules* 25(12):3129
159. Choi SH, Bates FS, Lodge TP (2009) *J Phys Chem B* 113(42):13840
160. Lai C, Russel WB, Register RA (2002) *Macromolecules* 35(3):841
161. Fredrickson GH, Bates FS (1996) *Annu Rev Mater Res* 26:501
162. Li Z, Dormidontova EE (2010) *Macromolecules* 43(7):3521
163. Nicolai T, Colombani O, Chassenieux C (2010) *Soft Matter* 6(14):3111
164. Grason GM (2007) *J Chem Phys* 126(11):114904
165. Mortensen K (1996) *J Phys Condens Matter* 8:A103
166. Kresheck GC, Hamori E, Davenport G, Scheraga HA (1966) *J Am Chem Soc* 88(2):246
167. Bennion B, Eyring E (1970) *J Colloid Interface Sci* 32(2):286
168. Lang J, Eyring E (1972) *J Polym Sci Part a-2-Polym Phys* 10(1):89
169. Honda C, Hasegawa Y, Hirunuma R, Nose T (1994) *Macromolecules* 27:7660
170. Honda C, Abe Y, Nose T (1996) *Macromolecules* 29(21):6778
171. Ye X, Lu Y, Liu S, Zhang G, Wu C (2007) *Langmuir* 23:10366
172. Zhang Y, Wu T, Liu S (2007) *Macromol Chem Phys* 208(23):2492
173. Bednář B, Edwards K, Almgren M, Tormod S, Tuzar Z (1988) *Makromolekulare Chemie-Rapid Communications* 9(12):785
174. Johnson B, Prud'homme RK (2003) *Phys Rev Lett* 91:118302
175. Wang D, Yin J, Zhu Z, Ge Z, Liu H, Armes SP, Liu S (2006) *Macromolecules* 39(21):7378
176. Zhang J, Li Y, Armes SP, Liu S (2007) *J Phys Chem B* 111(42):12111
177. Zhang J, Xu J, Liu S (2008) *J Phys Chem B* 112(36):11284
178. Zhu Z, Xu J, Zhou Y, Jiang X, Armes S (2007) *Macromolecules* 40:6393
179. Ge Z, Cai Y, Yin J, Zhu Z, Rao J, Liu S (2007) *Langmuir* 23(3):1114
180. Sweeney J, Scriven L, Davis H (1987) *J Chem Phys* 87(10):6120
181. Noguchi H, Takasu M (2001) *Phys Rev E* 64:041913
182. Sevink GJA, Zvelindovsky AV (2005) *Macromolecules* 38(17):7502

183. Lund R, Willner L, Monkenbusch M, Panine P, Narayanan T, Colmenero J, Richter D (2009) *Phys Rev Lett* 102:188301
184. Wang Y, Mattice WL, Napper D (1993) *Langmuir* 9(1):66
185. Marrink SJ, Tieleman DP, Mark AE (2000) *J Phys Chem B* 104(51):12165
186. Chen T, Hynninen AP, Prud'homme RK, Kevrekidis IG, Panagiotopoulos AZ (2008) *J Phys Chem B* 112(51):16357
187. Egelhaaf SU, Schurtenberger P (1999) *Phys Rev Lett* 82(13):2804
188. Egelhaaf SU, Olsson U, Schurtenberger P (2000) *Physica B Condens Matter* 276–278:326
189. Bressel K, Muthig M, Prévost S, Grillo I, Gradzielski M (2010) *Colloid Polym Sci* 288(8):827
190. Leng J, Egelhaaf SU, Cates M (2002) *Europhys Lett* 59(2):311
191. Leng J, Egelhaaf SU, Cates M (2003) *Biophys J* 85(3):1624
192. Schmölzer S, Gräbner D, Gradzielski M, Narayanan T (2002) *Phys Rev Lett* 88(25):258301
193. Weiss T, Narayanan T, Wolf C, Gradzielski M, Panine P, Finet S, Helsby W (2005) *Phys Rev Lett* 94(3):1
194. Gummel J, Sztucki M, Narayanan T, Gradzielski M (2011) *Soft Matter* 7(12):5731
195. Egelhaaf SU (1998) *Curr Opin Colloid Interface Sci* 3(6):608
196. Nie H, Bansil R, Ludwig K, Steinhart M, Konak C, Bang J (2003) *Macromolecules* 36(21):8097
197. Jeong U, Lee HH, Yang H, Kim JK, Okamoto S, Aida S, Sakurai S (2003) *Macromolecules* 36(5):1685
198. Krishnamoorti R, Modi MA, Tse MF, Wang HC (2000) *Macromolecules* 33(10):3810
199. Wang CY, Lodge TP (2002) *Macromolecules* 35(18):6997
200. Mai Y, Eisenberg A (2012) *Chem Soc Rev* 41(18):5969–5985
201. Antonietti M, Förster S (2003) *Adv Mater* 15(16):1323
202. Won YY, Brannan AK, Davis HT, Bates FS (2002) *J Phys Chem B* 106(13):3354
203. Shen H, Eisenberg A (1999) *J Phys Chem B* 103(44):9473
204. Wang L, Yu X, Yang S, Zheng JX, Van Horn RM, Zhang WB, Xu J, Cheng SZD (2012) *Macromolecules* 45(8):3634
205. Bhargava P, Tu Y, Zheng JX, Xiong H, Quirk RP, Cheng SZD (2007) *J Am Chem Soc* 129(5):1113
206. Burke SE, Eisenberg A (2001) *Langmuir* 17(21):6705
207. Chen L, Shen H, Eisenberg A (1999) *J Phys Chem B* 103(44):9488
208. Burke S, Eisenberg A (2001) *Polymer* 42(21):9111
209. Nakano M, Fukuda M, Kudo T, Endo H, Handa T (2007) *Phys Rev Lett* 98:238101
210. Nakano M, Fukuda M, Kudo T, Matsuzaki N, Azuma T, Sekine K, Endo H, Handa T (2009) *J Phys Chem B* 113(19):6745

Controlled Polymerization and Polymeric Structures
Flow Microreactor Polymerization, Micelles Kinetics,
Polypeptide Ordering, Light Emitting Nanostructures
Abe, A.; Lee, K.-S.; Leibler, L.; Kobayashi, S. (Eds.)
2013, V, 248 p. 143 illus., 72 illus. in color., Hardcover
ISBN: 978-3-319-02918-4